

USING MICROTREMORS TO ASSESS SITE CHARACTERISTICS IN THE
NEW MADRID SEISMIC ZONE

Except where reference is made to the work of others, the work described in this thesis is my own or was done in collaboration with my advisory committee. This thesis does not include proprietary or classified information.

Kelli April Hardesty

Certificate of Approval:

Ming-Kuo Lee
Professor
Geology and Geography

Lorraine W. Wolf, Chair
Professor
Geology and Geography

Mark G. Steltenpohl
Professor
Geology and Geography

Ashraf Uddin
Associate Professor
Geology and Geography

George T. Flowers
Interim Dean
Graduate School

USING MICROTREMORS TO ASSESS SITE CHARACTERISTICS IN THE
NEW MADRID SEISMIC ZONE

Kelli April Hardesty

A Thesis

Submitted to

the Graduate Faculty of

Auburn University

in Partial Fulfillment of the

Requirements for the

Degree of

Master of Science

Auburn, Alabama
August 9, 2008

USING MICROTREMORS TO ASSESS SITE CHARACTERISTICS IN THE
NEW MADRID SEISMIC ZONE

Kelli April Hardesty

Permission is granted to Auburn University to make copies of this thesis at its discretion, upon request of individuals or institutions and at their expense. The author reserves all publication rights.

Signature of Author

Date of Graduation

VITA

Kelli Hardesty, daughter of Tim and Beth Hardesty, was born on April 6, 1981, in Springfield, Missouri. She graduated from Richland High School in 1999. She attended Missouri State University, formerly known as Southwest Missouri State University, in Springfield, Missouri, and graduated with a Bachelor of Science degree in Geology in August, 2005. In August of 2005, she entered the Graduate School at Auburn University to pursue a Master of Science degree in Geology.

THESIS ABSTRACT

USING MICROTREMORS TO ASSESS SITE CHARACTERISTICS IN THE
NEW MADRID SEISMIC ZONE

Kelli A. Hardesty

Master of Science, August 9, 2008
(B.S., Missouri State University, 2005)

95 Typed Pages

Directed by Lorraine W. Wolf

Results are presented from a study in the New Madrid seismic zone (NMSZ) utilizing the microtremor method. The study analyzes and interprets horizontal to vertical (H/V) spectral ratios to determine resonant periods, wave amplification factors, and liquefaction vulnerability at sites across the Mississippi embayment. Data were collected from areas that experienced earthquake-induced soil liquefaction due to strong ground motion during historic and prehistoric earthquake sequences. Results from 15 sites show resonant fundamental periods of 0.5 s to 4.5 s for embayment thicknesses of ~100 m to 900 m and average shear-wave velocity of 800 m/s. These fundamental periods are associated with a strong impedance contrast between embayment sediments and underlying basement rock. The basin configuration and a strong impedance contrast between sediments and basement rocks could contribute significantly to wave

amplification at these resonant periods. Other spectral peaks are correlated with major stratigraphic boundaries within basin sediments. Results also indicate higher amplification factors and liquefaction vulnerability at sites located in meandering stream deposits near the basin axis, where embayment thickness is greatest.

ACKNOWLEDGEMENTS

I would like to thank the Geological Society of America, the Alabama Geological Society, and the Gulf Coast Association of Geological Societies for funding this project through grants and scholarships. I would like to thank Drs. Steve Horton, Glenn Rix, Buddy Schweig, and Martitia Tuttle for their expertise and research support. I would like to especially thank Dr. Paul Bodin for his expertise, time, guidance, and assistance towards making this project possible. Appreciation is also extended to the Center for Earthquake Research and Information in Memphis, Tennessee for allowing me to use their equipment that was essential to completing this research. To my committee members Drs. Ming-Kuo Lee, Mark Steltenpohl, and Ashraf Uddin goes my profound gratitude for their patience, knowledge, and contribution. My deepest appreciation goes to the head of my committee, Dr. Lorraine Wolf. Her wisdom, intelligence, patience, and dedication were essential to the completion of this thesis; her encouragement, support, and friendship provided the motivation and inspiration I needed to see it through. Thanks are also extended to the rest of the faculty and staff in the Auburn University Geology department who provided much needed support and assistance.

I would like to thank God for giving me the strength and knowledge to complete this project. I would like to thank my parents and my sister for their support, encouragement, enthusiasm, and sacrifice as I pursued this degree. Without the love and support of my family, this accomplishment would not be possible.

Style manual or journal used: GEOPHYSICS

Computer software used: Microsoft Office Word 2007®, Microsoft Office Excel 2007®, Microsoft Office Power Point 2007®, MATLAB R2007a®, ArcGIS 9®, Adobe Illustrator CS3®

TABLE OF CONTENTS

	<u>Page</u>
LIST OF FIGURES	xi
LIST OF TABLES	xiii
INTRODUCTION	1
BACKGROUND	3
Tectonic History	3
Geologic Background	4
Seismicity	10
The Microtremor Technique	13
Application of the Microtremor Method	15
METHODOLOGY	17
Data Acquisition	17
Site Selection	17
Microtremor Data Acquisition	19
Supporting Data Acquisition	21
Data Processing	22
Microtremor Analysis	22
Supporting Data Analysis	25
RESULTS	27
INTERPRETATION	43
Resonant Periods	43
Microtremor Robustness	55
DISCUSSION	56
Resonant Periods in the Mississippi Embayment	56
Nakamura's Kg Index	59
Significance of Resonant Periods	64

Considerations	65
Suggestions for Future Investigations	65
CONCLUSIONS	67
REFERENCES	69
APPENDIX A	75
APPENDIX B	77
APPENDIX C	87

LIST OF FIGURES

		<u>Page</u>
Figure 1.	Surface geology of the Mississippi Embayment and geologic cross-section through embayment.	5
Figure 2.	General stratigraphic column of units in the northern Mississippi Embayment.	6
Figure 3.	Surface geology and deposit type of the Mississippi Embayment as mapped by Saucier (1994b).	9
Figure 4.	Map of NMSZ displaying seismicity, rift zone, and liquefaction deposits.	11
Figure 5.	Microtremor data collection sites.	18
Figure 6.	Components of data acquisition system.	20
Figure 7.	Field set-up of data acquisition system.	20
Figure 8.	Recordings at two sites showing data transients.	23
Figure 9.	Processing sequence in calculating HVPSRs.	24
Figure 10.	Selected microtremor sites with nearby geotechnical and well-log data.	26
Figure 11.	HVPSR at site Lake Ashbaugh.	29
Figure 12.	HVPSR at sites Black River, Shirley Bay, and Lester.	30
Figure 13.	HVPSR at site Lake City.	31
Figure 14.	HVPSR at site Payneway.	32
Figure 15.	HVPSR at site Marked Tree.	33
Figure 16.	HVPSR at site Big Lake.	34

Figure 17.	HVPSR at site Hornersville.	35
Figure 18.	HVPSR at site Gilbert.	36
Figure 19.	HVPSR at sites Archway and R. P. Haynes.	37
Figure 20.	HVPSR at site Chickasaw.	38
Figure 21.	HVPSR at sites Bogota and Reelfoot.	39
Figure 22.	Peak periods observed in HVPSR and respective embayment thickness at each site.	40
Figure 23.	Comparison of HVSPR repeatability at sites Lester and Lake City, Archway and RP Haynes.	41
Figure 24.	Comparison of HVPSR repeatability at sites Payneaway and Marked Tree, Hornersville and Gilbert.	42
Figure 25.	Observed and predicted periods at five selected sites and their respective HVPSRs.	44
Figure 26.	Comparison of observed and predicted periods for the Cretaceous-Paleozoic interface.	48
Figure 27.	Comparison of observed and predicted periods for the Paleocene-Cretaceous interface.	50
Figure 28.	Comparison of observed and predicted periods for the Eocene-Paleocene unit.	52
Figure 29.	Comparison of observed and predicted periods for the Quaternary-Eocene interface.	54
Figure 30.	Resonant frequency, amplification factor, and calculated Kg values representing basement interface at 15 sites across embayment.	61
Figure 31.	Calculated Kg values for sites corresponding to the Quaternary-Eocene interface, and respective geotechnical and sand-blow data close to sites.	63

LIST OF TABLES

		<u>Page</u>
Table 1.	Names and abbreviations of site locations.	18
Table 2.	Data sources for embayment thicknesses, shear-wave velocities, Geotechnical information, well-logs, and seismic hazard.	21
Table 3.	Length of time segments used in analysis for each site.	28
Table 4.	Observed periods seen in the HVPSR grouped into short, intermediate and long-period ranges for each site.	40
Table 5.	Sources of thickness and shear-wave velocity of embayment units used in this study.	45
Table 6.	Calculated and observed periods for the Cretaceous-Paleozoic interface.	47
Table 7.	Calculated and observed periods for the Paleocene-Cretaceous interface.	49
Table 8.	Calculated and observed periods for the Eocene-Paleocene interface.	51
Table 9.	Calculated and observed periods for the Quaternary-Eocene interface.	53
Table 10.	Average densities and velocities associated with rock types.	55
Table 11.	Interfaces between the four embayment units, their respective rock types, and their estimated impedance contrast.	55
Table 12.	Peak ranges and observed periods with associated embayment interfaces for this study.	56
Table 13.	Peak ranges and observed periods with associated embayment units from Smith (2000).	57

INTRODUCTION

The New Madrid seismic zone (NMSZ) is located within the Mississippi Embayment in the central United States. The embayment forms a southwest-plunging syncline containing unconsolidated and loosely consolidated alluvial and marine sediments, which are Cretaceous, Tertiary, and Quaternary. Embayment sediments overlie Paleozoic basement rocks, forming a high acoustic impedance contrast at this interface. A high impedance contrast can cause seismic waves to become trapped and amplified in a basin, leading to longer seismic wave durations and wave amplification (Bullen and Bolt, 1985).

Much of the NMSZ seismicity occurs along well-defined trends thought to be associated with a failed rift system; outside the rift zone, seismicity is diffuse. Most present-day seismicity in the NMSZ is of low to moderate magnitude; however, paleoseismologic evidence indicates that the area has experienced at least three large earthquake sequences (i.e., $M > 7.0$), strong enough to induce soil liquefaction (Tuttle et al., 2002). Studies in the NMSZ have utilized geophysical techniques such as seismic refraction and reflection, well-logging, gravity, and electromagnetics to improve the understanding of geologic structures in the zone and to provide insight on the source of seismicity. Geotechnical methods have been used to predict the response of sediments to a large seismic event and to assess seismic hazard.

In this study, I use microtremors, or ambient noise, to assess the effects of embayment sediments in the NMSZ in response to strong ground motion. Microtremors are small vibrations, or noise, caused by both natural sources, such as sea waves and wind, and anthropogenic sources, such as traffic, footsteps, and well pumps. Introduced by Nakamura in 1989, the microtremor method has been utilized to analyze subsurface geologic structures, and subsurface site characteristics, such as resonant frequency, wave amplification, and liquefaction vulnerability (Lermo and Chavez-Garcia, 1993; Konno and Ohmachi, 1998; Bodin and Horton, 1999; Smith, 2000; Huang and Tseng, 2002). This study uses Nakamura's method of microtremors to investigate subsurface stratigraphic units and site characteristics in the Mississippi Embayment. In contrast with other geophysical methods used in the NMSZ, the microtremor method requires minimal manpower and provides a low-cost, time-effective, non-invasive alternative, thus making it an attractive technique.

BACKGROUND

Tectonic History

The tectonic history of the NMSZ involves periods of extension, compression, and uplift, followed by subsidence and sedimentary deposition (Kane et al., 1981; Howe and Thompson, 1984; Braile et al., 1986; Johnston and Shedlock, 1992; Saucier, 1994a). Tectonism in this intracontinental setting is thought to control various processes, such as sediment accumulation, drainage-basin location, igneous intrusion, fault reactivation, and ore-deposit localization (Braile et al., 1986).

Initial rifting in the central United States occurred during Late Proterozoic to Early Cambrian (Howe and Thompson, 1984) and is associated with the opening of the Iapetus Ocean (Johnston and Shedlock, 1992). During the active stages of rifting, mafic bodies were emplaced in the lower crust along the rift axis; however, the rift failed and the region subsequently subsided (Johnston and Shedlock, 1992). Crustal extension during this rifting phase was accompanied by normal faults that trend northeast and are parallel to the strike of the rift (Howe and Thompson, 1984).

Continued cooling and subsidence due to the rifting during Early Cambrian led to crustal downwarping in the NMSZ region during Middle Cambrian to Middle Ordovician (Howe and Thompson, 1984). An interior seaway allowed a thick accumulation of carbonate sediments (Howe and Thompson, 1984). From Middle Ordovician to Late

Pennsylvanian, the region continued to subside between episodic periods of uplift and erosion in response to compression during the Taconic, Acadian, and Alleghanian orogenies (Howe and Thompson, 1984; Johnston and Shedlock, 1992). Throughout Paleozoic, the NMSZ region formed a sedimentary basin above the failed rift, accumulating a sequence of clastic and carbonate rocks with thicknesses ranging from 1 to 4 km (Braile et al., 1986).

During Mesozoic, the NMSZ region experienced uplift and erosion related to the extension and opening of the modern Atlantic Ocean during the break up of Pangaea (Johnston and Shedlock, 1992). During the uplift, it is estimated that between 2 and 5 km of Paleozoic sedimentary rock were eroded (Johnston and Shedlock, 1992). The uplift also allowed the reactivation of faults and the emplacement of igneous intrusions in the original rifted area (Braile et al., 1986). The cooling and contraction of Mesozoic-emplaced igneous bodies caused the NMSZ region, once more, to subside and downwarp during Late Cretaceous (Kane et al., 1981). From Late Cretaceous to Quaternary, faults were reactivated due to compressional stress in response to the continued widening of the Atlantic (Braile et al., 1986). Continued sedimentation and subsidence allowed the formation of the modern-day Mississippi Embayment.

Geologic Background

The Mississippi Embayment is a sedimentary basin that contains a thick sequence of interbedded alluvial and marine gravels, sands, silts, clays, and carbonates derived from various sources (Figures 1 and 2). In the upper Mississippi Embayment, Upper

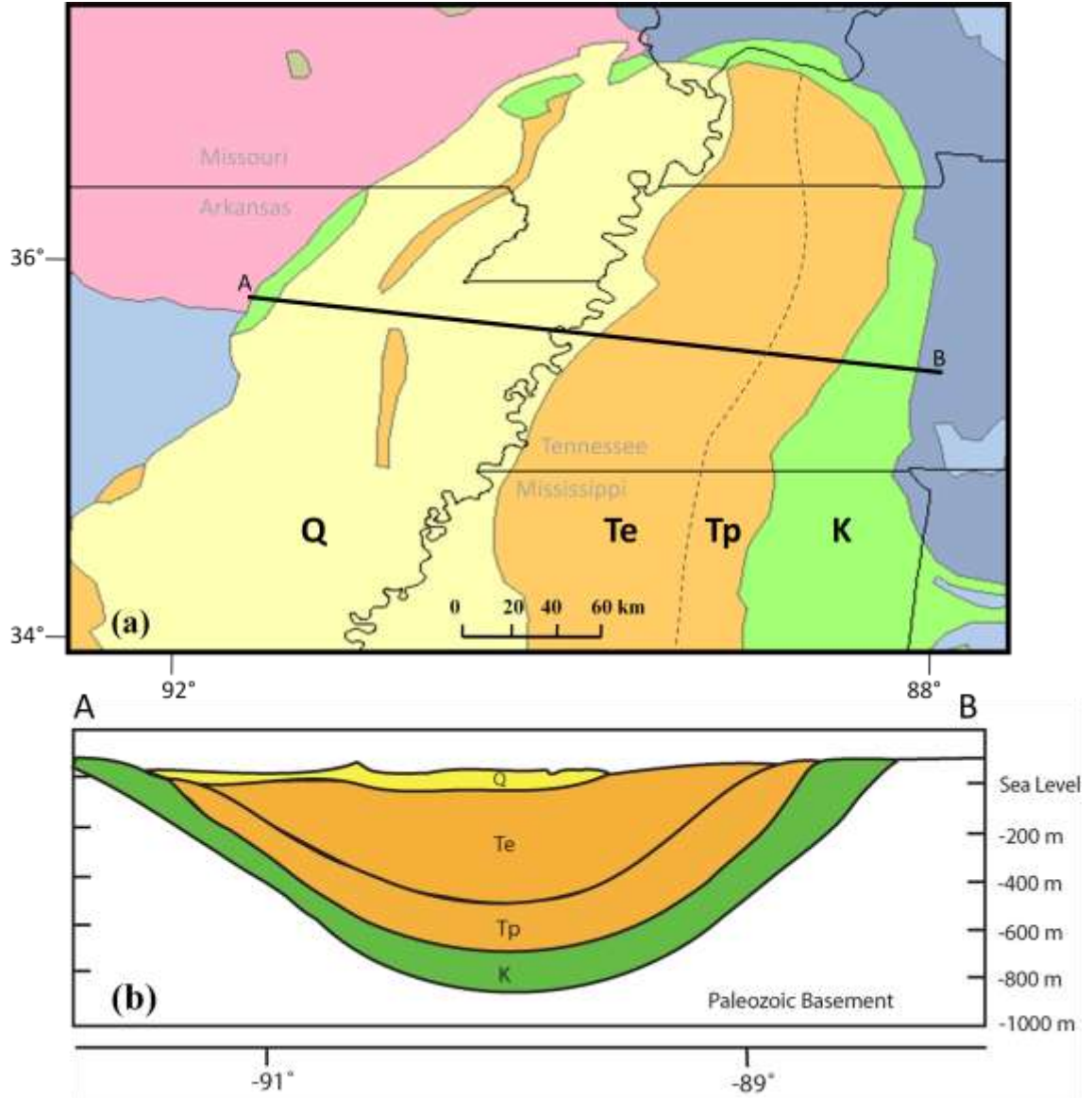


Figure 1. (a) Surface geology of the Mississippi Embayment (USGS, 2005). Labeled are cross-section line A-B, and ages Q (Quaternary), T_e (Tertiary- Eocene), T_p (Tertiary- Paleocene), and K (Cretaceous). (b) Cross-section profile along A-B (Modified from Street et al., 2004). Note huge vertical exaggeration.

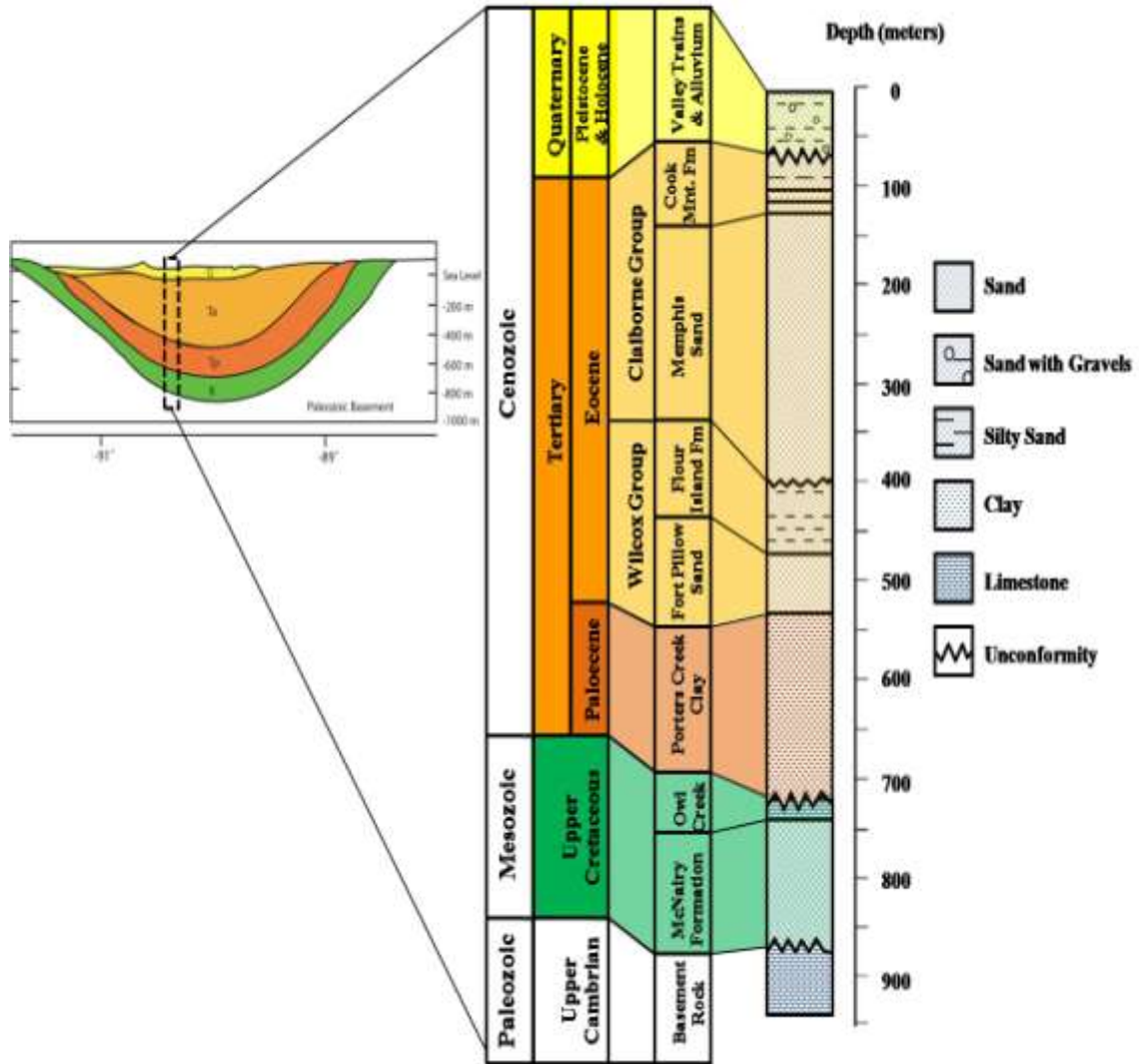


Figure 2. General stratigraphic column of units in the northern part of the Mississippi Embayment (Modified from Street et al., 2004). This study groups the units by age into four packages: Cretaceous, Paleocene, Eocene, and Quaternary.

Cretaceous sedimentary deposits are of marine origin, whereas Tertiary sediments are of both marine and non-marine origin (Howe and Thompson, 1984). Quaternary sediments are primarily of glacial and fluvial origin (Saucier, 1994a). During Pleistocene, the Mississippi Embayment experienced sediment deposition related to cyclic glaciations.

Although the continental glaciers did not extend into the embayment region, they distributed large volumes of meltwater and outwash into the embayment via braided streams (Obermeier, 1989). As the ratio of sediment to meltwater declined during the Holocene, stream characteristics changed from braided to meandering (Obermeier, 1989).

For this study, we group embayment units by age into four packages: Cretaceous, Paleocene, Eocene, and Quaternary (Figure 1). Figure 2 is a generalized stratigraphic column of northern embayment units relating to the four grouped stratigraphic packages. Cretaceous units include the McNairy Formation, which is overlain by the Owl Creek Formation. The McNairy Formation is a massively bedded, fine- to coarse-grained sandstone; the Owl Creek Formation is a sandy limestone (Crone, 1981). The total thickness of the Cretaceous section ranges from 95 to 200 m (Van Arsdale and TenBrink, 2000). Overlying the Cretaceous unit are Paleocene sediments, consisting of the Porters Creek Clay (Crone, 1981). The Porters Creek is a hard, clay unit that ranges in thickness from 150 to 200 m (Van Arsdale and TenBrink, 2000). The Porters Creek Clay acts as a major hydrostratigraphic confining unit. Overlying the Paleocene sediments is a 235 to 450 m-thick Eocene sequence, consisting of the Wilcox and Claiborne Groups (Crone, 1981; Van Arsdale and TenBrink, 2000). The Wilcox Group consists of the Fort Pillow Sand and the Flour Island Formation. Massive sands and sandy clays dominate the Wilcox Group. The Claiborne Group consists of the Memphis Sand and the Cook Mountain Formation. Massive sands, silty sands, and clays comprise the Claiborne Group. The Fort Pillow Sand and the Memphis Sand are the predominant Eocene units. The Eocene unit is unconformably overlain by the 33 to 61 m Quaternary unit, consisting of valley trains and alluvium (Crone, 1981; Van Arsdale and TenBrink, 2000). Valley

trains are glacial outwash deposits consisting of sands and gravels (Saucier, 1994a). The valley trains and alluvium are Pleistocene and Holocene, respectively.

The complexity of Quaternary surface sediments in the Mississippi Embayment has been described by Saucier (1994a). Saucier (1994a) classifies surface deposits in the embayment into four main groups: lowlands, braided stream, meandering, and transitional (mixed braided and meandering) (Figure 3). These groups comprise sediments that can be further classified on the basis of age, depositional environment, and lithology.

The lowlands, braided stream and transitional surface deposits are glacial outwash sediments of different ages and from different sources (Obermeier, 1989; Saucier, 1994a). Lowland deposits are early Wisconsin and were derived from the Missouri and Mississippi River drainage basins. Braided stream and transitional deposits are late Wisconsin and are derived from the Missouri, Mississippi, and Ohio River drainage basins. Although the lowland, braided stream and transitional deposits have near-similar lithologies, they differ in source and age (Obermeier, 1989). The lithologies of these three deposit types are described on the basis of stratigraphic position: substratum, near-surface, and surface, from bottom to top, respectively. Substratum deposits are coarse-grained, consisting of coarse sands and gravels; near-surface and surface deposits are fine-grained, consisting of silty and sandy clays, silts, silty sands, and sands (Obermeier, 1989; Saucier, 1994a).

Meandering deposits are Holocene and were derived from successive lateral migrations of individual river courses (Obermeier, 1989). These deposits are more complex in terms of lithology because they include depositional environments such as

natural levees, point bars, and abandoned channels. Natural levees consist of silty clay, sandy clay, and silty sand that are moderately stiff to stiff (Saucier, 1994a). Point-bar deposits typically fine upward, from medium to coarse sands with gravel, into well-sorted, medium- to fine-grained sands, and finally into sandy or silty clays, or silty sands. The fine-grained sediments in the upper portion are more cohesive than the coarse-grained sediments in the lower portion of the point-bar deposit (Saucier, 1994a). Abandoned channels consist of fine- to medium-grained sands, overlain by a sequence of (1) silts and silty clays, (2) silty clays and clays, and (3) clays with silts and fine sands (Obermeier, 1989).

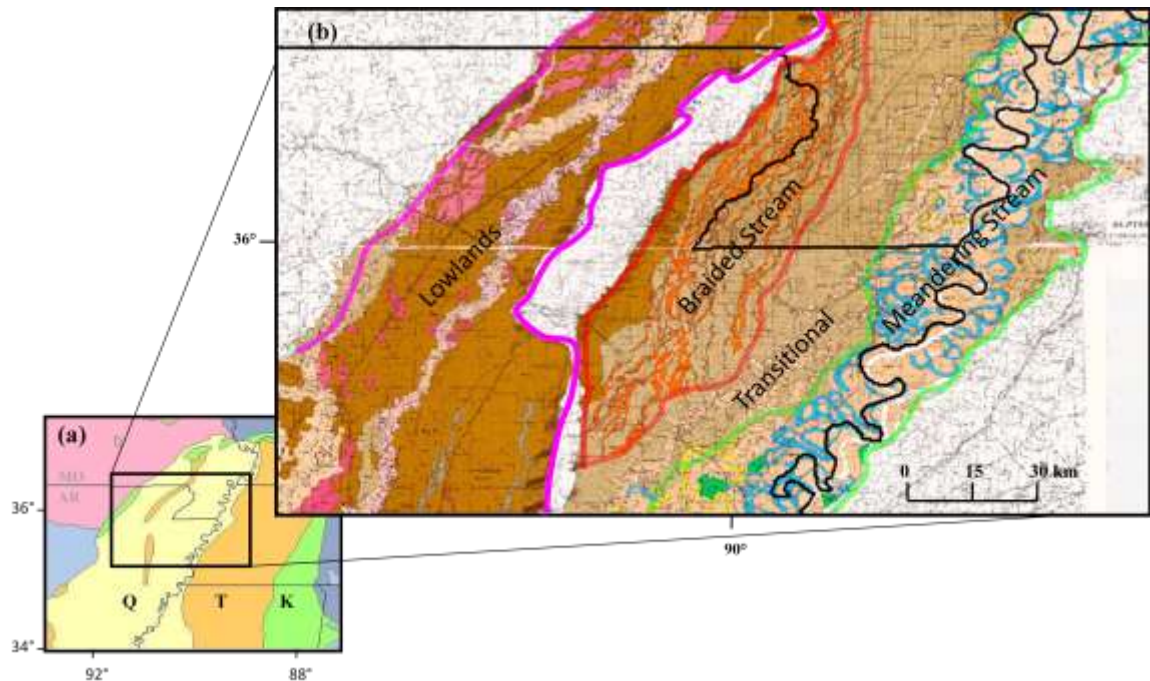


Figure 3. (a) Geologic map of Mississippi Embayment: Q (Quaternary), T (Tertiary), K (Cretaceous). (b) Map of surface sediments and deposit type as classified by Saucier (1994b): Lowlands, braided stream, transitional, and meandering stream outlined in magenta, red, and green, respectively.

Seismicity

Historical records and paleoseismological evidence together indicate that the NMSZ experienced at least three large earthquake sequences ($M \geq 7.0$) strong enough to induce soil liquefaction (Obermeier, 1989; Tuttle et al., 2002). The most recent sequence was the earthquakes of 1811 and 1812, which was responsible for devastating settlements along the Mississippi River and inducing liquefaction in an area of $\sim 10,000 \text{ km}^2$ in the New Madrid region (Tuttle et al., 2002). Liquefaction is a process in which saturated sediments respond to seismic energy by behaving as a viscous fluid. It is dependent upon factors such as duration of seismic waves, amplitude of seismic wave energy, depth to water table, and depth and type of sediments (Obermeier, 1996). Liquefaction occurs in areas of overpressure when cyclic strains from seismic ground motion exceed a given threshold (Seed and Idriss, 1982). Figure 4 illustrates the approximate extent of liquefaction deposits in the NMSZ.

Much of the present-day seismicity in the NMSZ is of low to moderate magnitude and occurs along well-defined trends thought to be associated with the failed Cambrian rift system (Figure 4). These trends are thought to reflect two northeast-oriented right-lateral strike-slip faults, offset by a northwest-trending step-over thrust (Gomberg, 1992). Outside of the rift zone, seismicity is diffuse, as is characteristic of intraplate regions. The source of seismic activity, recurrence rates of large earthquakes, and potential for seismic hazard in the NMSZ are the focus of ongoing study (Gomberg, 1992; Liu et al., 1992; Liu and Zoback, 1997; Newman et al., 1999; Tuttle, 2001; Tuttle et al., 2002).

Many hypotheses have been suggested about the origin of seismicity in the NMSZ. Some propose that seismicity is concentrated in zones of crustal weakness

(Hinze et al., 1988); others propose that seismicity occurs in localized areas of concentrated stress (Campbell, 1978; Gangopadhyay et al., 2004). Of the many mechanisms proposed for the origin of the zone's seismicity, the most accepted is that most earthquakes in the NMSZ are associated with structurally weak, reworked crust responding to far-field plate-boundary forces (Liu and Zoback, 1997).

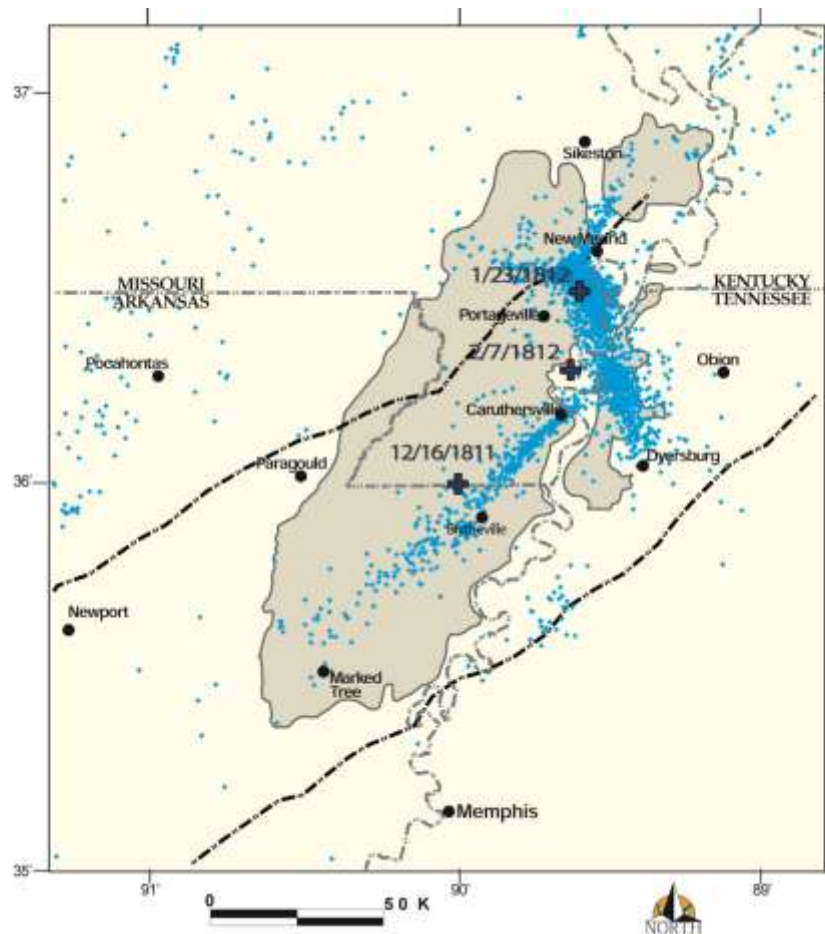


Figure 4. Map of seismicity (blue dots) in the NMSZ. Shown are boundaries of Reelfoot rift zone (dashed line), 1811-1812 earthquake epicenters (black crosses), and liquefaction deposits (gray shading). Modified from Tuttle et al. (2002).

Recurrence rates of moderate to large seismic events in the NMSZ have been estimated using a variety of approaches. In paleoliquefaction studies, the timing of major seismic events is constrained by radiocarbon-dating and by artifacts that are diagnostic of specific cultural periods (Tuttle, 2001). Based on the geologic record and liquefaction deposits, it is estimated that the recurrence rate for a magnitude 7 or 8 earthquake is ~500 years (Tuttle et al., 2002). In 1991, GPS networks were established in the NMSZ region to obtain information about strain rates (Liu et al., 1992; Newman et al., 1999). Liu et al. (1992) concluded that slip rates between 5 to 7 mm/yr in the NMSZ region indicate that it takes ~1,000 years to accumulate the strain energy needed to produce earthquakes of magnitudes similar to 1811 and 1812. Newman et al. (1999) concluded that either previous recurrence rates had been overestimated, or that the magnitudes of the 1811 and 1812 earthquakes were smaller than estimated. They observed negligible slip rates of 2 mm/yr in the NMSZ and proposed a recurrence rate of ~2,500 years. Based on the observed rate of smaller earthquakes in the NMSZ, Newman et al. (1999) report a recurrence rate of ~1,700 and 15,000 years for a magnitude 7 and 8 earthquake, respectively.

In addition to research aimed at estimating recurrence rates, some studies have focused on understanding how embayment sediments might respond to seismic energy from large earthquakes. Embayment sediments and underlying Paleozoic basement rock form a high acoustic impedance contrast that can cause seismic waves to become trapped and amplified in the basin. Impedance is the product of a layer's velocity and density. A high impedance contrast can lead to longer seismic wave durations and to wave amplification, thus increasing the potential for surface sediments to liquefy (Bullen and

Bolt, 1985). In this study, we use microtremors, or ambient noise, to assess the effects of embayment sediments in the NMSZ on seismic ground motions.

The Microtremor Technique

Microtremors have been used to analyze site characteristics and estimate site effect on earthquake ground motion (Katz, 1976; Nakamura, 1989; Lermo and Chavez-Garcia, 1993; Huang and Tseng, 2002). Site characteristics include fundamental period, liquefaction vulnerability, and wave amplification, all of which are influenced by sediment type, sediment consolidation and saturation, and location and thickness of lithologic units. Site effect (also known as the transfer function) is the response of surface sediment due to the source and propagation of released seismic energy.

Although the methods of collecting and processing microtremor data are varied, the basic assumptions of the microtremor method remain unchanged.

Two approaches for determining the site effect are the standard spectral ratio (S_T) and the H/V ratio methods (Katz, 1976; Nakamura, 1989; Huang and Tseng, 2002). The standard spectral ratio is computed by taking the ratio of the horizontal spectrum of ground motion on a soft sediment site, S_{HS} , relative to the horizontal spectrum on a hard (or reference) site S_{HB} ,

$$S_T = \frac{S_{HS}}{S_{HB}} \quad (1)$$

Nakamura (1989) investigated the use of microtremors for estimating site effect by first looking at seismic waveforms of different earthquakes at various observation points. He observed that regardless of earthquake magnitude or propagation path,

waveforms recorded at the same observation point shared similarities. Based on this observation, Nakamura (1989) proposed using a spectral ratio of the vertical spectrum of ground motion on a soft site, S_{VS} , and hard site, S_{VB} , to estimate the effect of the source, E_S , on amplitude of recorded motion, where

$$E_S = \frac{S_{VS}}{S_{VB}} \quad (2)$$

To compensate for the source effect, Lermo and Chavez-Garcia (1993) and Nakamura (1989) proposed a modified spectral ratio, S_{TT} , where

$$S_{TT} = \frac{S_T}{E_S} \approx \frac{S_{HS}}{S_{VS}} \quad (3)$$

Several studies have shown empirically that the ratio of S_{HB}/S_{VB} is approximately 1, thus yielding a transfer function based only on ground motion at a soft sediment site (Nakamura, 1989; Lermo and Chavez-Garcia, 1993; Huang, 2002). This technique eliminates the need for a reference site, which is important for studies in basins like the NMSZ, where a hard-rock reference is not locally accessible. In application, this quantity is known as the H/V power spectral ratio (HVPSR),

$$HVPSR = \frac{\frac{H_N + H_E}{2}}{V_Z} \quad (4)$$

where H_N and H_E are the power spectra of the recorded horizontal components (N-S, E-W) of ground motion and V_Z is the vertical component. The HVPSR method assumes that the vertical component is uninfluenced by low-velocity sediments and that the

Rayleigh wave affects the vertical and horizontal components equally (Nakamura, 1989; Woolery and Street, 2002). The resulting spectrum is assumed to be independent of source and path and can be used to determine resonant frequencies, which appear in the HVPSR as peak amplitudes.

Application of the Microtremor Method

Since Nakamura (1989) introduced the HVPSR method, others have applied it to determine fundamental period (also known as “resonant frequency” or “predominate period”), site amplification, sediment thickness, and liquefaction vulnerability in sedimentary basins. Field et al. (1990) collected microtremor data and used the standard spectral ratio to compare observed and predicted resonant frequencies, determine amplification factors, and correlate spectral peaks with specific soil layers at a site in Flushing Meadows, New York. Although Field et al. did not apply Nakamura’s method of HVPSRs in their 1990 study, Field and Jacob (1993) later applied the HVPSR method in the same study area and determined that it compared favorably with their earlier investigation.

Lermo and Chavez-Garcia (1993) employed the HVPSR method to estimate the transfer function and determine fundamental period and local site amplification in three cities in Mexico with different geologic and tectonic settings. They compared these results with results from a study using standard spectral ratios and determined good agreement between the two methods. Ibs-von Seht and Wohlenberg (1999) applied the HVPSR method to relate fundamental frequency with sediment thickness at sites in the Rhine Embayment, Germany. They used sediment thickness known from drillings to

compare the HVPSRs with standard spectral ratios and determined that results using the HVPSRs were more reliable than the standard spectral ratios because the HVPSRs were less influenced by high-amplitude noise.

Huang and Tseng (2002) utilized Nakamura's method in the area of Yuan-Lin, Taiwan, not only to determine fundamental frequencies and amplification factors, but also to assess liquefaction vulnerability of basin sediments. The Yuan-Lin area experienced intense liquefaction during the 1999 Chi-Chi earthquake. Huang and Tseng (2002) found that their calculated values of liquefaction vulnerability were higher in areas with obvious liquefaction and lower in areas that did not display noticeable liquefaction. They proposed using the application of the microtremor method for mapping liquefaction susceptibility in other areas.

Most closely related to the present study is a microtremor study conducted by Smith (2000) in the southern portion of the NMSZ. Smith (2000) collected data at 113 sites in the metropolitan Memphis area and along a west-east transect from Eagle Lake, TN, west of the Mississippi River to Somerville, TN, 30 miles east of Eagle Lake. Smith (2000) used the HVPSR technique to investigate resonant periods. He correlated three distinct resonant frequencies with depth to basement and to specific lithologic units within the Mississippi Embayment. Two longer period peaks ($1.0 \text{ s} \leq T \leq 2.0 \text{ s}$, and $4.0 \text{ s} \leq T \leq 4.5 \text{ s}$) were associated with deep sediments that overlie the Paleozoic basement rock; a shorter period peak ($0.05 \text{ s} \leq T \leq 0.3 \text{ s}$) was associated with a shallow subsurface loess unit.

METHODOLOGY

This section describes both the data acquisition and data processing methods of the study. Data acquisition involved selecting site locations, acquiring microtremor data, and gathering supporting data. Data processing involved analyzing microtremor data and supporting data.

Data Acquisition

Site Selection

Sites for this study were located in the central part of the NMSZ zone, close to the postulated epicenters of the 1811-1812 earthquakes and to areas where liquefaction deposits are abundant (Figure 4). Some sites were selected because they were close to sites where geotechnical and paleoseismological data had been collected. Other sites were selected to represent the common types of sedimentary deposits (lowlands, braided streams, meandering streams, and transitional) as classified by Saucier (1994a) (Figure 3). At least 3 sites of each deposit type were chosen for data collection, and 18 sites were collected in all (Figure 5). Site names and abbreviations are defined in Table 1. Information pertaining to each site, such as site name, latitude-longitude, quality of collected data, and other site details, is displayed in Appendix A.

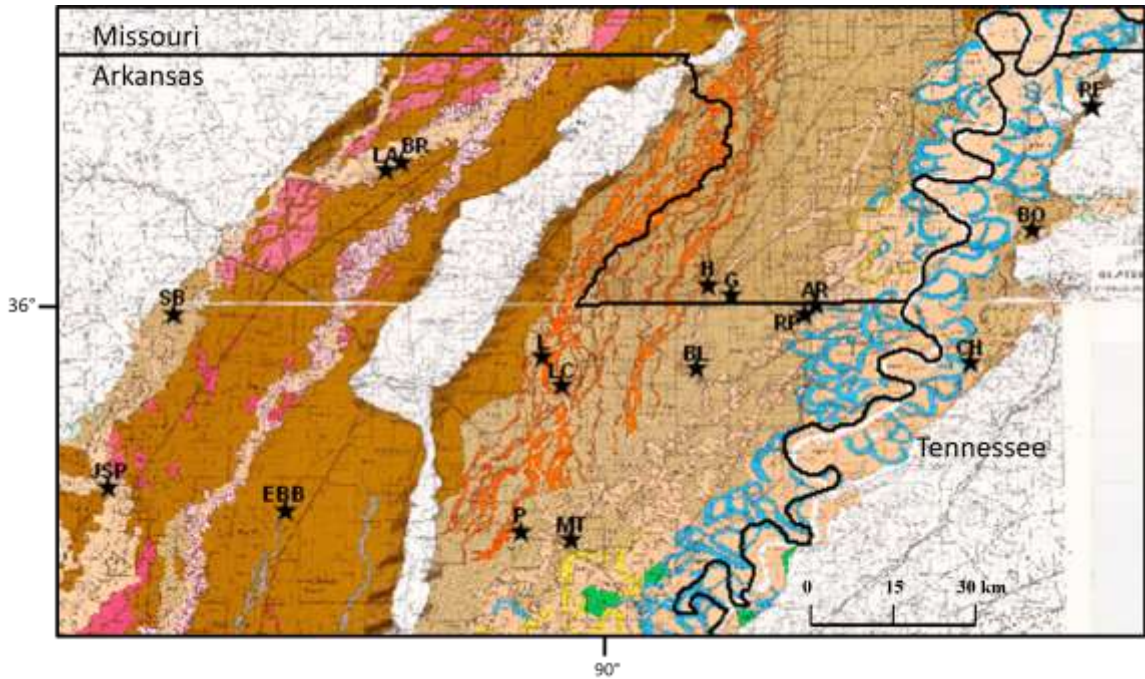


Figure 5. Microtremor data collection sites represented by stars and abbreviations (Saucier, 1994b).

Table 1. Names and abbreviations of site locations as depicted in figures and text.

Site Name	Site Abbreviation
Marked Tree	MT
Chickasaw	CH
Reelfoot	RF
Bogota	BO
Big Lake	BL
Hornersville	H
Gilbert	G
Black River WMA	BR
Lake Ashbaugh	LA
Shirley Bay WMA	SB
Jacksonport SP	JSP
Earl Buss Bayou	EBB
Payneway	P
Lake City	LC
Lester	L
RP Haynes	RP
Archway	AR

Microtremor Data Acquisition

Microtremor data were collected on a Guralp CMG-6TD, 3-component, broadband seismometer, borrowed from the Center for Earthquake and Research Information (CERI), Memphis, TN (Figure 6). These seismometers have a flat instrument response between 0.03 Hz and 50 Hz. The seismometer detects ground motion and outputs a signal representing ground velocity. A 12-volt marine battery was used to power the seismometer. A standard procedure for installing the seismometer was followed. Each seismometer was leveled and oriented north, placed in a plastic bag for protection, and then buried in an $\approx 30 \text{ cm} \times 45 \text{ cm}$ hole (Figure 7). Leveling and orienting the seismometer is required to achieve accurate recordings for each component, horizontal (north-south and east-west) and vertical; burying the seismometer reduces wind noise and provides a relatively constant temperature environment. Once positioned, the instrument was allowed to settle for 10 minutes, and data acquisition continued for an additional 20 minutes. Data were acquired using Guralp's data-recording software "SCREAM!"; this program allowed the data stream to be viewed on a laptop to ensure that a signal was being detected and recorded by the seismometer. A GPS receiver was used to identify the latitude-longitude of each site and to establish the timing and duration of each recording. Recordings were made at 200 samples per second. Longer recording times potentially increase the amount of useable data. The recorded data were stored on the seismometer and later transferred to storage media for future processing.

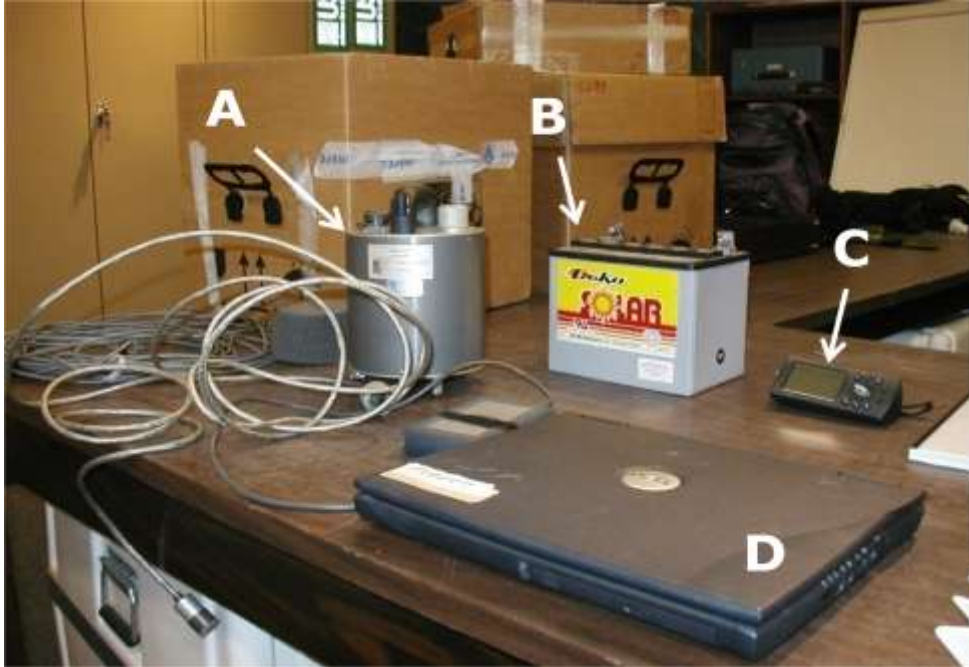


Figure 6. Components of the data acquisition system: (A) Guralp CMG-6TD seismometer, (B) battery, (C) GPS unit, and (D) laptop.

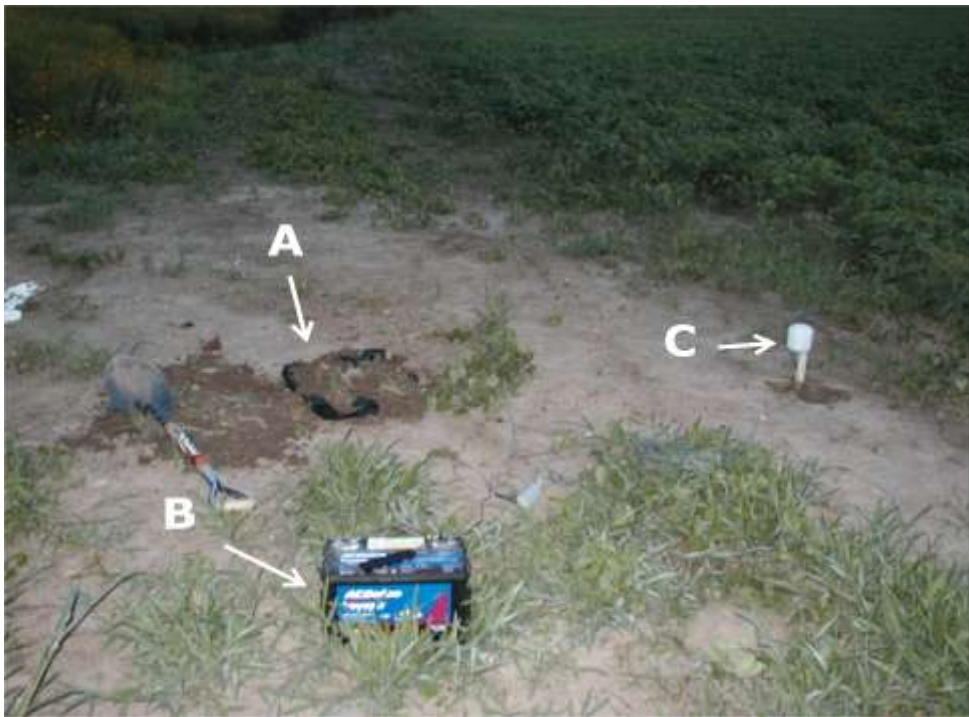


Figure 7. Microtremor recording set-up: (A) buried seismometer, (B) power source, (C) GPS antenna.

Supporting Data Acquisition

In addition to microtremor data, supporting data such as seismic, stratigraphic, well-log and geotechnical information were collected for the study. Supporting data are used to help constrain site characteristics. Sources of information consisted of published data sets and personal communications (Table 2). Seismic, stratigraphic, and well-log data were used to determine depth and thickness of major stratigraphic units within the embayment. Lithologic and geotechnical data were used to characterize the shallow subsurface lithologies, structures, and liquefaction potential.

Table 2. Data type and sources.

Data Type	Data Source
Embayment thickness	Saucier (1994); Stearns (1982); Van Arsdale and TenBrink (2000)
Shear-wave velocity	Romero and Rix (2001); Personal communication (Rix, 2006)
Geotechnical	Obermeier (1989); Schneider and Mayne (1998)
Well-log	Personal communication (Ausbrooks, 2006; Hoyal, 2006; Seimens, 2006)
Seismic hazard	Personal communication (Blake, 2006)

Data Processing

Microtremor Analysis

Recordings from each site were examined for data transients and artifacts. A basic assumption of the method is that noise sources are azimuthally distributed around the recording site. A strong or loud noise close to the seismometer, such as a car door slamming or a running water pump, would constitute a data artifact and make that recorded time segment undesirable (Figure 8).

Clean time segments (260 s to 845 s) from each recording were then extracted for spectral analysis. Each time-series was transformed using the MATLAB™ power-spectral density function (PSD) to produce a power spectrum for calculating the HVPSR (Equation 4) for a given site (Figure 9). Spectra are plotted as relative power, or amplitude², versus frequency. Data were demeaned and tapered and then processed using Hanning windows of 16384, 8192, 4096, 2048, 1024, or 512 points in length, overlapping by half the window length. A window length of 16384 samples (~82 s) and 1024 samples (~5 s) were applied to deep and shallow stratigraphic units, respectively. Smaller window lengths resolved higher frequency components in the spectra. The fundamental periods, T , found in the HVPSR share a relationship with sediment thickness, H , and shear-wave velocity, V_s , as expressed in the quarter-wavelength equation,

$$T = \frac{4}{V_s} * H \quad (5)$$

The fundamental period observed in the H/V ratio can be used to relate the period to a particular depth or stratigraphic boundary, assuming an average shear-wave, or to determine an average shear-wave velocity for a given depth interval.

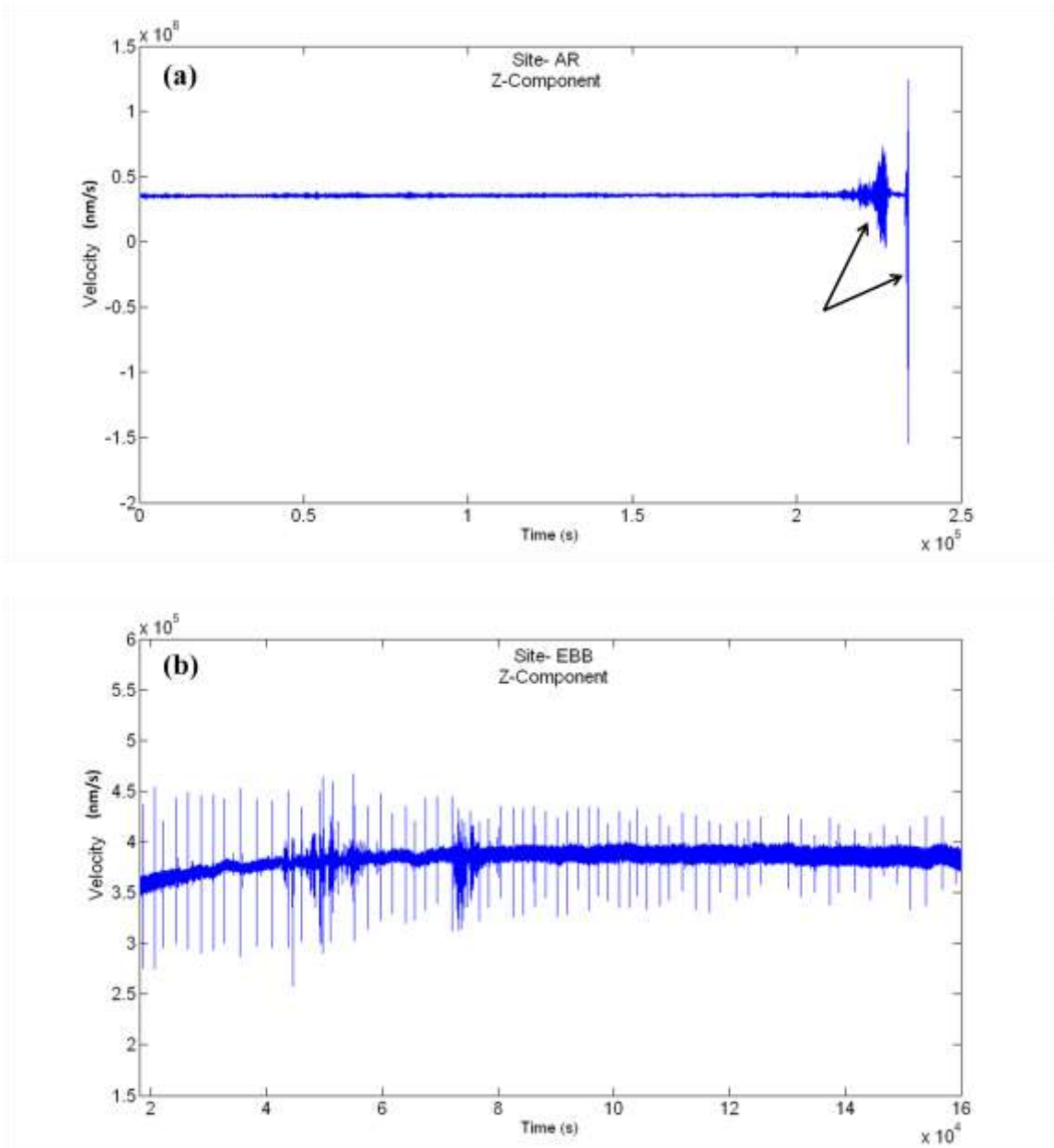


Figure 8. Recordings at two sites showing data transients. (a) Arrows indicate strong or loud noise that would not be selected in time segment for spectral analysis. (b) Time segment displaying cyclic noise (spikes) caused by unnatural source, making the record undesirable for spectral analysis.

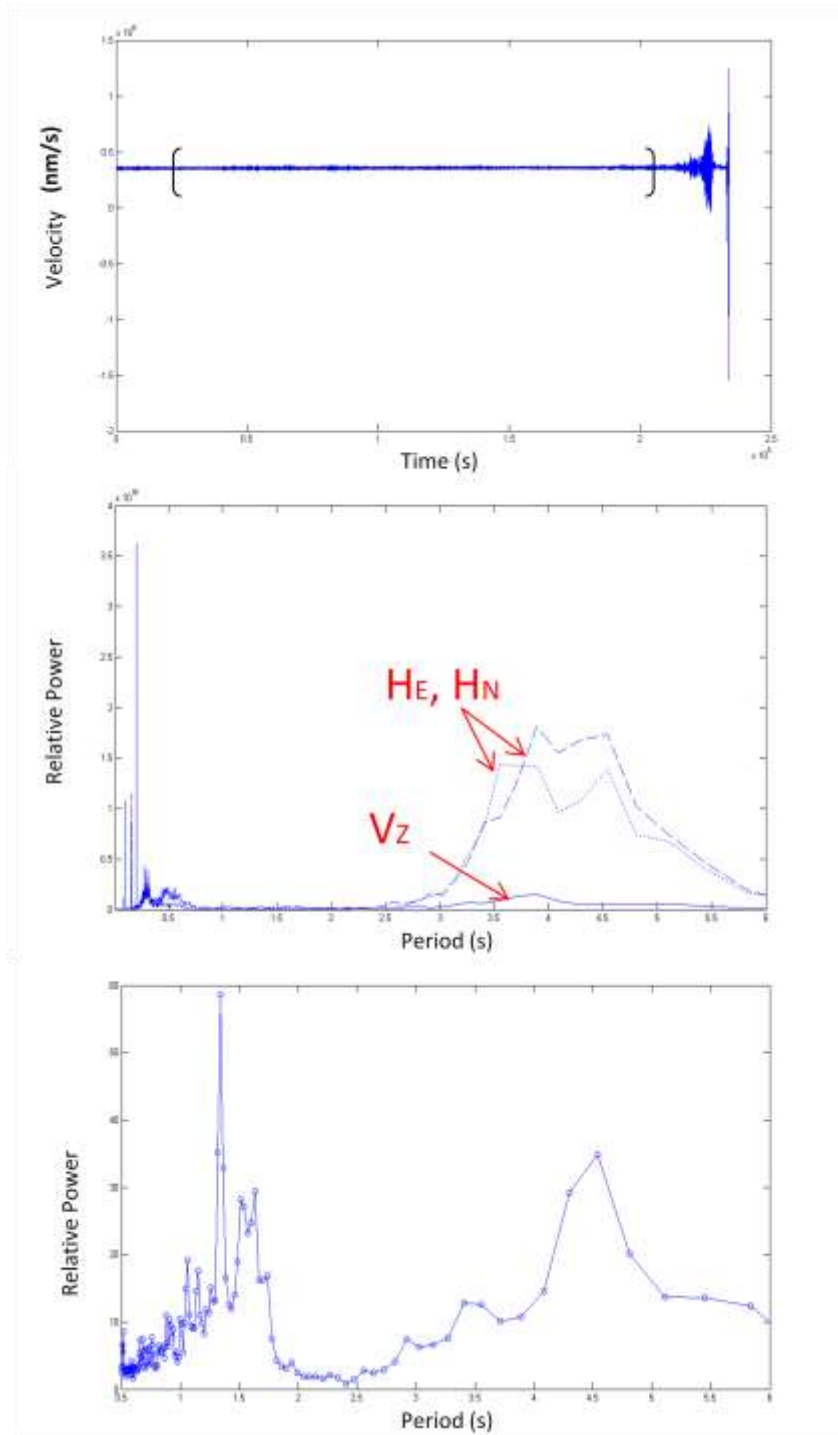


Figure 9. (a) Clean time segment (brackets) selected from raw data. (b) Computed power spectra for each wave component, horizontal (H_E , H_N) and vertical (V_Z). (c) Calculated H/V power spectral ratio showing resonant peaks.

Supporting Data Analysis

Collected seismic and stratigraphic data consist of contour and isopach maps of depth to embayment units and thickness of embayment units, respectively. Contour and isopach maps were uploaded in ArcMap™ and referenced with their respective geographic coordinate system. Once the maps were georeferenced, the locations of the microtremor sites were overlain by using their latitude-longitude coordinates. This process allowed the depth to, and thickness of, embayment units to be determined for each microtremor location.

Well-log and geotechnical data consist of descriptions of lithology and thickness to depths of ≤ 100 m and ≤ 20 m, respectively. Geotechnical data also include information on tip resistance, sleeve friction, pore pressure, and horizontal shear-wave velocity corresponding to specific depth intervals. This information allows the correlation of geotechnical parameters with lithology.

Latitude-longitude coordinates of well-log, geotechnical, and microtremor locations were entered and saved as a database in Microsoft Excel© and uploaded into ArcMap™. Once all the sites were displayed in ArcMap™, a buffer zone ranging from one to five kilometers was applied around each microtremor site and used to determine which well-log and geotechnical locations would be useful for interpreting the acquired microtremor data (Figure 10). Well-log and geotechnical sites within the buffer zone were analyzed first, and chosen to be a good representation of the microtremor site because of its spatial proximity. If a well-log or geotechnical site was not located within the buffer zone, the closest well-log or geotechnical sites were selected. Both well-log and geotechnical information provide valuable insight into the physical properties of

near-surface sediments and are useful in assessing the sediment response to earthquake ground motions.

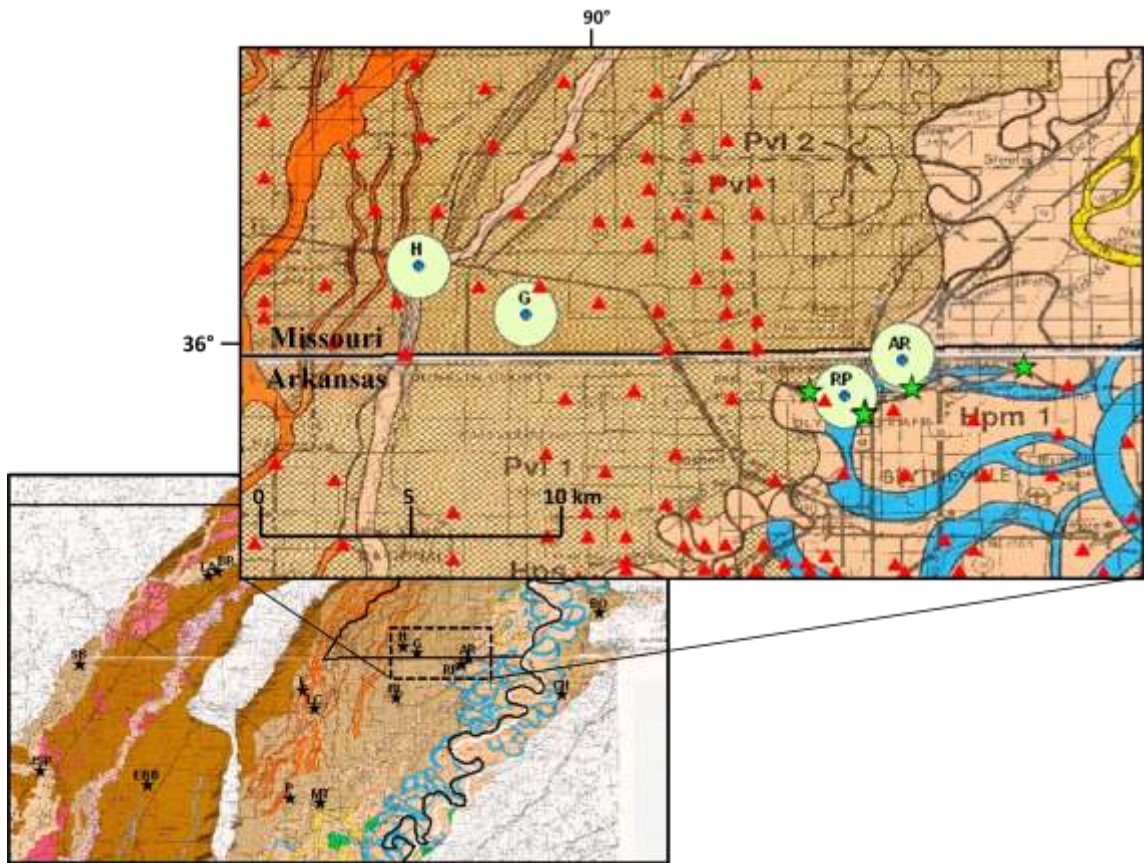


Figure 10. Selected microtremor sites (blue dots and name abbreviation from Table 1) with a 2-km buffer zone applied (light green circles) (Saucier, 1994b). Geotechnical data (green stars) and well-log data (red triangles) are added to determine which data could be useful in the microtremor analysis. See Table 1 for complete names of site locations.

RESULTS

Of the 18 sites at which microtremor data were collected, only 15 sites could be used for further analysis. The 3 sites excluded from analysis displayed coherent noise in the recorded signal. Appendix B displays raw data for all 15 sites and the time segments chosen for analysis. Table 3 displays the length of each time segment in samples per second (sps), seconds, and minutes. The length in seconds is determined by taking the difference between the start and end times and dividing by the sampling rate, 200 sps.

Figures 11 through 21 show the HVPSRs for each site. Some sites had several resonant periods that are grouped into short, intermediate, and long ranges. Each figure indicates the site name and its period range. Table 4 presents the chosen period and grouping for each site, as observed from the HVPSR. Periods not observed for a grouping are indicated on the table.

Other NMSZ studies (for example, Bodin and Horton, 1999, and Smith, 2000) have associated the long period peaks range with the embayment-basement interface. Figure 22 plots the long-period peaks observed in this study against embayment thickness at each site. The data in this figure indicates increasing observed periods with increasing embayment thickness. Results from 14 sites indicate resonant periods of 0.8 s to 4.4 s for embayment thicknesses of 100 m to 900 m, respectively. A linear regression of these data points yields an average shear-wave velocity of ~ 800 m/s for embayment sediments.

Some studies have taken multiple microtremor recordings at a reference site to test the reproducibility of the result at that site (for example, Dravinski et al., 1992, and Smith, 2000). In this study, the HVPSR at a given site is compared to other sites in spatial proximity to determine and show the observations of peak frequency to be robust (Figure 23 and 24). Distance between two sites in each example range from 3 km to 9 km. The similarity in peak and waveform suggests that the microtremor recordings are applicable to locals within several kilometers of the investigate site.

Table 3. Length of time segments used in analysis (samples per second, seconds, and minutes) for each site determined by the difference between the start and end times.

Site	Start	End	Length (sps)	Length (sec)	Length (min)
Shirley Bay	84000	250000	166000	830	14
Lake Ashbaugh	52220	176400	124180	621	10
Black River	247500	310300	62800	314	5
Payneway	112700	181100	68400	342	6
Lester	186400	308000	121600	608	10
Lake City	152200	290000	137800	689	11
Marked Tree	141400	303500	162100	811	14
Big Lake	88000	140000	52000	260	4
Hornersville	98450	147000	48550	243	4
Gilbert	150000	230000	80000	400	7
RP Haynes	146400	249500	103100	516	9
Archway	10000	179000	169000	845	14
Chickasaw	140500	200600	60100	301	5
Bogota	164700	215100	50400	252	4
Reelfoot	187500	335300	147800	739	12

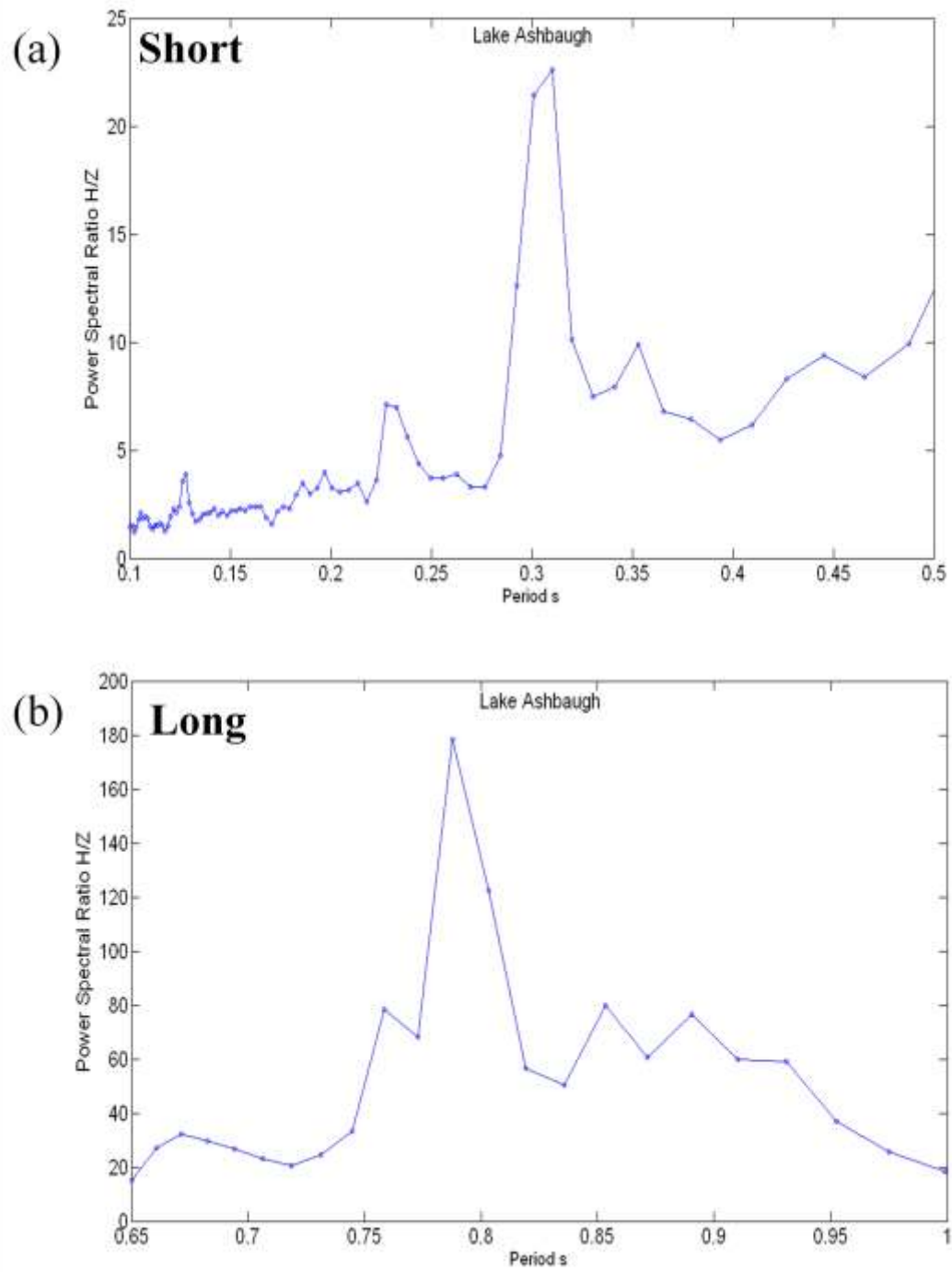


Figure 11. HVPSR at site Lake Ashbaugh with (a) short and (b) long periods observed.

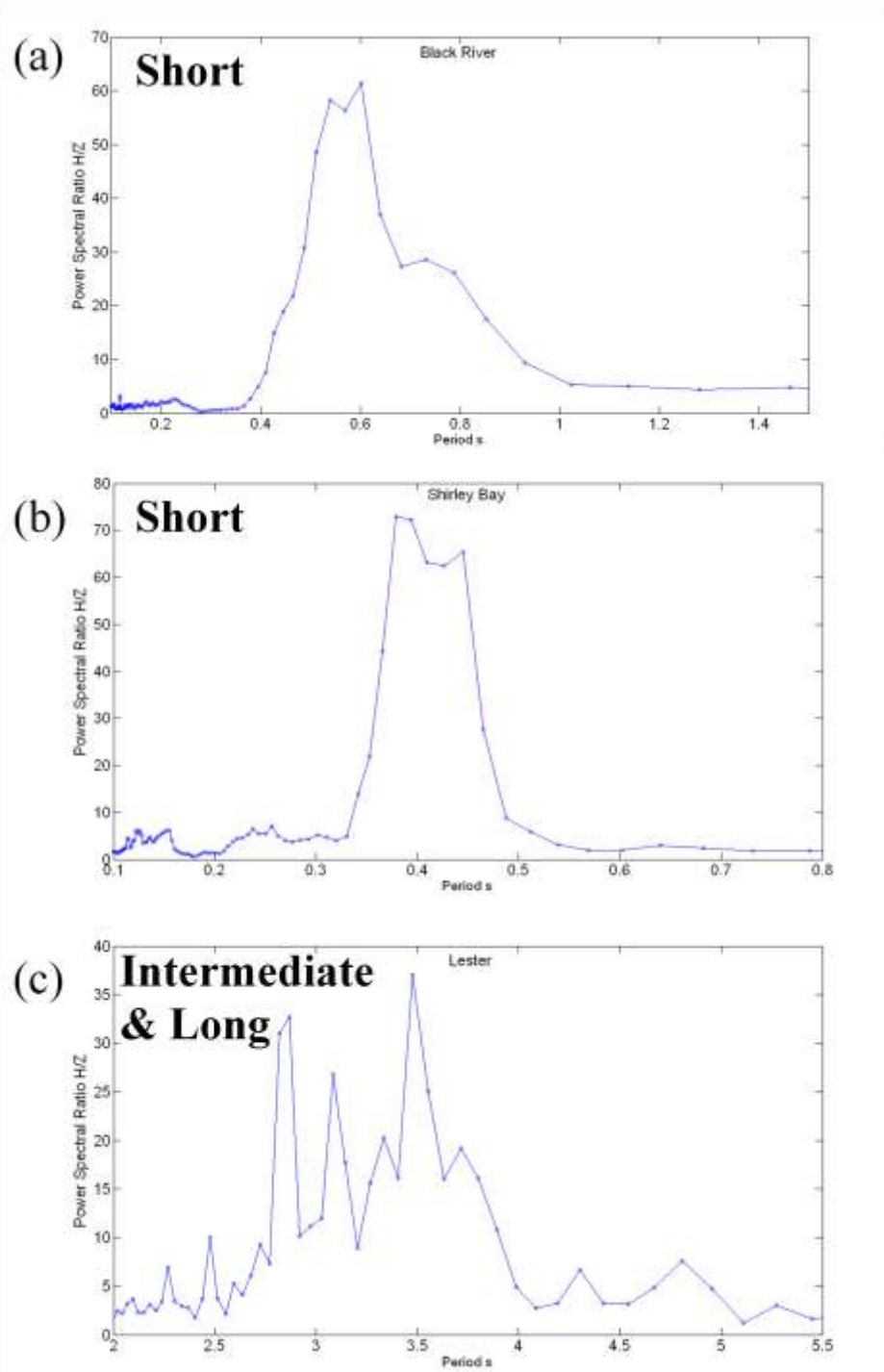


Figure 12. HVPSR at sites (a) Black River, (b) Shirley Bay, and (c) Lester. Short periods are observed at Black River and Shirley Bay, and intermediate and long periods at Lester.

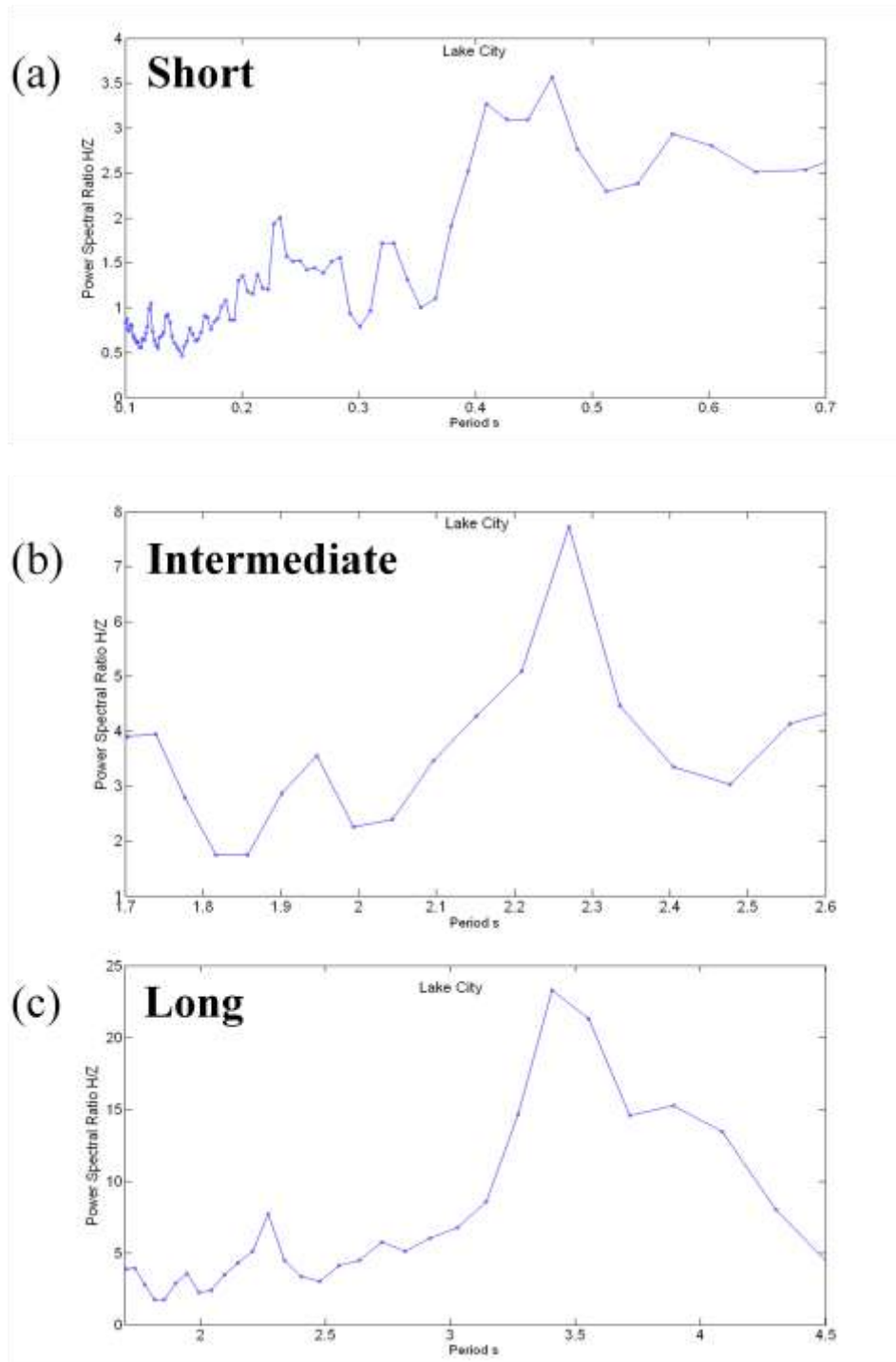


Figure 13. HVPSR at site Lake City with (a) short, (b) intermediate, and (c) long periods observed.

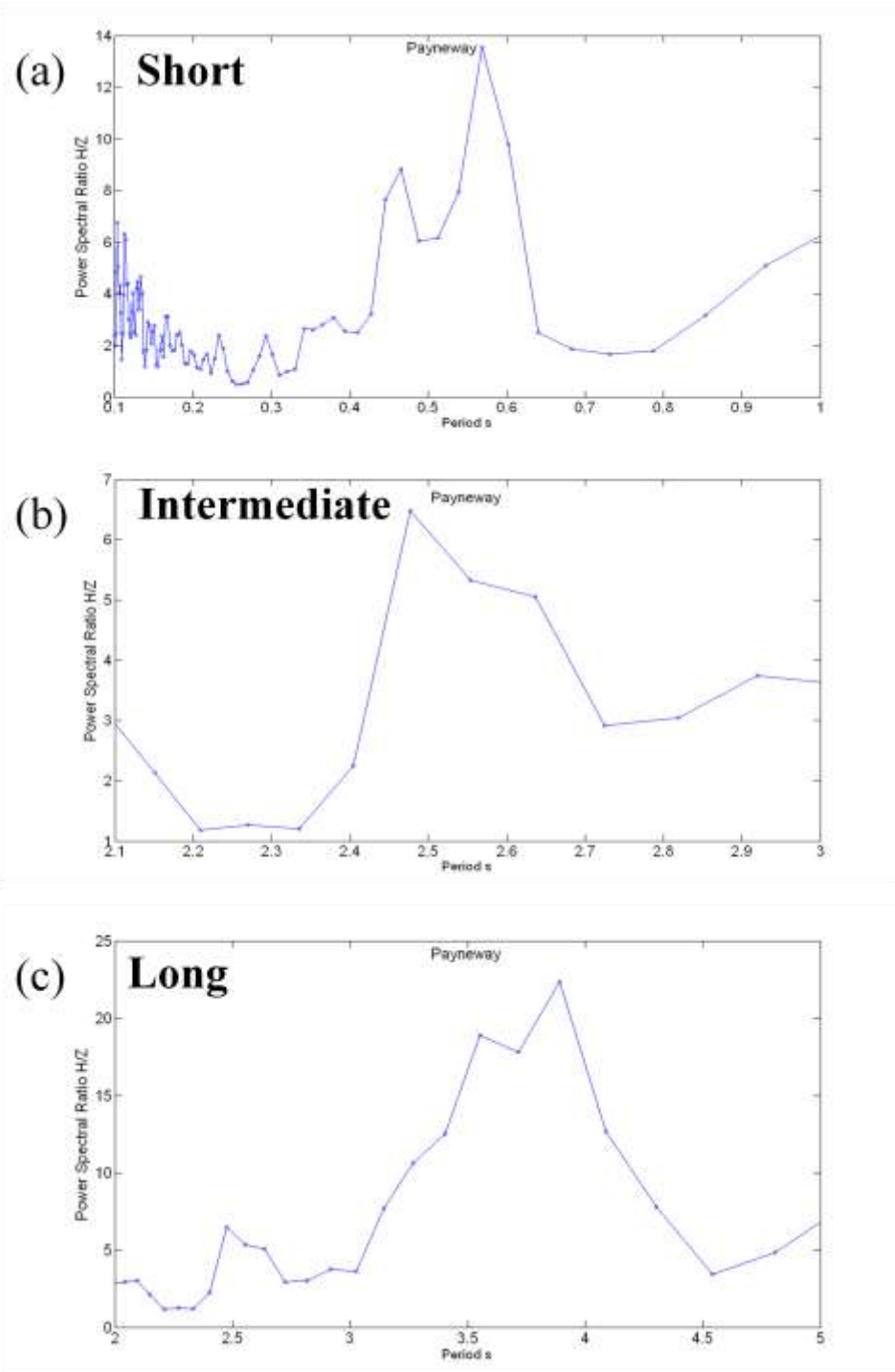


Figure 14. HVPSR at site Payneway with (a) short, (b) intermediate, and (c) long periods observed.

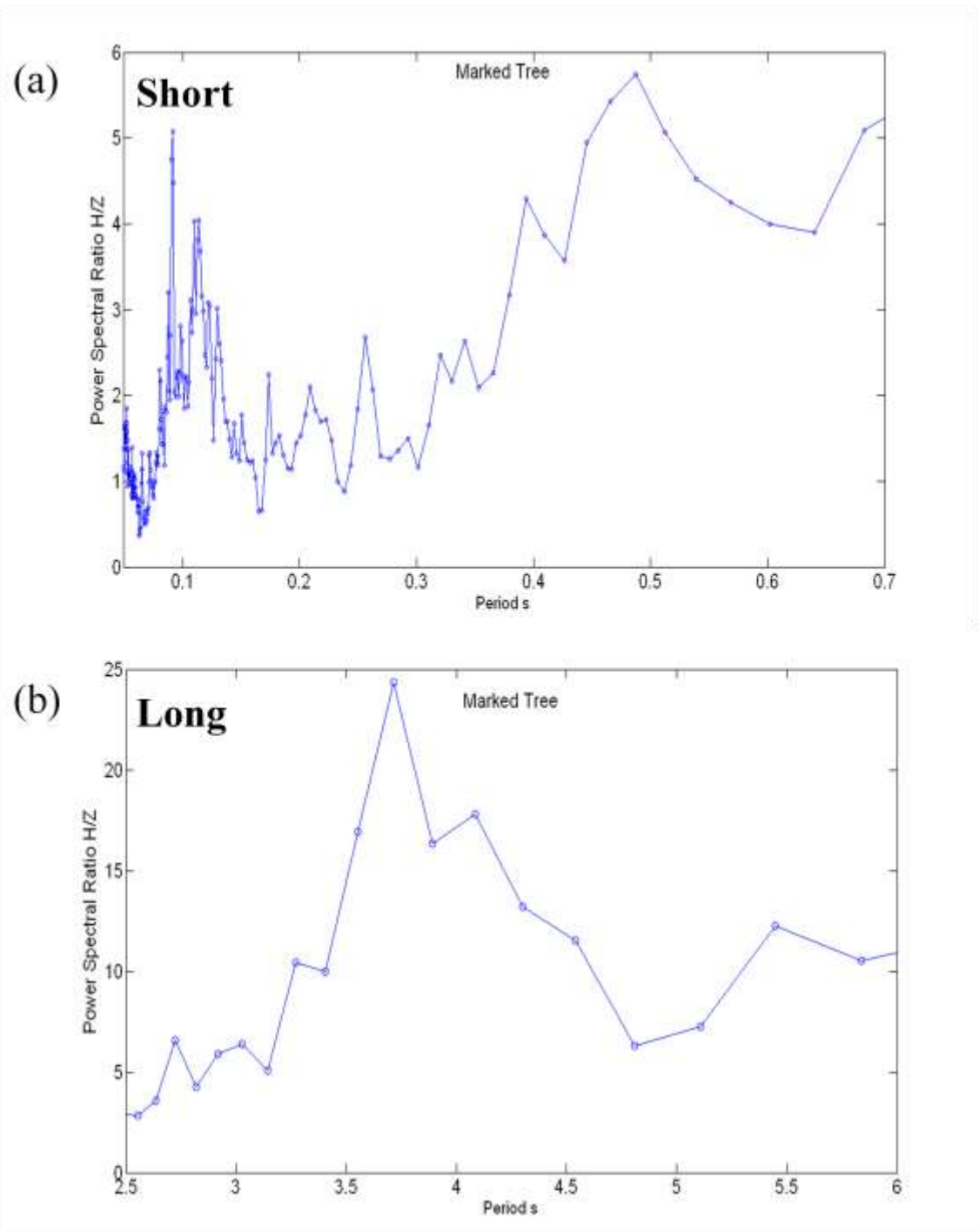


Figure 15. HVPSR at site Marked Tree with (a) short and (b) long periods observed.

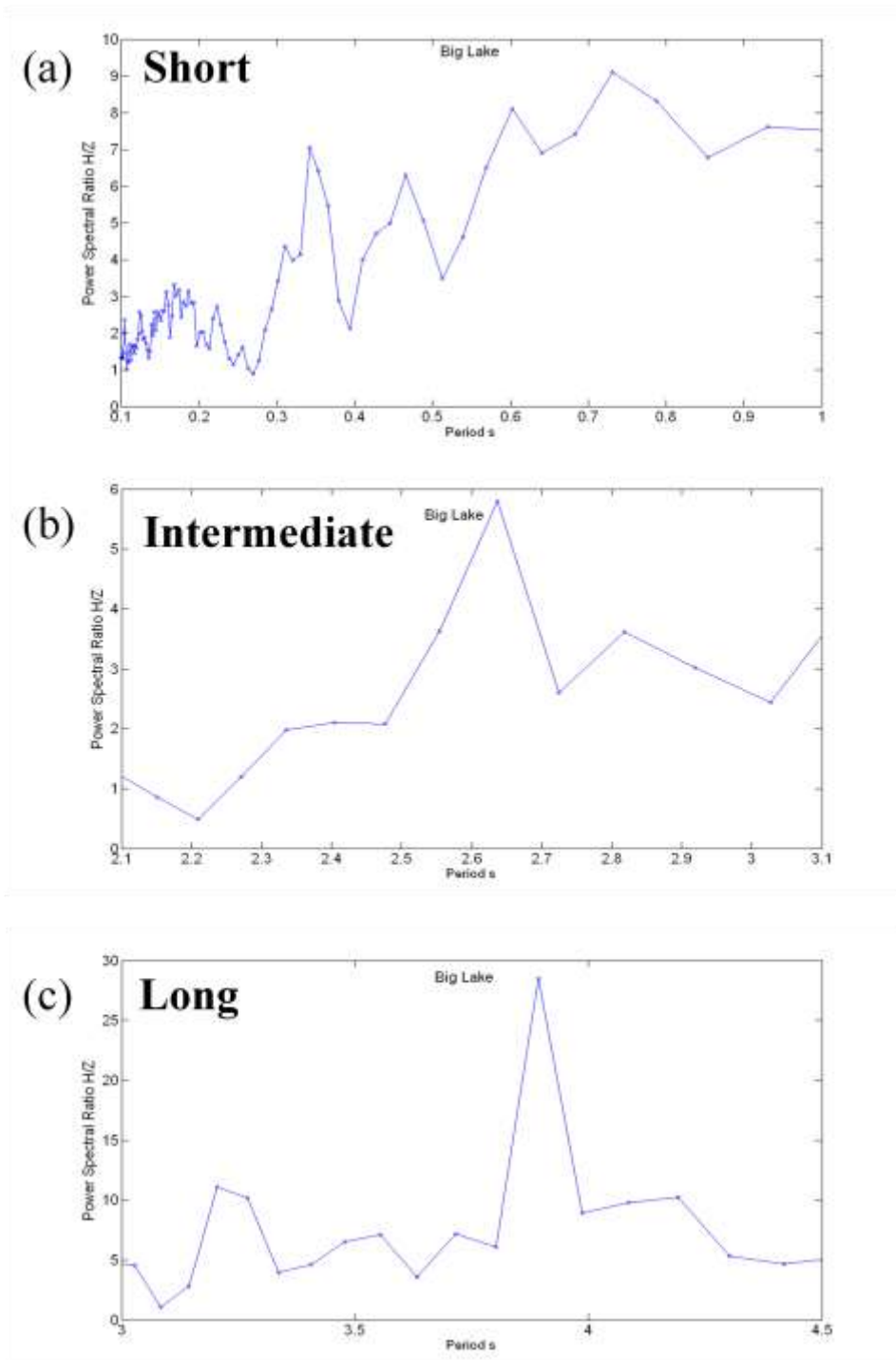


Figure 16. HVPSR at site Big Lake with (a) short, (b) intermediate, and (c) long periods observed.

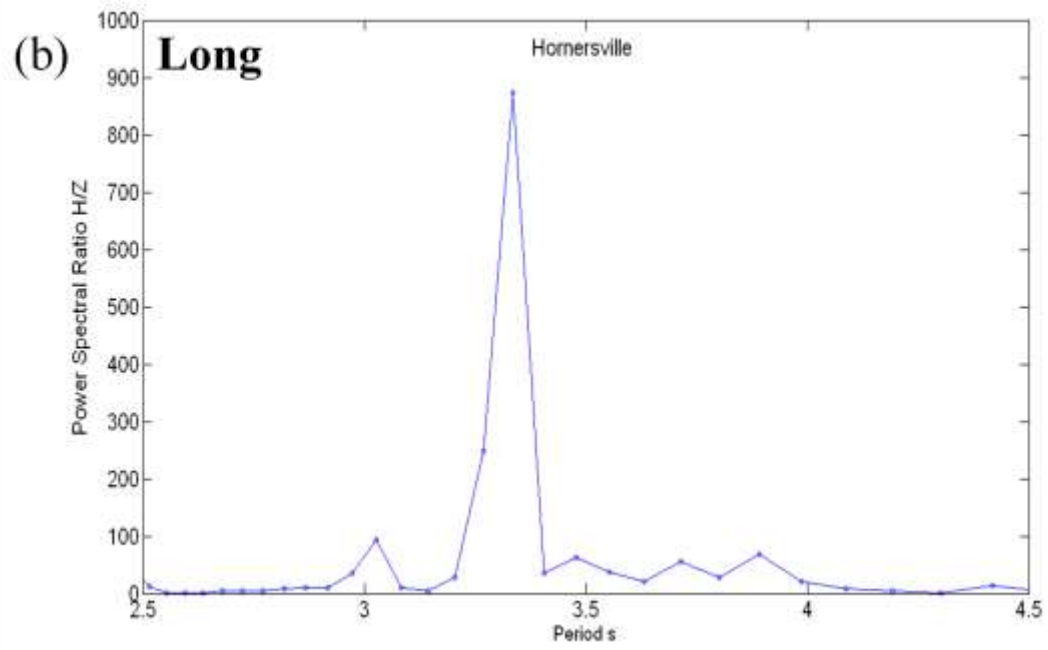
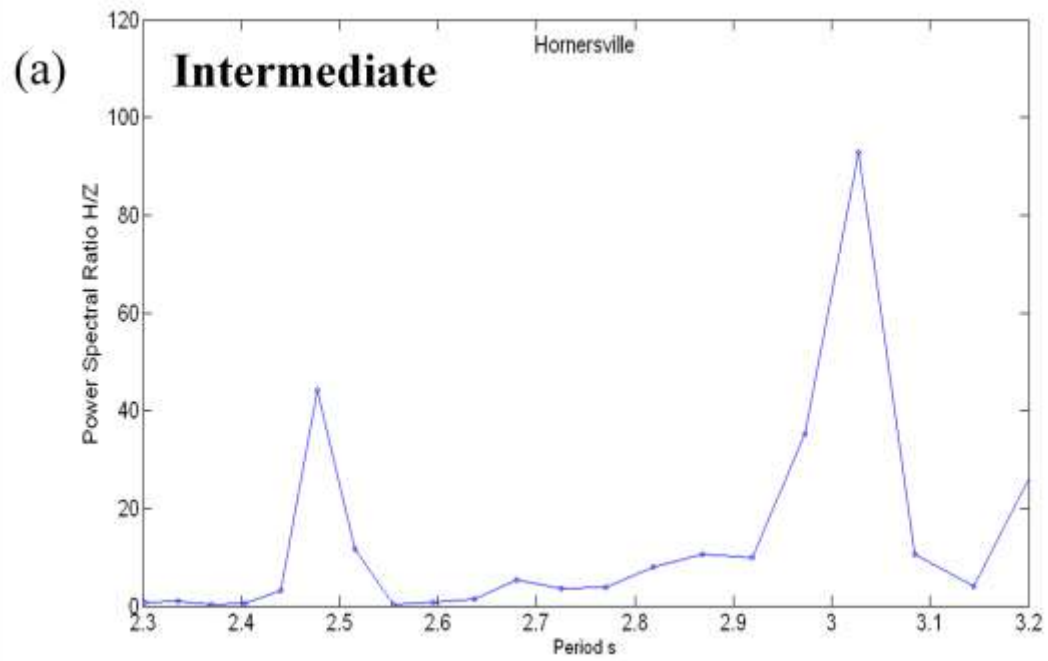


Figure 17. HVPSR at site Homersville with (a) intermediate and (b) long periods observed.

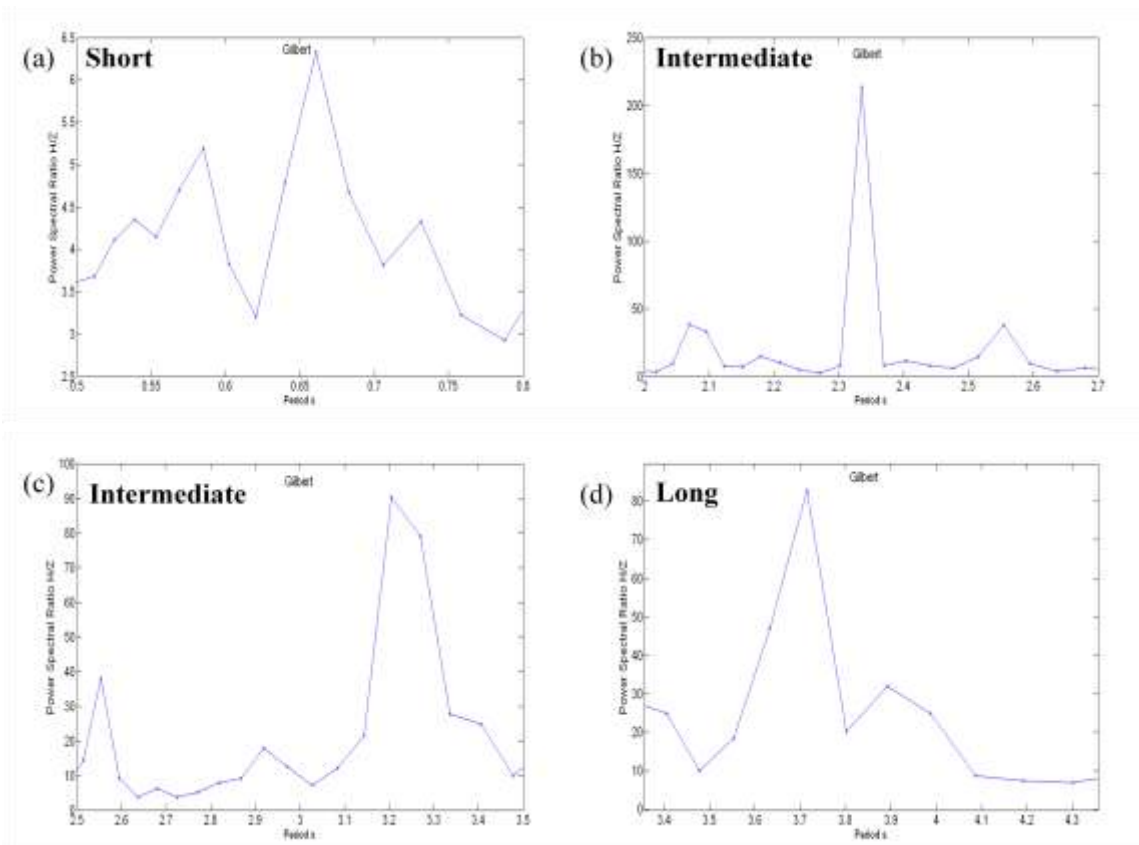


Figure 18. HVPSR at site Gilbert with (a) short, (b and c) intermediate, and (d) long periods observed.

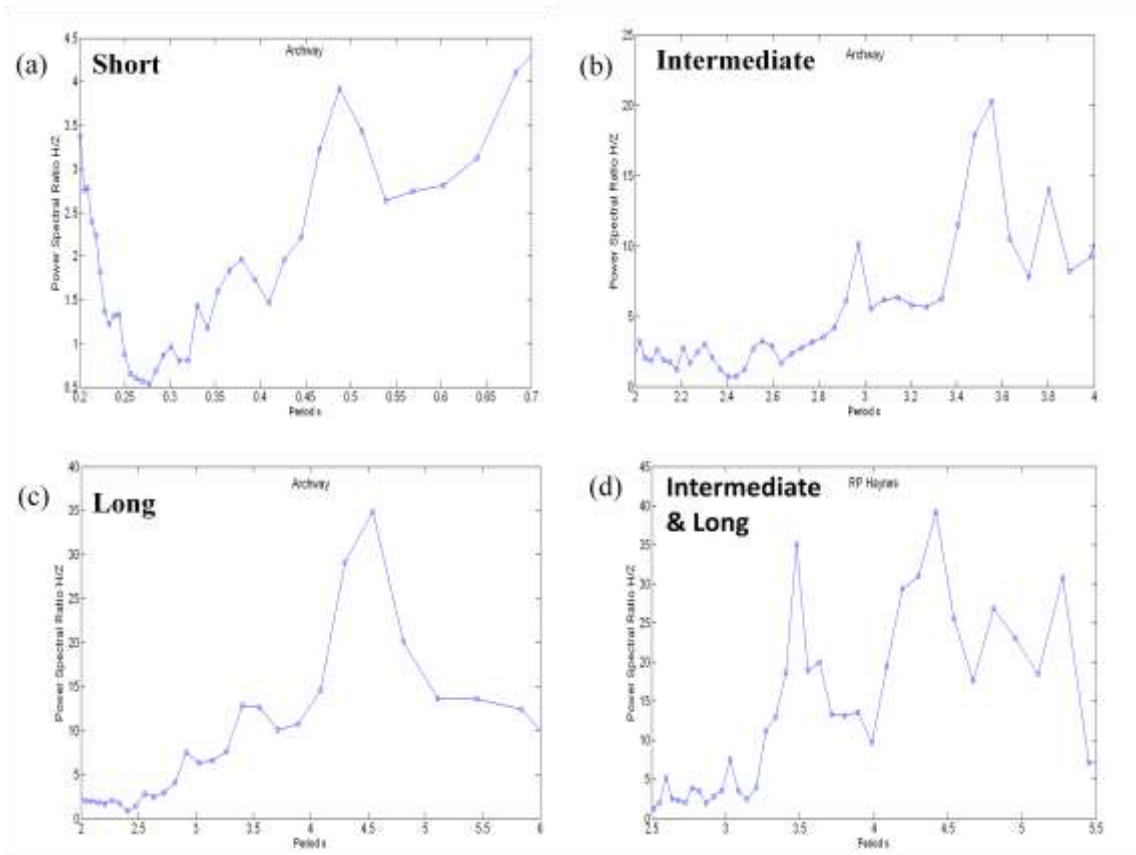


Figure 19. HVPSR at site Archway (a, b, c,) and R.P. Haynes (d) with short periods observed at Archway, and intermediate and long periods observed at both Archway and R. P. Haynes.

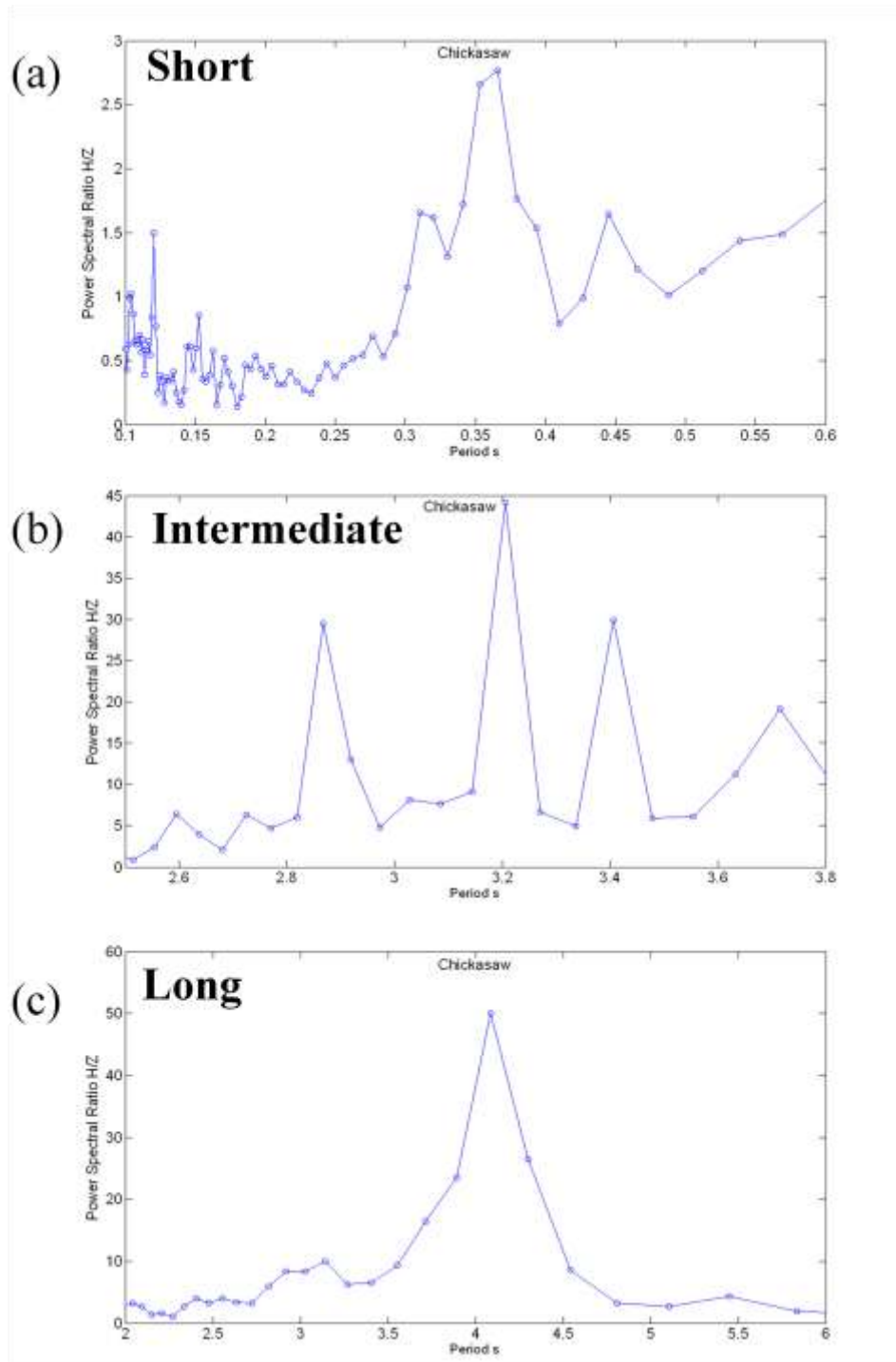


Figure 20. HVPSR at site Chickasaw with (a) short, (b) intermediate, and (c) long periods observed.

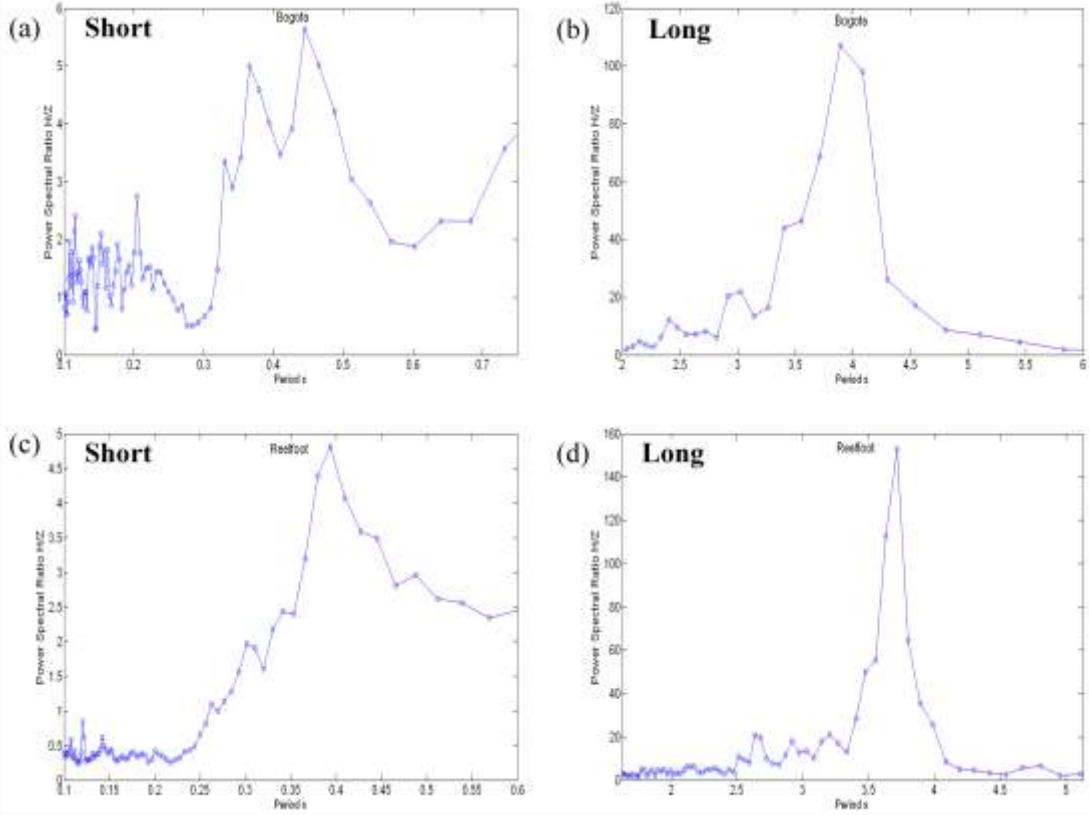


Figure 21. HVPSR at site Bogota (a and b) and Reelfoot (c and d) with short and long periods observed at both sites.

Table 4. Observed periods (T) seen in the HVPSR grouped into short, intermediate, and long period ranges. (-) indicates a period range not observed.

Site	Short Periods T (s)	Intermediate Periods T (s)	Long Periods T (s)
Shirley Bay	0.41	-	-
Lake Ashbaugh	0.31	-	0.79
Black River	0.55	-	0.6
Payneway	0.58	2.6	3.8
Lester	-	2.85	3.5
Lake City	0.55	2.2	3.4
Marked Tree	0.50	-	4.1
Big Lake	0.74	2.7	3.8
Hornersville	-	2.5, 3.0	3.4
Gilbert	0.62	2.3, 3.15	3.8
RP Haynes	-	3.55	4.3
Archway	0.49	3.0, 3.6	4.4
Chickasaw	0.35	2.8, 3.25	4.1
Bogota	0.45	3.1	3.85
Reelfoot	0.40	-	3.6

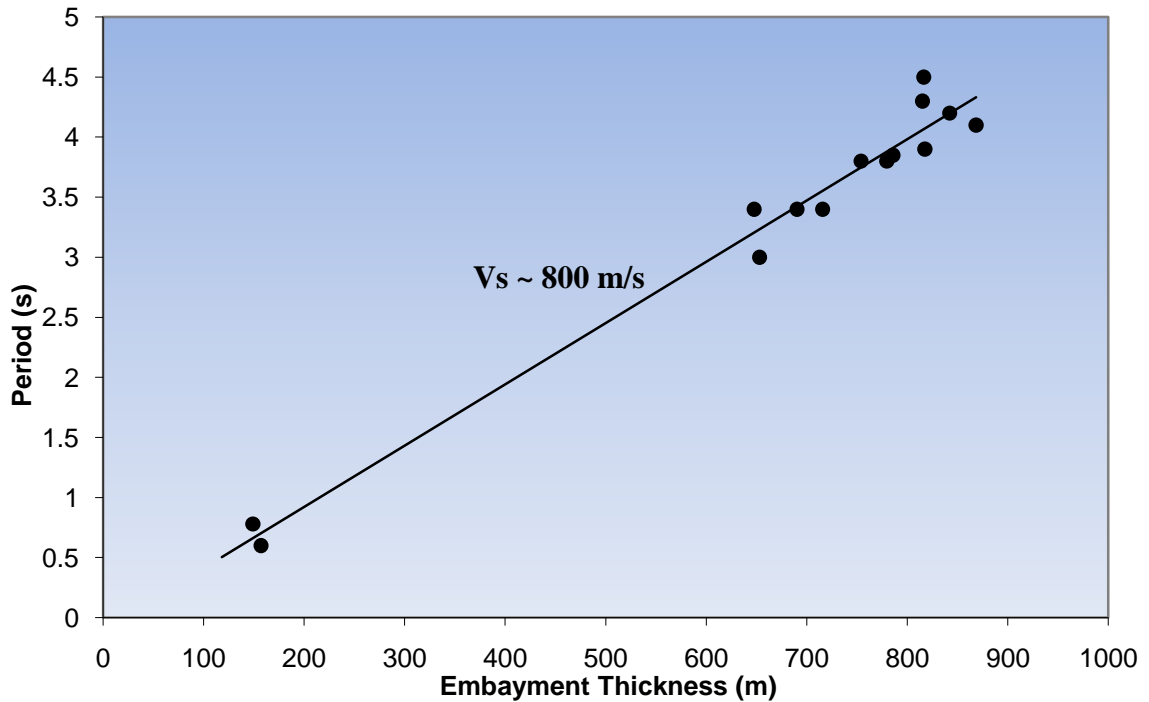


Figure 22. Long peak periods observed in HVPSR and respective embayment thickness at each site. Note an increase in period with increasing depth.

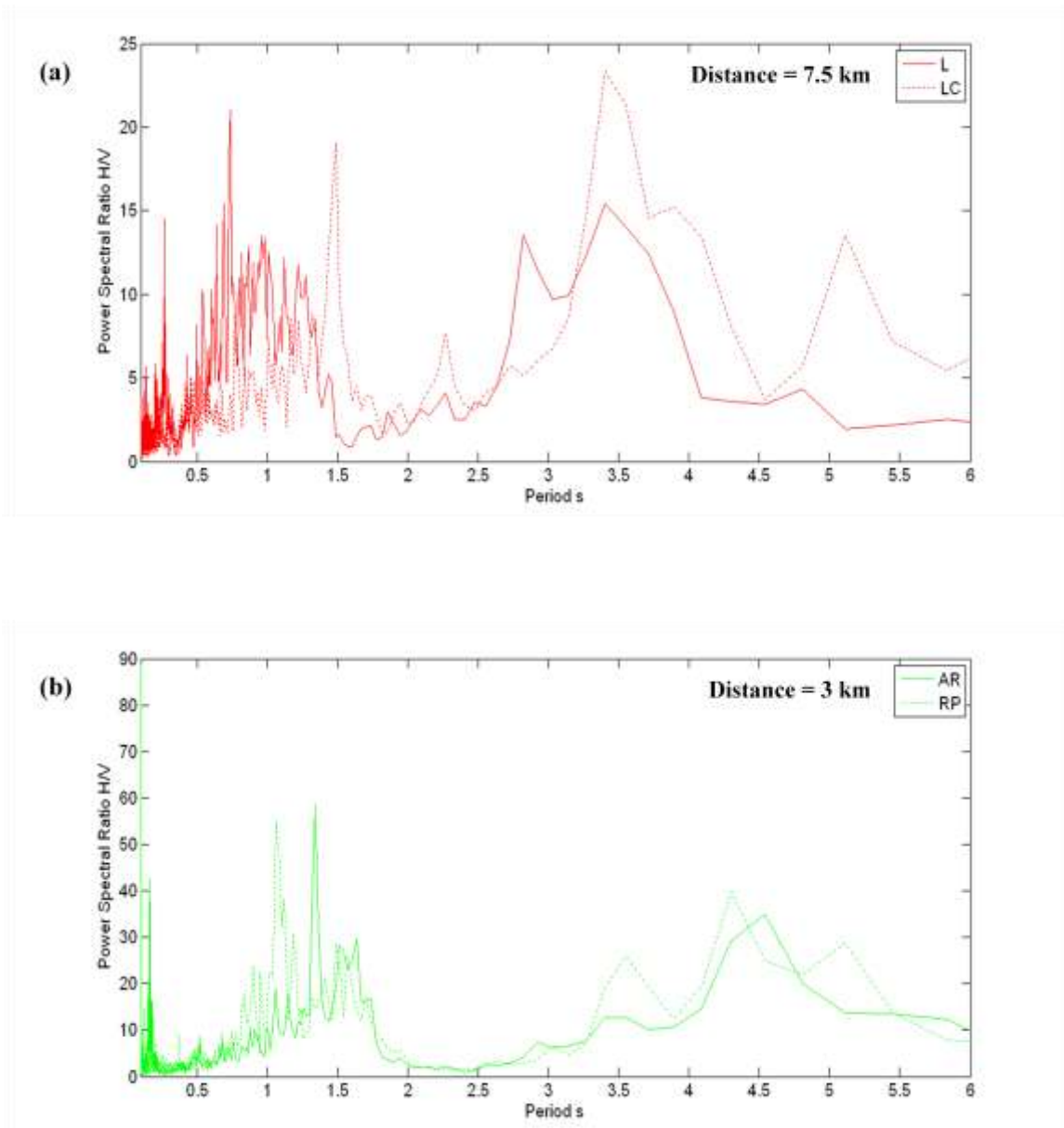


Figure 23. HVPSR comparison of sites (a) Lester and Lake City, and (b) Archway and R.P. Haynes. Compared sites have similar peaks and waveform characteristics. Distance between sites is given in kilometers. Colors indicate surface deposit type, braided stream (red) and meander (green).

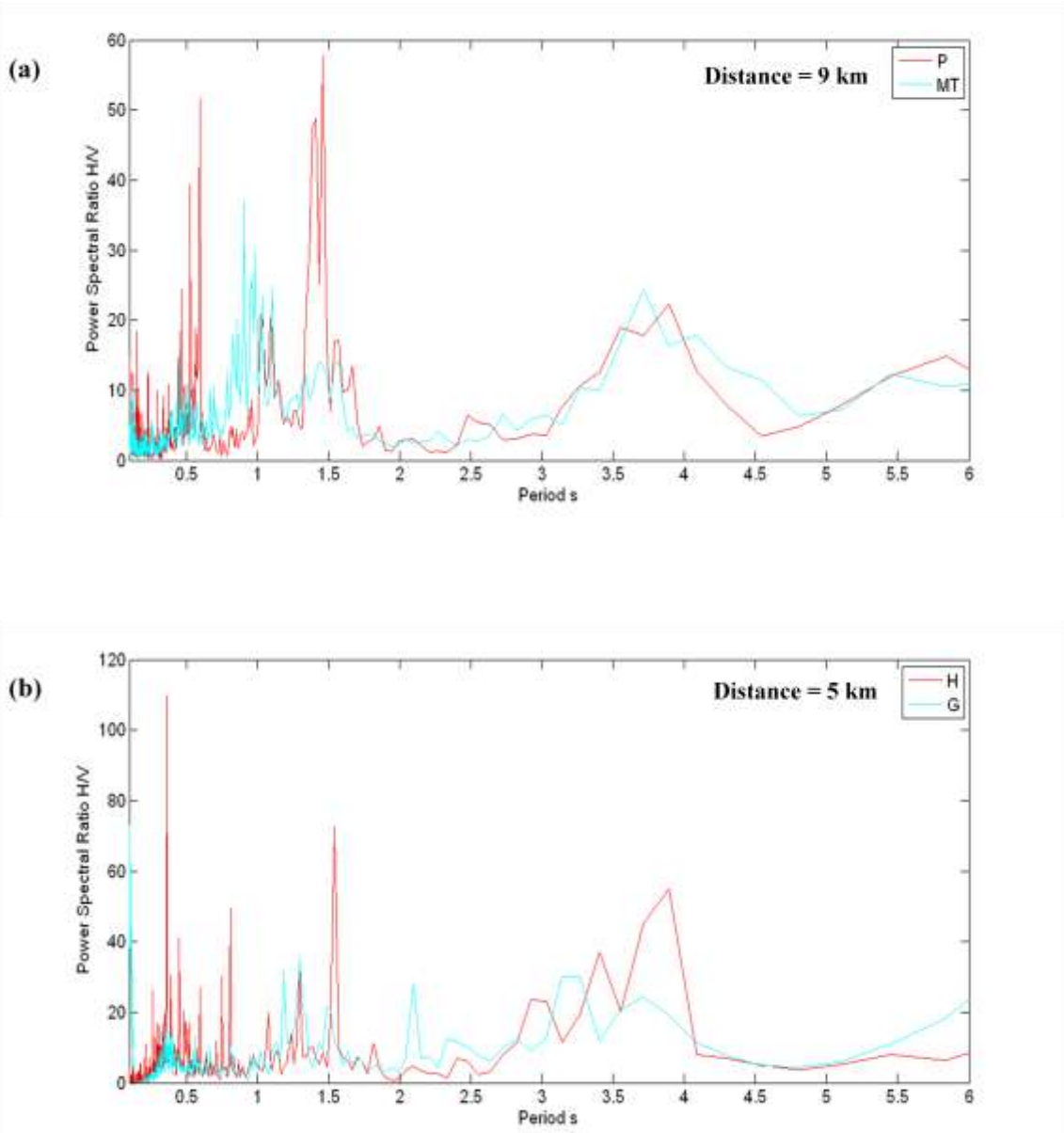


Figure 24. HVPSR comparison of sites (a) Payneway and Marked Tree, and (b) Hornersville and Gilbert. Compared sites have similar peaks and waveform characteristics. Distance between sites is given in kilometers. Colors indicate surface deposit type, braided stream (red) and transitional (cyan).

INTERPRETATION

Resonant Periods

For each of the four stratigraphic units in the study, observed peak frequencies are compared with predicted resonant frequencies. Here, five sites are selected from the data set to illustrate the procedures followed (Figure 25). The sites are Archway (AR), Black River (BR), Bogota (BO), Lake City (LC), and Reelfoot (RF). These sites represent a range of depths to the basement interface across the embayment from west to east (Figure 25b). Figure 25c contains the HVPSR for each of the five sites and documents resonant periods shifting to longer periods with increasing embayment thickness. Observed values for the peak periods shown in Figure 25c are compared with those predicted using equation 5. The total cumulative sediment thickness and average shear-wave velocity used in the calculations were taken from Table 5. Differences between the predicted and observed periods for each site range from 0.05 s to 0.19 s, or 10 m to 38 m, respectively (Figure 25a). Some peaks are broad and difficult to pick. Errors for determining the observed peak periods were estimated by taking the width at $2/3$ the maximum peak height (Figure 25c).

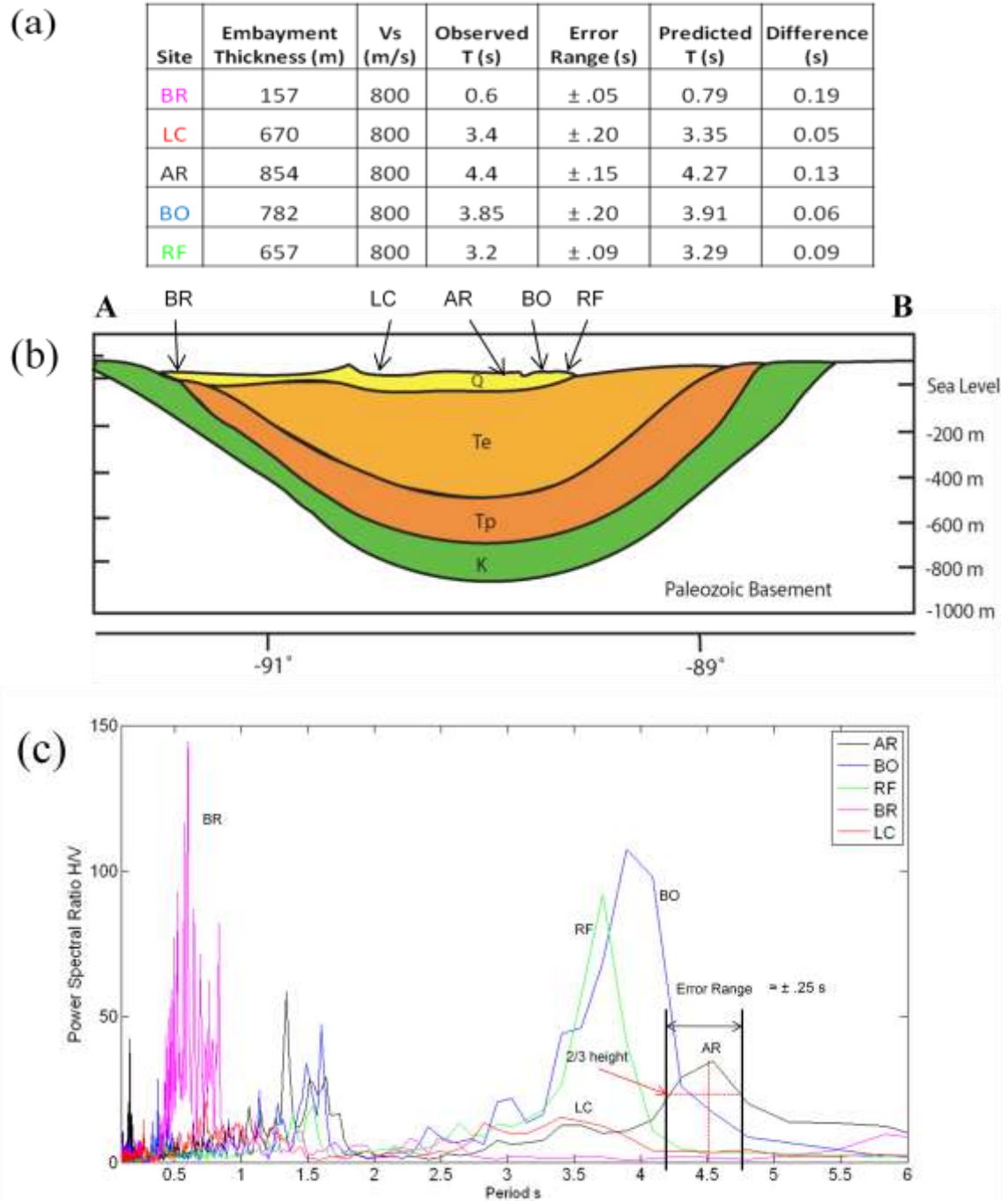


Figure 25. (a) Table listing five sites selected across the embayment and their predicted resonant periods as compared with observed periods. Predicted periods (T) are calculated by $T = 4H/V_s$, where H = embayment thickness and V_s = average shear-wave velocity. Errors associated with determining resonant periods are estimated as the width of peak taken at 2/3 peak height as shown in (c). (b) Cross-section through study area showing major stratigraphic units (see Figure 5 for locations), with sites indicated (Modified from Street et al., 2004). (c) H/V power spectral ratio of five selected sites. Note that peak shifts towards longer periods as embayment thickness increases.

In addition to large spectral peaks associated with the basement interface, small peaks in the HVPSR are also observed. These higher frequency peaks were compared with predicted peaks using thicknesses and shear-wave velocities illustrated in Tables 6 through 9. The difference between the predicted and observed periods is compared to the error range for each site. Figures 26 through 29 plot the calculated and observed periods at each site for each stratigraphic unit using the lower and upper end of shear-wave velocities for that unit. Not all sites have peaks for each of the four stratigraphic units. Where not observed, cells are marked (-) in Tables 6 through 9. The three lowland sites (Shirley Bay, Lake Ashbaugh, and Black River) do not indicate the presence of the Eocene or Paleocene stratigraphic units, and are therefore excluded from interpretation at these interfaces (indicated [n/a] in Tables 6 through 9).

Table 5. Parameters of grouped embayment units as used in this study.

	Unit Thickness (m)	Cumulative Thickness (m)	Source (Thickness data)	Vs (m/s)	Source (Velocity data)
Quaternary	33-61	33-61	Saucier (1994b)	275-325	Romero and Rix (2001)
Eocene	235-450	275-496	Van Arsdale and TenBrink (2000)	600-650	Romero and Rix (2001)
Paleocene	150-250	470-721	Van Arsdale and TenBrink (2000)	700-750	Romero and Rix (2001)
Cretaceous	95-200	605-886	Van Arsdale and TenBrink, (2000)	800-850	Romero and Rix (2001)

Peaks associated with the interfaces between the four stratigraphic units are attributed to significant impedance contrasts at these boundaries. A higher impedance contrast results in a higher percentage of energy being reflected back into the basin, amplifying ground motion. Using the predominant rock type for each stratigraphic unit (Figure 2) and Zoeppritz equation (Reynolds, 2003), the average density and velocity associated with that rock type was used to calculate impedance contrast at each interface (Tables 10 and 11).

Table 6 and Figure 26 show very good agreement between predicted and observed resonant periods for the Cretaceous-Paleozoic boundary, suggesting that these peaks are associated with the embayment-basement interface. The Cretaceous-Paleozoic boundary has a higher average impedance contrast than overlying sediments. 14 of 15 sites have similar predicted and observed resonant period values. Based on observed data, the best fit average shear-wave velocity is 800 m/s (Figure 26a).

Good agreement between predicted and observed frequencies for the intermediate depth boundaries suggests that these peaks may be associated with major lithologic changes; 6 of 12 sites, and 8 of 12 sites have similar predicted and observed frequency values for the Paleocene and Eocene interfaces, respectively. Based on the observed data, the best fit average shear-wave velocity is 750 m/s and 650 m/s for the Paleocene-Cretaceous and Eocene-Paleocene interfaces, respectively (Figure 27b and 26b). The three lowland sites were excluded from the intermediate depth boundary investigations (Paleocene-Cretaceous and Eocene-Paleocene interfaces) because these stratigraphic boundaries are not mapped in the subsurface in this particular region of the embayment.

Table 6. Calculated versus observed periods for the entire embayment thickness (QEPK), or the Cretaceous-basement interface. Predicted periods were derived using equation 5 and the values for thickness and shear-wave velocities indicated (a) $V_s = 800$ m/s and (b) $V_s = 850$ m/s. Sites where no corresponding peaks were observed are indicated (-). Difference between predicted and observed periods, and the determined error range for observed periods are also indicated. Data are plotted in Figure 26.

(a)

Site	Thickness QEPK (m)	Vs (m/s)	Predicted T (s)	Observed T (s)	Difference (s)	Error Range (s)
SB	118	800	0.59	-	-	-
LA	149	800	0.75	0.75	0.01	±.09
BR	157	800	0.79	0.6	0.19	±.05
P	853	800	4.26	3.8	0.46	±.15
L	620	800	3.10	3.5	0.40	±.08
LC	670	800	3.35	3.4	0.05	±.20
MT	871	800	4.35	4.1	0.25	±.30
BL	778	800	3.89	3.8	0.09	±.04
H	714	800	3.57	3.4	0.17	±.04
G	753	800	3.76	3.8	0.04	±.06
RP	836	800	4.18	4.3	0.12	±.19
AR	854	800	4.27	4.4	0.13	±.15
CH	837	800	4.19	4.1	0.09	±.20
BO	782	800	3.91	3.85	0.06	±.20
RF	657	800	3.29	3.6	0.31	±.09

(b)

Site	Thickness QEPK (m)	Vs (m/s)	Predicted T (s)	Observed T (s)	Difference (s)	Error Range (s)
SB	118	850	0.56	-	-	-
LA	149	850	0.70	0.75	0.05	±.09
BR	157	850	0.74	0.6	0.14	±.05
P	853	850	4.01	3.8	0.21	±.15
L	620	850	2.92	3.5	0.58	±.08
LC	670	850	3.15	3.4	0.25	±.20
MT	871	850	4.10	4.1	0.00	±.30
BL	778	850	3.66	3.8	0.14	±.04
H	714	850	3.36	3.4	0.04	±.04
G	753	850	3.54	3.8	0.26	±.06
RP	836	850	3.94	4.3	0.36	±.19
AR	854	850	4.02	4.4	0.38	±.15
CH	837	850	3.94	4.1	0.16	±.20
BO	782	850	3.68	3.85	0.17	±.20
RF	657	850	3.09	3.6	0.51	±.09

Cretaceous

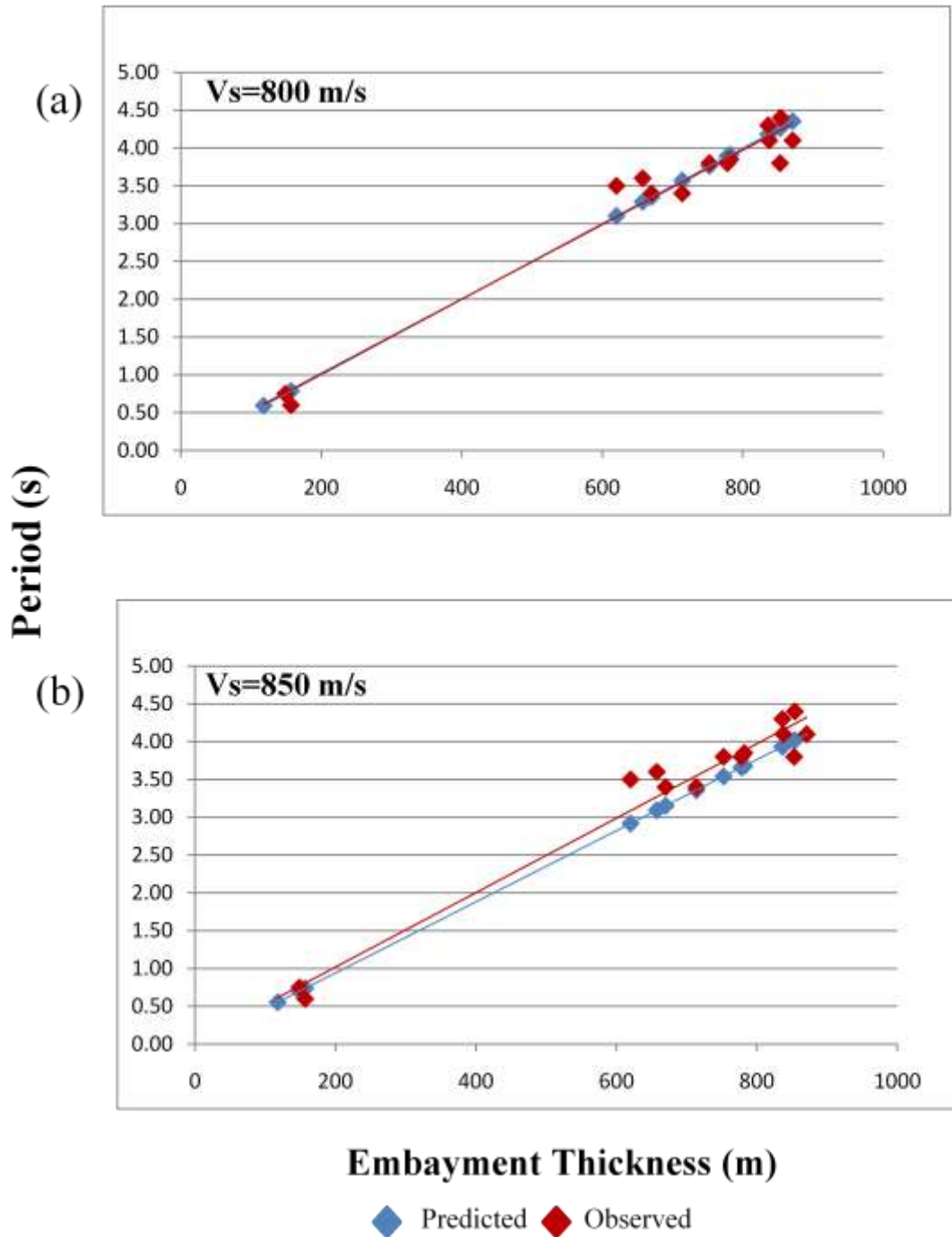


Figure 26. Comparison of observed (red) and predicted (blue) resonant periods associated with the Cretaceous-basement interface using (a) $V_s = 800 \text{ m/s}$ and (b) $V_s = 850 \text{ m/s}$. See Table 6. 14 of 15 sites have good agreement between observed and calculated periods, with the $V_s = 800 \text{ m/s}$ providing the best fit.

Table 7. Calculated versus observed periods for the Paleocene-Cretaceous interface (QEP). Predicted periods were derived using equation 5 and the values for thickness and shear-wave velocities indicated (a) $V_s = 700$ m/s and (b) $V_s = 750$ m/s. Three lowland sites (SB, LA, and BR) are excluded in this data set because this interface is not present (n/a). Sites where no corresponding peaks were observed are indicated (-). Difference between predicted and observed periods, and the determined error range for observed periods are also indicated. Data are plotted in Figure 27.

(a)

Site	Thickness QEP (m)	Vs (m/s)	Predicted T (s)	Observed T (s)	Difference (s)	Error Range (s)
SB	n/a	n/a	n/a	n/a	n/a	n/a
LA	n/a	n/a	n/a	n/a	n/a	n/a
BR	n/a	n/a	n/a	n/a	n/a	n/a
P	672	700	3.84	-	-	-
L	474	700	2.71	2.85	0.14	±.06
LC	538	700	3.07	-	-	-
MT	711	700	4.06	-	-	-
BL	645	700	3.68	-	-	-
H	567	700	3.24	3.00	0.24	±.03
G	560	700	3.20	3.15	0.05	±.06
RP	659	700	3.77	3.55	0.22	±.06
AR	684	700	3.91	3.60	0.31	±.10
CH	623	700	3.56	3.25	0.31	±.03
BO	665	700	3.80	-	-	-
RF	558	700	3.19	-	-	-

(b)

Site	Thickness QEP (m)	Vs (m/s)	Predicted T (s)	Observed T (s)	Difference (s)	Error Range (s)
SB	n/a	n/a	n/a	n/a	n/a	n/a
LA	n/a	n/a	n/a	n/a	n/a	n/a
BR	n/a	n/a	n/a	n/a	n/a	n/a
P	672	750	3.58	-	-	-
L	474	750	2.53	2.85	0.32	±.06
LC	538	750	2.87	-	-	-
MT	711	750	3.79	-	-	-
BL	645	750	3.44	-	-	-
H	567	750	3.02	3.00	0.02	±.03
G	560	750	2.99	3.15	0.16	±.06
RP	659	750	3.52	3.55	0.03	±.06
AR	684	750	3.65	3.60	0.05	±.10
CH	623	750	3.32	3.25	0.07	±.03
BO	665	750	3.55	-	-	-
RF	558	750	2.98	-	-	-

Paleocene

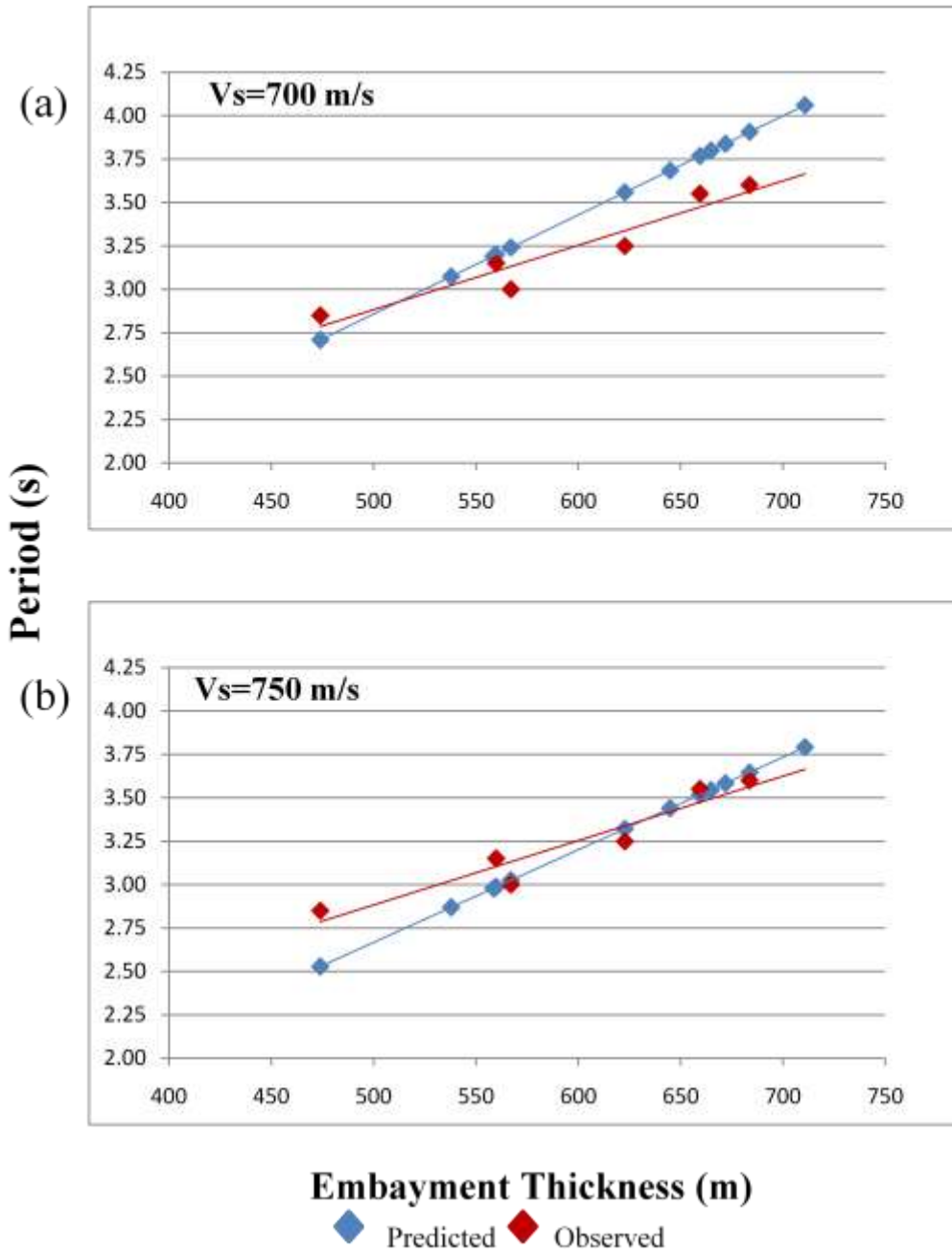


Figure 27. Comparison of observed (red) and predicted (blue) resonant periods associated with the Cretaceous-basement interface using (a) $V_s = 700$ m/s and (b) $V_s = 750$ m/s. See Table 7. 6 of 12 sites have good agreement between observed and calculated periods, with the $V_s = 750$ m/s providing the best fit.

Table 8. Calculated versus observed periods for Eocene-Paleocene interface (QE). Predicted periods were derived using equation 5 and the values for thickness and shear-wave velocities indicated (a) $V_s = 600$ m/s and (b) $V_s = 650$ m/s. Three lowland sites (SB, LA, and BR) are excluded in this data set because this interface is not present (n/a). Sites where no corresponding peaks were observed are indicated (-). Difference between predicted and observed periods, and the determined error range for observed periods are also indicated. Data are plotted in Figure 28.

(a)

Site	Thickness QE (m)	Vs (m/s)	Predicted T (s)	Observed T (s)	Difference (s)	Error Range (s)
SB	n/a	n/a	n/a	n/a	n/a	n/a
LA	n/a	n/a	n/a	n/a	n/a	n/a
BR	n/a	n/a	n/a	n/a	n/a	n/a
P	422	600	2.81	2.60	0.21	±.10
L	279	600	1.86	-	-	-
LC	318	600	2.12	2.20	0.08	±.05
MT	486	600	3.24	-	-	-
BL	410	600	2.73	2.70	0.03	±.06
H	402	600	2.68	2.50	0.18	±.04
G	375	600	2.50	2.30	0.20	±.02
RP	449	600	3.00	-	-	-
AR	464	600	3.09	3.00	0.09	±.04
CH	453	600	3.02	2.80	0.22	±.08
BO	495	600	3.30	3.10	0.20	±.06
RF	408	600	2.72	-	-	-

(b)

Site	Thickness QE (m)	Vs (m/s)	Predicted T (s)	Observed T (s)	Difference (s)	Error Range (s)
SB	n/a	n/a	n/a	n/a	n/a	n/a
LA	n/a	n/a	n/a	n/a	n/a	n/a
BR	n/a	n/a	n/a	n/a	n/a	n/a
P	422	650	2.60	2.60	0.00	±.10
L	279	650	1.72	-	-	-
LC	318	650	1.96	2.20	0.24	±.05
MT	486	650	2.99	-	-	-
BL	410	650	2.52	2.70	0.18	±.06
H	402	650	2.47	2.50	0.03	±.04
G	375	650	2.31	2.30	0.01	±.02
RP	449	650	2.77	-	-	-
AR	464	650	2.85	3.00	0.15	±.04
CH	453	650	2.79	2.80	0.01	±.08
BO	495	650	3.05	3.10	0.05	±.06
RF	408	650	2.51	-	-	-

Eocene

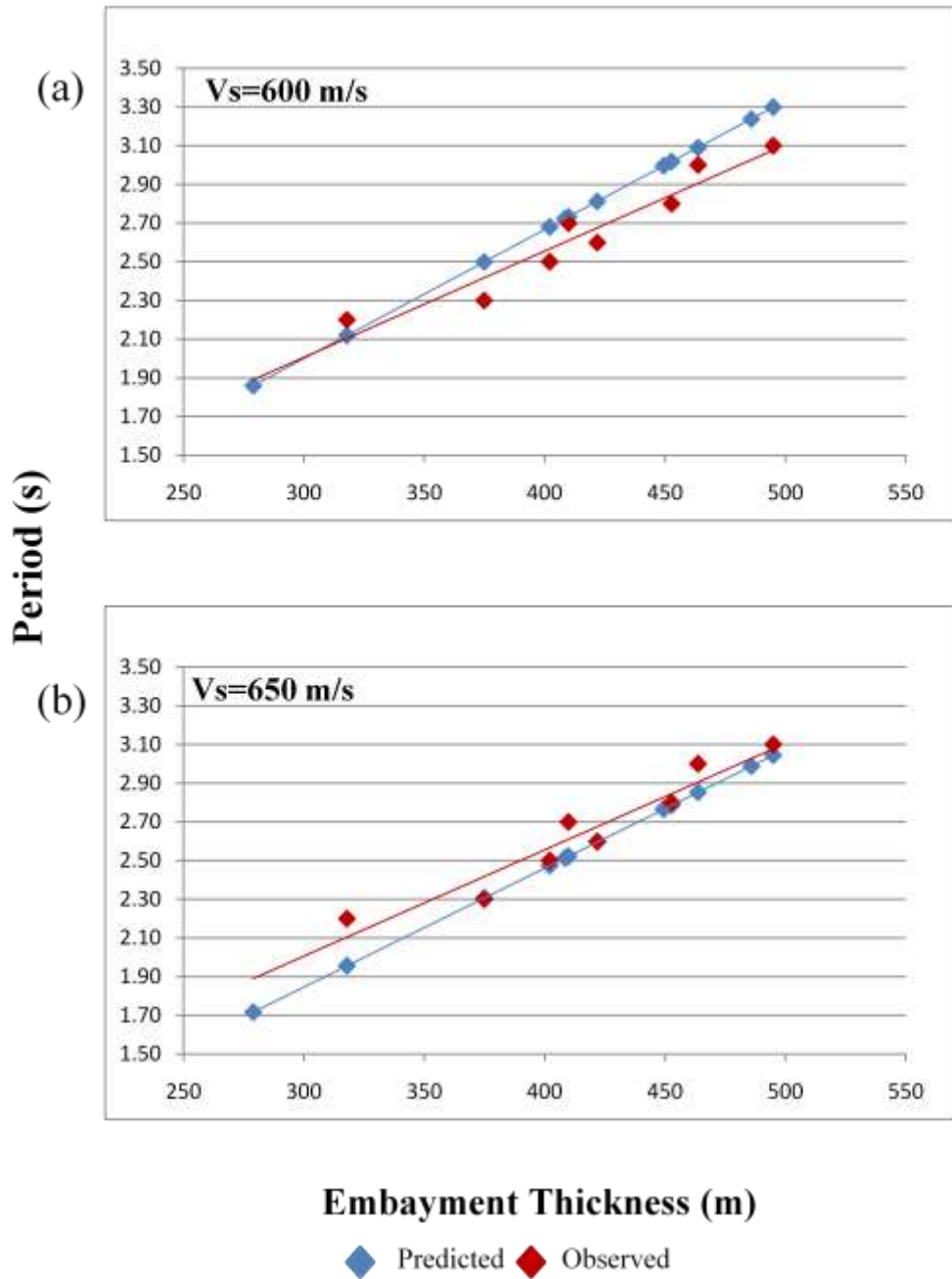


Figure 28. Comparison of observed (red) and predicted (blue) resonant periods associated with the Cretaceous-basement interface using (a) $V_s = 600$ m/s and (b) $V_s = 650$ m/s. See Table 8. 8 of 12 sites have good agreement between observed and calculated periods, with the $V_s = 650$ m/s providing the best fit.

Table 9. Calculated versus observed periods for the Quaternary-Eocene interface (Q). Predicted periods were derived using equation 5 and the values for thickness and shear-wave velocities indicated (a) $V_s = 275$ m/s and (b) $V_s = 325$ m/s. Sites where no corresponding peaks were observed are indicated (-). Difference between predicted and observed periods and the determined error range for observed periods are also indicated. Data are plotted in Figure 29.

(a)

Site	Thickness Q (m)	Vs (m/s)	Predicted T (s)	Observed T (s)	Difference (s)	Error Range (s)
SB	30	275	0.44	0.43	0.01	±.04
LA	33	275	0.48	0.31	0.17	±.01
BR	30	275	0.44	0.55	0.11	±.09
P	42	275	0.61	0.58	0.03	±.03
L	44	275	0.64	-	-	-
LC	48	275	0.70	0.55	0.15	±.06
MT	46	275	0.67	0.50	0.17	±.10
BL	45	275	0.65	0.74	0.09	±.07
H	52	275	0.76	-	-	-
G	45	275	0.65	0.62	0.03	±.07
RP	39	275	0.57	-	-	-
AR	44	275	0.63	0.49	0.14	±.04
CH	33	275	0.48	0.38	0.10	±.04
BO	45	275	0.65	0.45	0.20	±.04
RF	38	275	0.56	0.40	0.16	±.04

(b)

Site	Thickness Q (m)	Vs (m/s)	Predicted T (s)	Observed T (s)	Difference (s)	Error Range (s)
SB	30	325	0.37	0.43	0.06	±.04
LA	33	325	0.41	0.31	0.10	±.01
BR	30	325	0.37	0.55	0.18	±.09
P	42	325	0.51	0.58	0.07	±.03
L	44	325	0.54	-	-	-
LC	48	325	0.59	0.55	0.04	±.06
MT	46	325	0.56	0.50	0.06	±.10
BL	45	325	0.55	0.74	0.19	±.07
H	52	325	0.64	-	-	-
G	45	325	0.55	0.62	0.07	±.07
RP	39	325	0.48	-	-	-
AR	44	325	0.54	0.49	0.05	±.04
CH	33	325	0.41	0.38	0.03	±.04
BO	45	325	0.55	0.45	0.10	±.04
RF	38	325	0.47	0.40	0.07	±.04

Quaternary

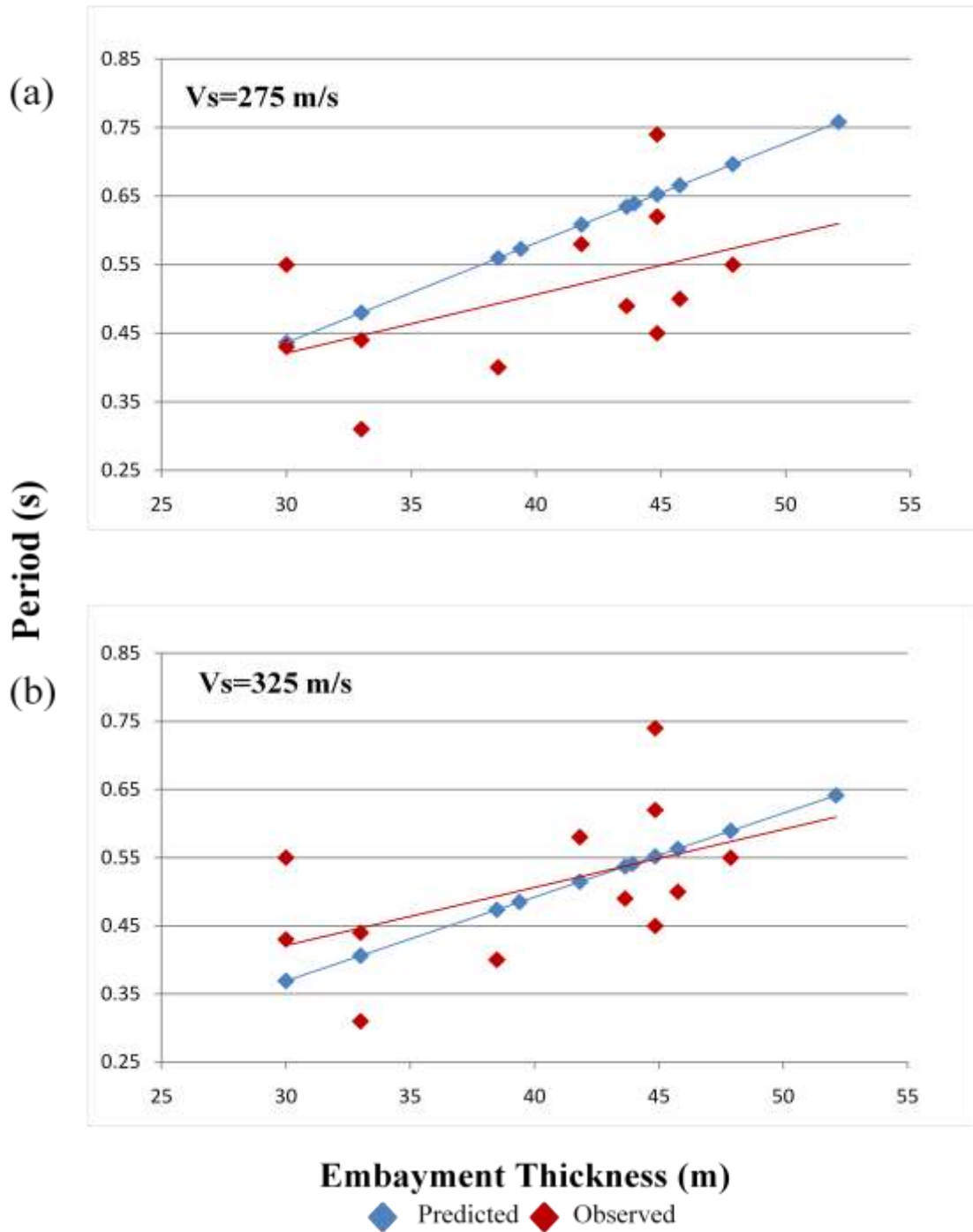


Figure 29. Comparison of observed (red) and predicted (blue) resonant periods associated with the Cretaceous-basement interface using (a) $V_s = 275$ m/s and (b) $V_s = 325$ m/s. See Table 9. Observed periods are quite variable due to variation in the shallow, subsurface shear-wave velocities.

Table 10. Average densities and velocities associated with rock types (Reynolds, 2003).

Rock Type	Average Density (Mg/m³)	Average Velocity (m/s)
Alluvium	1.98	2000
Sandstone	2.35	2900
Clay	2.21	1750
Limestone	2.55	4900

Table 11. Interfaces between the four embayment units and their respective rock type (Figure 2). Average impedance contrast is determined using Zoeppritz equation and the values of average density and velocity seen in Table 10 (Reynolds, 2003).

Interface	Rock Type	Impedance Contrast
Quaternary-Eocene	Alluvium-Sandstone	0.07
Eocene-Paleocene	Sandstone-Clay	0.07
Paleocene-Cretaceous	Clay-Sandstone	0.07
Cretaceous-Basement	Sandstone-Limestone	0.09

Spectra associated with shallow Quaternary-Eocene interface demonstrate significant variability. This variability is likely the result of higher frequencies (e.g., shorter wavelengths) reflecting the differences in near-surface shear-wave velocities related to the Quaternary unit. Based on similar trend lines, the best fit average shear-wave velocity is 325 m/s for the Quaternary-Eocene interface (Figure 29b).

Microtremor Robustness

The robustness of microtremor recordings at a site suggests that microtremors could be used for reliable site characterization. Figures 23 and 24 revealed similarities in both peaks and waveform of longer periods, although the peaks are shifted. The shift in peak is most likely related to the depth to the same interface. The similarity in waveform implies that microtremors could be used to characterize a general area, especially in locations that do not have abundant well-log data.

DISCUSSION

Resonant Periods in the Mississippi Embayment

Peaks in the HVPSRs are interpreted to represent site resonance. Four peak ranges ($T_1 - T_4$) are thought to be associated with different interfaces within the Mississippi embayment; one observed peak range (T_5) is not correlated with any specific embayment interface (Table 12). Of the peaks observed in the HVPSRs, T_1 , T_4 , and T_5 , are present at most sites. T_1 and T_4 correlate with stratigraphic boundaries, whereas the relationship between T_5 and embayment stratigraphy remains elusive.

Table 12. Periods observed in the HVPSRs for this study. Periods are grouped into peak ranges representing the different embayment interfaces.

Peak Range	Periods (s)	Embayment Unit
T_1	0.3 - 0.75	Quaternary
T_2	2.2 - 3.0	Eocene
T_3	2.85 - 3.6	Paleocene
T_4	3.4 - 4.5	Cretaceous
T_5	1.0 - 1.8	Unknown

In microtremor studies located further south in the embayment, Bodin and Horton (1999) and Smith (2000) observe peak ranges similar to those determined in this study. Bodin and Horton (1999) observe a range of 1.5 s to 4.5 s which they correlate with

Paleozoic basement rock ranging in depth from 350 m to 950 m, respectively. Their observations in this frequency range correspond well with the observed periods of T_4 in this study.

Smith (2000) reports three peak ranges and investigates their relation to different interfaces within the embayment (Table 13). He correlates T_1 to interfaces at a depth of about 30 m in the subsurface, T_m to a structure in the upper 125 m of the embayment, and T_p to the basement interface. Smith (2000) divides his study transect into three segments (A, B, and C). Segment A crosses a section of the embayment that would correspond to the eastern part of my study area, and segments B and C would be located east of my study area.

Table 13. Periods observed in the HVPSRs and grouped into peak ranges representing the different embayment boundaries observed by Smith (2000).

Peak Range	Periods (s)	Embayment Unit
T_1	0.03 - 0.3	Quaternary, Loess
T_m	1.0 - 2.0	Unknown
T_p	4.0 - 4.5	Cretaceous

Smith (2000) suggests that T_1 corresponds to the Quaternary-Eocene boundary along Segment A, to a loess layer in Segment B, and to the Claiborne-Wilcox interface (Eocene units) in Segment C. He further speculates that the T_1 in Segment C could be related to a change in rigidity of sediments. T_1 from Segment A in Smith's study and T_1 from the present study relate the shorter period with shallow subsurface sediments, in particular the Quaternary-Eocene interface.

Smith (2000) observes a stable peak at his sites which he refers to as a mid-range peak, T_m . He correlates the period range to a structure in the upper 125 m of the embayment; however, he is unable to identify a particular feature. He then suggests that T_m could be a harmonic multiple of the longer period T_p . Smith (2000) tests this idea of T_m , but is unable to make a correlation between the relationship of T_m and T_p . I observe a range similar to Smith's mid-peak range, T_5 , in which no correlation between the peak and an embayment interface is identified.

Smith (2000) observes a third peak range, T_p , which he correlates to the basement interface. His correlation of T_p to the Paleozoic interface agrees with the relation of resonant periods to basement rock made by Bodin and Horton (1999). I also observe a similar peak range, T_4 , corresponding to Smith's T_p range, which I relate to the interface between embayment sediments and Paleozoic bedrock. In all three studies, the impedance contrast between embayment sediments and basin interface is interpreted to be high and a resonant peak is consistently observed in the spectral ratios.

Based on my observations, I suggest that peak ranges T_1 , T_2 , T_3 , and T_4 correlate to the basal Quaternary, Eocene, Paleocene, and Cretaceous interfaces, respectively. Resonant periods associated with these boundaries are observed at sites where an impedance contrast is inferred from well-logs and other seismic data. Sites in which the peak ranges are not observed could indicate that there is a more gradational change in velocity between these interfaces, or that depth to these units is not appropriately constrained.

Nakamura's K_g Index

Nakamura (1997) proposed use of a vulnerability index, K_g , to represent the degree to which a site or area might experience destructive ground motions, or high shear strains, during earthquakes. High shear strains ($> 10^{-6}$) can lead to soil liquefaction, landslide, and settlement. Since Nakamura (1997) introduced the technique, others have used it to assess vulnerability in areas that have experienced intense liquefaction due to strong ground motion (Konno and Ohmachi, 1998; Huang and Tseng, 2002).

K_g is derived from resonant frequencies, F_p , and amplification factor, A_p , as determined from the HVPSRs, where

$$K_g = A_p^2 / F_p \quad (6)$$

The amplitude of the resonant frequency observed in the HVPSR (Equation 4) is considered the amplification factor.

Nakamura (1997) investigated two areas in Japan, one largely occupied by railway lines and the other occupied by rigid-frame viaducts. Microtremor measurements were taken along railway sections that were damaged in an earthquake. These railway sections were repaired but damaged again by another earthquake. Results corresponding to K_g values along the railway line indicate that damage occurred where K_g values were relatively large (Nakamura, 1997). Similar results were also observed in another area, where large K_g values corresponded to the amount of damage to viaducts. Nakamura (1997) asserts that the K_g values obtained prior to earthquakes can be expected to predict accurately the future earthquake damage at a site.

Huang and Tseng (2002) investigated liquefaction vulnerability for sites in Taiwan that experienced severe liquefaction resulting from the 1999 Chi-Chi earthquake. They took microtremor data in an alluvial fan setting at 42 sites and applied Nakamura's method of estimating liquefaction potential by use of K_g values. Sites that revealed a higher calculated K_g value corresponded with sites that had experienced serious liquefaction.

Figure 30 shows resonant frequencies, amplification factors and liquefaction vulnerability for the 15 sites in this study. Sites are ordered from west to east across the embayment, and corresponding from shallower to deeper depths to basement. Type of deposit, following Saucier's classification, at each site location is indicated by color on the data plots. Fundamental frequencies are progressively lower for thicker portions of the embayment, and corresponding amplification factors are typically higher. For example, the LA site along the basin's margin exhibits the highest value of resonant frequency of 0.6 Hz and the lowest amplification factor of 4. By contrast, the RF site in the basin center has a resonant frequency of 0.32 Hz and an amplification factor of 80. Calculated K_g values range from 2 to 2177, increasing by three orders of magnitude in the central basin. The highest vulnerability indices are associated with sites located in the meandering stream deposits slightly east of the Mississippi River, and east of the embayment axis. Liquefaction deposits are most abundant in this area where higher K_g values have been calculated.

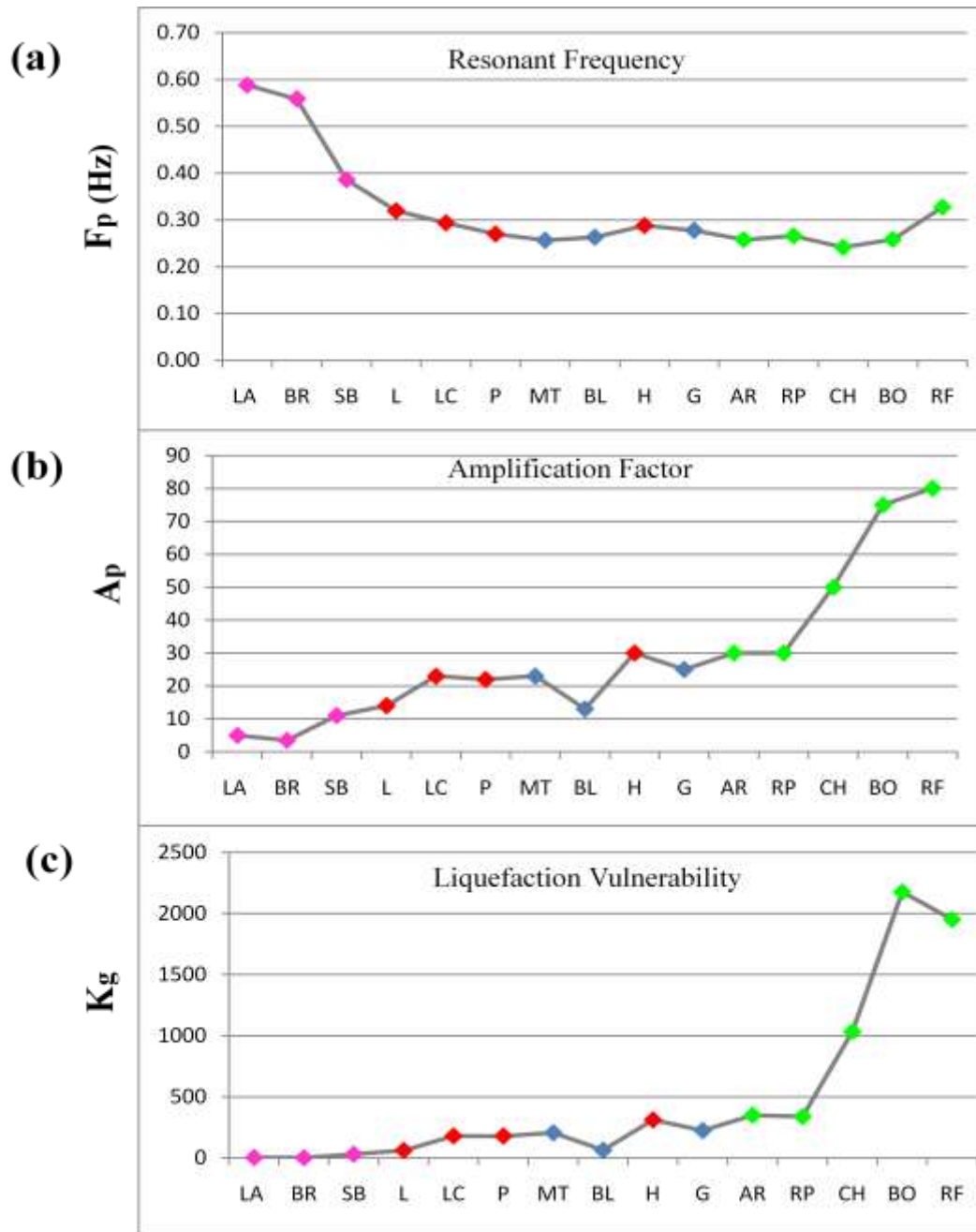


Figure 30: (a) Resonant frequencies (F_p) of embayment-basement interface at 15 sites listed from west to east, with increasing embayment thickness to east. Sites are color-coded by depositional type: lowlands (magenta), braided stream (red), transitional (blue), and meandering stream (green). (b) Observed amplification factor (A_p) for each site as determined from amplitude of predominant periods in HVPSRs. (c) Calculated liquefaction vulnerability (K_g) value for each site, as defined by Nakamura (1997, 2000). Although some variability exists, sites located in the meandering stream deposits generally exhibit stronger liquefaction vulnerability and higher amplification factors relative to other depositional environments.

Konno and Ohmachi (1998) took microtremor measurements in Tokyo to correlate subsurface geology with fundamental periods and amplification factors. The periods and amplification factors observed in the HVPSRs were compared to surface sediments, and other microtremor measurements made prior to their study. The fundamental periods indicate good correlation with sediment type and previous microtremor measurements, whereas the amplification factor did not have a strong correlation to surface sediments.

As with the study of Konno and Ohmachi (1998), I investigate a possible relationship between amplification and K_g with near-surface layers (Figure 31). Whereas Konno and Ohmachi (1998) found little agreement between amplification and alluvial sediment, this study suggests association of higher amplification factors to meandering surface deposits. Figure 31a compares the calculated K_g value with the percentage of sand blow material as taken from paleoliquefaction and liquefaction maps of surface deposits. Some correlation is observed between higher K_g values and sites containing observed liquefaction deposits. However, due to the limited area covered in this study, these results are inconclusive.

(a)

Sites	Geotechnical data	Sand Blow %	Kg- Q
L	N	10 - 15	123
LC	N	10 - 15	53
P	N	Forested	94
MT	Y	10 - 15	254
BL	N	Forested	155
H	N	10 - 15	867
G	N	Forested	26
AR	Y	10 - 15	531
RP	Y	10 - 15	956
CH	N	Forested	87
BO	N	10 - 15	353
RF	N	Forested	62

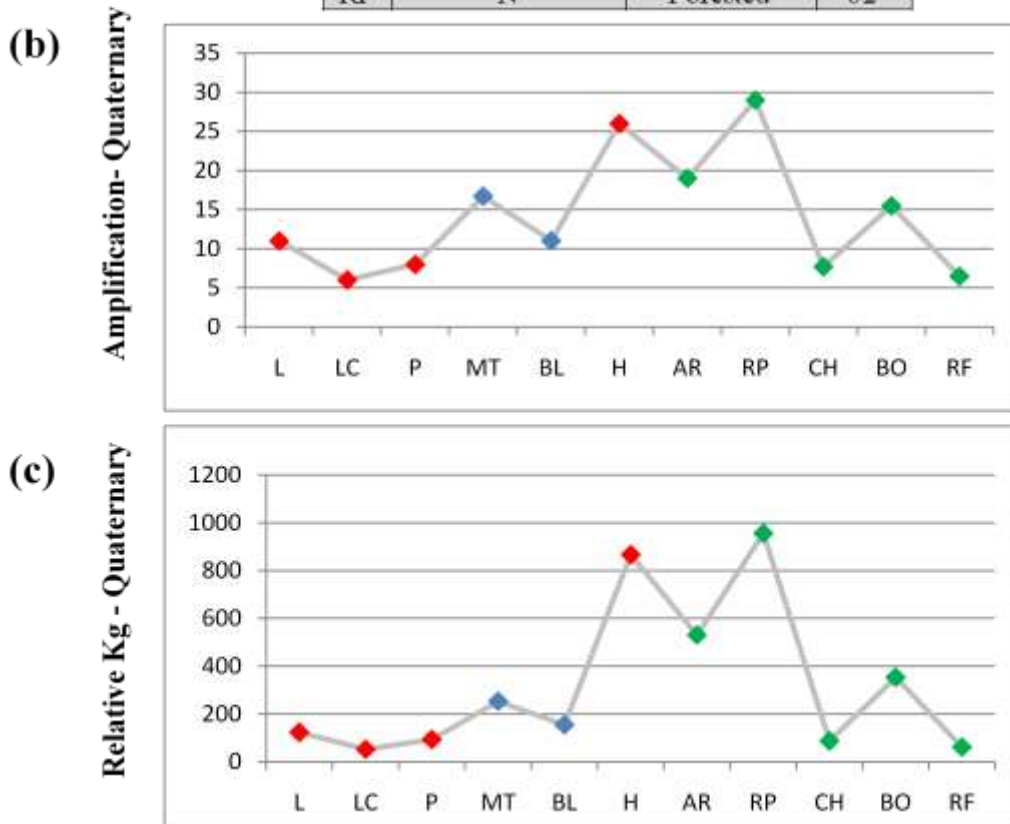


Figure 31. (a) Sites and their calculated K_g values relating to the basal Quaternary interface. Also indicated are geotechnical data available for sites (Y- yes, N- no), and percentage of sand blows expressed at the surface at the location of each site as determined from aerial photography (Obermeier, 1989). Sites labeled forested indicate that sand blow percentages could not be determined due to vegetation. (b) Observed amplification factors at sites listed from west to east and color coded by deposit type: braided stream (red), transitional (blue), and meandering (green). (c) Calculated K_g values. Sites with a high relative K_g value agree well with areas that have a high percentage of sand blows observed at the surface.

Previous studies (Baher and Davis, 2003; Hruby and Beresnev, 2003; Choi et al., 2005) have suggested that basin configuration can focus seismic energy towards the deeper portions of a basin. This phenomenon occurs because the curvature of the basin focuses energy to the basin's center and the overlying younger alluvial sediments of lower seismic velocity can trap wave energy within the basin. These phenomena can lead to more intense shaking and longer durations (Baher and Davis, 2003; Hruby and Beresnev, 2003). Focusing effects may provide one explanation for why the highest amplitude is found at sites near the basin center. Figure 30 shows the relationship of relative amplification factor and site location within the embayment. Sites are shown from the western edge towards the basin center; generally, amplification becomes larger towards the center of the basin.

Significance of Resonant Periods

Large earthquakes ($M > 6.5$) radiate high energy at periods of 4 s and above, and are capable of initiating soil liquefaction in unconsolidated sediments like those found in the Mississippi Embayment (Obermeier, 1996; Bodin and Horton, 1999). Earthquake energy at these periods coincides with the resonant period bands observed in this study, as well as other studies (Bodin and Horton, 1999; Smith, 2000). Earthquake energy excited in this period range, may partially explain the high occurrence of liquefaction deposits observed in the central basin. The resonant periods of embayment sediments as revealed in this and previous studies are essential considerations for studies of seismic hazard.

Considerations

Although the advantages of the microtremor method are significant, there are some cautionary aspects of the technique to consider. Whereas this study used single-stations to collect microtremor data and analyze site characteristics, some studies have used arrays of different sizes to investigate the variation of incoming microtremors over a spatial extent (Lermo and Chavez-Garcia, 1993; Horike et al., 2001; Chavez-Garcia and Luzon, 2005). The microtremor method is best used as an additional tool in conjunction with geotechnical, well-log, and seismic data. K_g values represent the relative potential of a site to experience wave amplification, but whether that will lead to liquefaction depends on other factors (i.e. - seismic duration, sediment type and cohesion, presence of fluids, ambient pore pressure, etc.). Geotechnical tests designed to determine site-specific characteristics are needed to assess soil liquefaction susceptibility. However, these tests are sometime not affordable or logistically practical. The microtremor measurements can be used to assess and target an area vulnerable to seismic waves.

Suggestions for Future Investigations

Results of this study have brought about some interesting findings that could be further investigated in future studies. First is the peak range, T_5 , in which no correlation was made between the observed periods and embayment sediments. This peak range was also recognized in a study further south of my study area (Smith, 2000), and was not correlated to any specific structure in the embayment. Second are the K_g values. Microtremor measurements should be taken at more sites that are closer in spatial distribution in an effort to map and contour high liquefaction potential in the NMSZ and

in other sedimentary basins that are susceptible to strong earthquakes. Contouring K_g values could be useful in providing target areas for geotechnical investigations, as higher values would indicate the potential of a site to liquefy.

CONCLUSIONS

Microtremor data collected for this study suggests that Nakamura's (1989) method of using H/V spectral ratios can be a useful tool in determining site characteristics such as fundamental period, amplification factor, and liquefaction susceptibility. This study correlated observed periods from the H/V spectral ratios to different embayment interfaces and used this information to target areas within the embayment that are more vulnerable to wave amplification and liquefaction.

H/V ratios indicate that the resonant periods are longer at sites that have thicker embayment sediments. Sites that have thicknesses ranging from 600 m to 900 m have fundamental resonant periods ranging from 3.2 s to 4.5 s, respectively, indicating that earthquake ground motions in this period range might be amplified by basin sediments and have longer durations. Although all sites have peaks associated with the sediment-basement interface, the intermediate Paleocene and Eocene boundaries are observed in spectral ratios only at some sites. Peaks related to the intermediate boundaries are associated with the significant impedance contrasts at those interfaces.

In addition to high impedance contrasts, results are also consistent with the idea that basin configuration contributes to the observed large spectral amplitudes and high relative vulnerability. Although the spectral amplification might be better estimated by other techniques, such as the standard spectral ratio or instrument arrays, the ease of data

collection combined with the elimination of the need for a hard rock reference site make the HVPSR method a worthwhile choice for seismic hazard studies in deep sedimentary basins. Results of this study are consistent with previous work that suggests the HVPSR method is useful in evaluating areas susceptible to liquefaction. The application of microtremors is a fast, non-invasive, and cost-efficient method requiring minimal woman-power, thus making it an appealing technique. However, it is suggested that the microtremor technique be used in conjunction to other geophysical and geotechnical studies.

REFERENCES

- Ausbrooks, S., 2006, Arkansas Oil and Gas Commission: personal communication.
- Baier, S. A., and P. M. Davis, 2003, An application of seismic tomography to basin focusing of seismic waves and Northridge earthquake damage: *Journal of Geophysical Research*, **108**, B22122.
- Blake, B., 2006, Central United States Earthquake Consortium: personal communication.
- Bodin, P. and S. Horton, 1999, Broadband microtremor observation of basin resonance in the Mississippi embayment, Central United States: *Geophysical Research Letters*, **26**, 903-906.
- Braile, L. W., W. J. Hinze, G. R. Keller, E. G. Lidiak, and J. L. Sexton, 1986, Tectonic development of the New Madrid Rift Complex, Mississippi Embayment, North America: *Tectonophysics*, **131**, 1-21.
- Bullen, K., and B. Bolt, 1985, *An Introduction to the Theory of Seismology*: Cambridge University Press.
- Campbell, D. A., 1978, Investigation of the stress-concentration mechanism for intraplate earthquakes: *Geophysical Research Letters*, **5**, 477-479.
- Chavez-Garcia, F., and F. Luzon, 2005, On the correlation of seismic microtremors: *Journal of Geophysical Research*, **110**, B11313.

- Choi, Y., J. P. Stewart, and R. W. Graves, 2005, Empirical model for basin effects accounts for basin depth and source location: *Bulletin of the Seismological Society of America*, **95**, 1412-1427.
- Crone, A. J., 1981, Sample description and stratigraphic correlation of the New Madrid test well-1-X, New Madrid County, Missouri: U. S. Geological Survey Open-File Report, 81-426.
- Dravinski, M., H. Yamanaka, and H. Kagami, 1992, Site amplification through measurement of long period microtremors: Predominant period of motion: *Proceedings of the 10th World Conference on Earthquake and Engineering*, 1037-1041.
- Field, E. H., S. E. Hough, and K. H. Jacob, 1990, Using microtremors to assess potential earthquake site response: A case study in Flushing Meadows, New York City: *Bulletin of the Seismological Society of America*, **80**, 1456-1480.
- Field, E. H., and K. H. Jacob, 1993, The theoretical response of sedimentary layers to ambient seismic noise: *Geophysical Research Letters*, **20**, 2925-2928.
- Gangopadhyay, A., J. Dickerson, and P. Talwani, 2004, A two-dimensional numerical model for current seismicity in the New Madrid seismic zone: *Seismological Research Letters*, **75**, 406-418.
- Gomberg, J. S., 1992, Tectonic deformation in the New Madrid seismic zone: inferences from boundary element modeling: *Seismological Research Letters*, **63**, 407-425.
- Hinze, W. J., L. W. Braile, G. R. Keller, and E. G. Lidiak, 1988, Models for midcontinent tectonism- An update: *Reviews of Geophysics*, **26**, 699-717.

- Horike, M., B. Zhao, and H. Kawase, 2001, Comparison of site response characteristics inferred from microtremors and earthquake shear waves: *Bulletin of the Seismological Society of America*, **91**, 1562-1536.
- Howe, J. R., and T. L. Thompson, 1984, Tectonics, sedimentation, and hydrocarbon potential of the Reelfoot rift: *Oil and Gas Journal*, **82**, 179-190.
- Hoyal, M. L., 2006, Tennessee Department of Environment and Conservation: personal communication.
- Hruby, C. E., and I. A. Beresnev, 2003, Empirical corrections for basin effects in stochastic ground-motion prediction, based on the Los Angeles basin analysis: *Bulletin of the Seismological Society of America*, **93**, 1679-1690.
- Huang, H. C., 2002, Characteristics of earthquake ground motions and the H/V of microtremors in the southwestern part of Taiwan: *Earthquake Engineering and Structural Dynamics*, **31**, 1815-1829.
- Huang, H.C., and Y. Tseng, 2002, Characteristics of soil liquefaction using H/V of microtremors in Yan-Lin area, Taiwan: *Terrestrial, Atmospheric, and Oceanic Sciences*, **13**, 325-338.
- Ibs-von Seht, M., and J. Wohlenburg, 1999, Microtremor measurements used to map thickness of soft sediments: *Bulletin of the Seismological Society of America*, **89**, 250-259.
- Johnston, A. C., and K. M. Shedlock, 1992, Overview of research in the New Madrid seismic zone: *Seismological Research Letters*, **63**, 193-208.

- Kane, M. F., T. G. Hildenbrand, and J. D. Hendricks, 1981, Model for the tectonic evolution of the Mississippi Embayment and its contemporary seismicity: *Geology*, **9**, 563-568.
- Katz, L. J., 1976, Microtremor analysis of local geological conditions: *Bulletin of the Seismological Society of America*, **66**, 45-60.
- Konno, K., and T. Ohmachi, 1998, Ground-motion characteristics estimated from spectral ratios between horizontal and vertical components of microtremor: *Bulletin of the Seismological Society of America*, **88**, 228-241.
- Lermo, J., and F. Chavez-Garcia, 1993, Site effect evaluation using spectral ratios with only one station: *Bulletin of the Seismological Society of America*, **83**, 1574-1594.
- Liu, L., M. D. Zoback, and P. Segall, 1992, Rapid intraplate strain accumulation in the New Madrid seismic zone: *Science*, **257**, 1666-1669.
- Liu, L., and M. Zoback, 1997, Lithospheric strength and intraplate seismicity in the New Madrid seismic zone: *Tectonics*, **16**, 585-595.
- Nakamura, Y., 1989, A method for dynamic characteristics estimation of subsurface using microtremor on the ground surface: *Quarterly Report of Railway Technical Research Institute*, **30**, 25-33.
- Nakamura, Y., 1997, Seismic vulnerability indices for ground and structures using microtremor: *World Congress and Railway Research in Florence, Italy*.
- Nakamura, Y., 2000, Clear identification of fundamental idea of Nakamura's technique and its applications: *Proceedings of the 12th World Conference on Earthquake and Engineering*, 2656-2664.

- Newman, A., S. Stein, J. Weber, J. Engeln, A. Mao, and T. Dixon, 1999, Slow deformation and lower seismic hazard at the New Madrid seismic zone: *Science*, **284**, 619-21.
- Obermeier, S. F., 1989, The New Madrid earthquakes: an engineering-geologic interpretation of relict liquefaction features: U. S. Geological Survey Professional Paper, 1336-B.
- Obermeier, S. F., 1996, Using liquefaction-induced features for paleoseismic analysis, *in* J.P. McCalpin, ed., *Paleoseismology*: Academic Press, 331-396.
- Reynolds, J. M., 2003, *An introduction to applied and environmental geophysics*: John Wiley and Sons Inc.
- Rix, G., 2006, Georgia Institute of Technology: personal communication.
- Romero, S., and G. Rix, 2001, Ground motion amplification of soils in the upper Mississippi embayment: GIT-CEE/GEO-01-1.
- Saucier, R., 1994a, Geomorphology and Quaternary geologic history of the lower Mississippi Valley: United States Army Corps of Engineers, Waterways Experiment Station, **1**, 364.
- Saucier, R., 1994b, Geomorphology and Quaternary geologic history of the lower Mississippi Valley: United States Army Corps of Engineers, Waterways Experiment Station, **2**, 28.
- Schneider, J. A., and P. W. Mayne, 1998, Results of seismic piezocone and flat plate dilatometer tests performed in Blythville, AR, Steele, MO, and Shelby County, TN: Interim Report, Mid-America Earthquake Center Project No. GT-3.

- Seed, H., and I. Idriss, 1982, Ground motions and soil liquefaction during earthquakes: Earthquake Engineering Research Institute.
- Siemens, M., 2006, Missouri Department of Natural Resources: personal communication.
- Smith, K., 2000, Using microtremor to illuminate subsurface geology of Memphis, Tennessee: M.S. Thesis, University of Memphis.
- Stearns, R. G., 1982, Configuration of the base Cretaceous – top of Paleozoic surface: Tennessee Division of Geology, scale 1:500,000.
- Street, R., E. W. Woolery, and J. Chiu, 2004, Shear-wave velocities of the Post-Paleozoic sediments across the Upper Mississippi Embayment: Seismological Research Letters, **75**, 390-405.
- Tuttle, M. P., 2001, The use of liquefaction features in paleoseismology: Lessons learned in the New Madrid seismic zone, central United States: Journal of Seismology, **5**, 361-380.
- Tuttle, M., E. Schweig, J. Sims, R. Lafferty, L. Wolf, and M. Haynes, 2002, The earthquake potential of the New Madrid seismic zone: Bulletin and the Seismological Society of America, **92**, 2080-2089.
- U. S. Geological Survey, 2005, Surface geology of the Mississippi Embayment, <http://nmviewogc.cr.usgs.gov/viewer.htm>, accessed November 7, 2007.
- Van Arsdale, R., and R. TenBrink, 2000, Late Cretaceous and Cenozoic geology of the New Madrid seismic zone: Bulletin of the Seismological Society of America, **90**, 345-356.
- Woolery, E. and R. Street, 2002, 3D near-surface soil response from H/V ambient-noise ratios: Soil Dynamics and Earthquake Engineering, **22**, 865-876.

APPENDIX A – Site Information

The following table includes the following information pertaining to each site:

Site Name:	Names and abbreviations of sites at which microtremor data were collected
Site Number:	Order in which microtremor data were collected
Comment:	Good- site used for spectral analysis, Bad- site excluded from spectral analysis
Latitude:	Decimal degrees
Longitude:	Decimal degrees
County:	County of site location
State:	State of site location
Deposit Type:	Surface deposit type as classified by Saucier (1994b)
Guralp Number:	Number of specific Guralp unit used for data collection

SITE NAME	SITE	COMMENT	LATITUDE	LONGITUDE	COUNTY	STATE	DEPOSIT TYPE	GURALP
Marked Tree (MT)	1	Good	35.52522	-90.38544	Poinsett	AR	Transitional	6299
Chickasaw (CH)	2	Good	35.88091	-89.58448	Lauderdale	TN	Flood Plain	6299
Chickasaw 2 (CH)	2	Good	35.88091	-89.58448	Lauderdale	TN	Flood Plain	6242
Reeffoot 2 (RF)	3	Good	36.39708	-89.33857	Obion	TN	Flood Plain	6242
Reeffoot 1 (RF)	4	Good	36.39725	-89.33876	Obion	TN	Flood Plain	6299
Bogota (BO)	5	Good	36.14711	-89.46036	Dyer	TN	Flood Plain	6299
Big Lake (BL)	6	Good	35.87019	-90.13098	Mississippi	AR	Transitional	6242
Hornersville (H)	7	Good	36.03769	-90.11026	Dunklin	MO	Braided Stream	6299
Gilbert (G)	8	Good	36.01625	-90.06191	Dunklin	MO	Transitional	6242
Black River (BR)	9	Good	36.28407	-90.72336	Clay	AR	Lowlands	6299
Lake Ashbaugh (LA)	10	Good	36.26711	-90.75298	Clay	AR	Lowlands	6299
Shirley Bay (SB)	11	Good	35.97893	-91.18088	Lawrence	AR	Lowlands	6242
Jacksonport State Park (JSP)	12	Bad	35.63104	-91.31296	Jackson	AR	Lowlands	6242
Earl Buss Bayou (EBB)	13	Bad	35.58490	-90.95720	Poinsett	AR	Lowlands	6242
Payneway (P)	14	Good	35.54329	-90.48471	Poinsett	AR	Braided Stream	6299
Lake City (LC)	15	Good	35.83382	-90.40435	Craighead	AR	Braided Stream	6299
Lester (L)	16	Good	35.89348	-90.44321	Craighead	AR	Braided Stream	6299
RP Haynes (RP)	17	Good	35.98851	-89.91750	Mississippi	AR	Flood Plain	6032
Archway (AR)	18	Good	35.99611	-89.89139	Pemiscot	MO	Flood Plain	6032
Dillihunty (D)	19	Bad	35.99806	-89.89139	Pemiscot	MO	Flood Plain	6239

APPENDIX B – Raw Data

Raw data collected from 18 sites and used in this study are included here (Figure 5). The site name is displayed at the top of each figure and the time segment chosen for analysis is contained within the black-dashed rectangle of each figure.

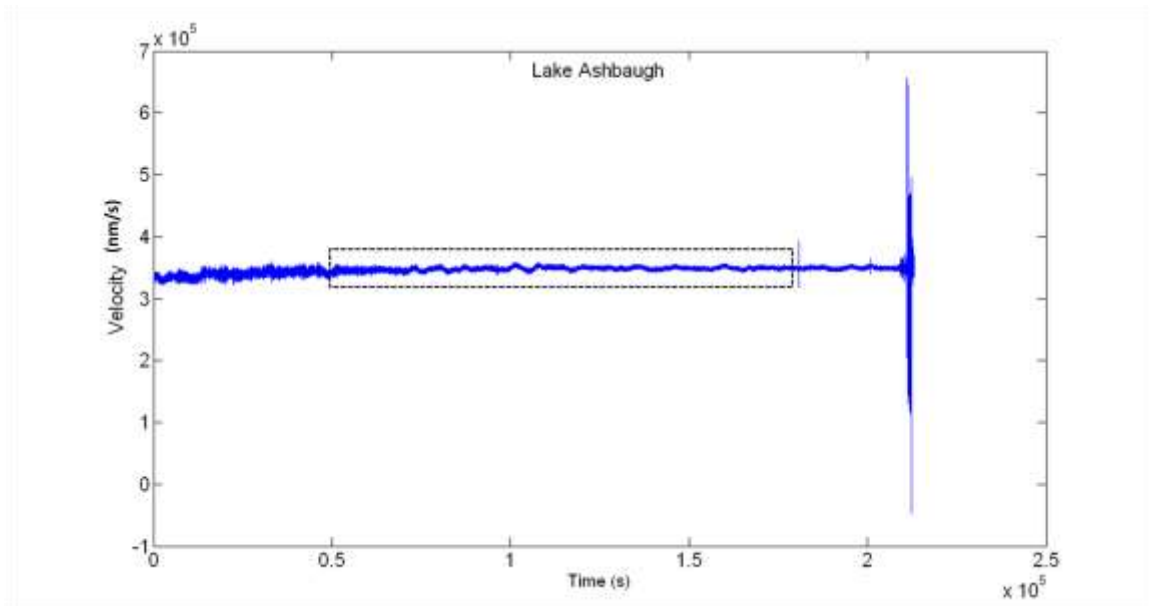


Figure B-1. Raw data and selected time segment used in analysis for site Lake Ashbaugh.

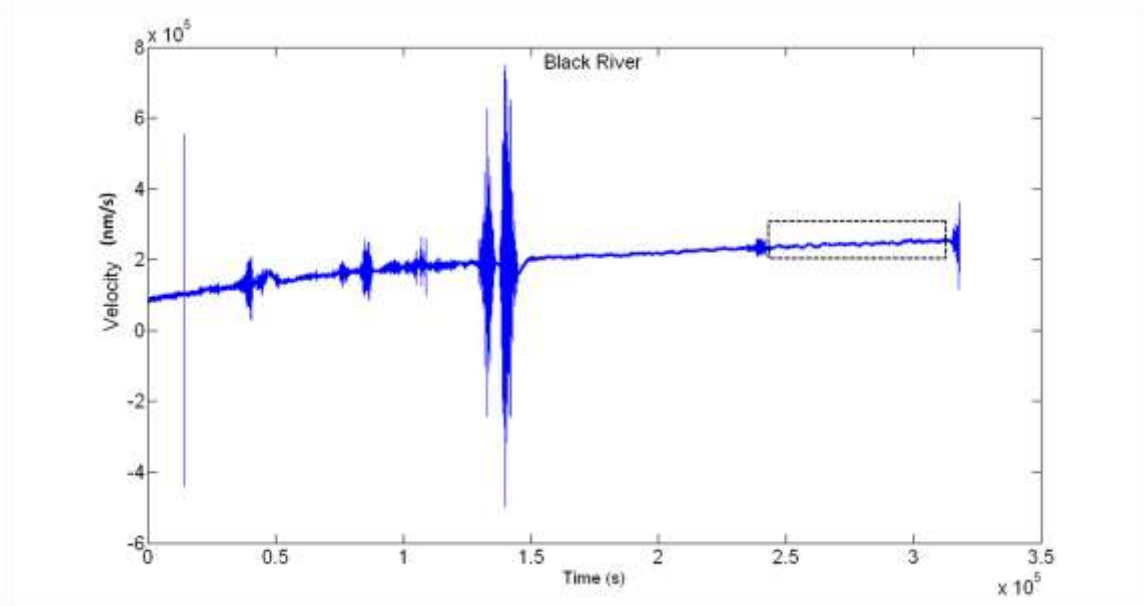


Figure B-2. Raw data and selected time segment used in analysis for site Black River.

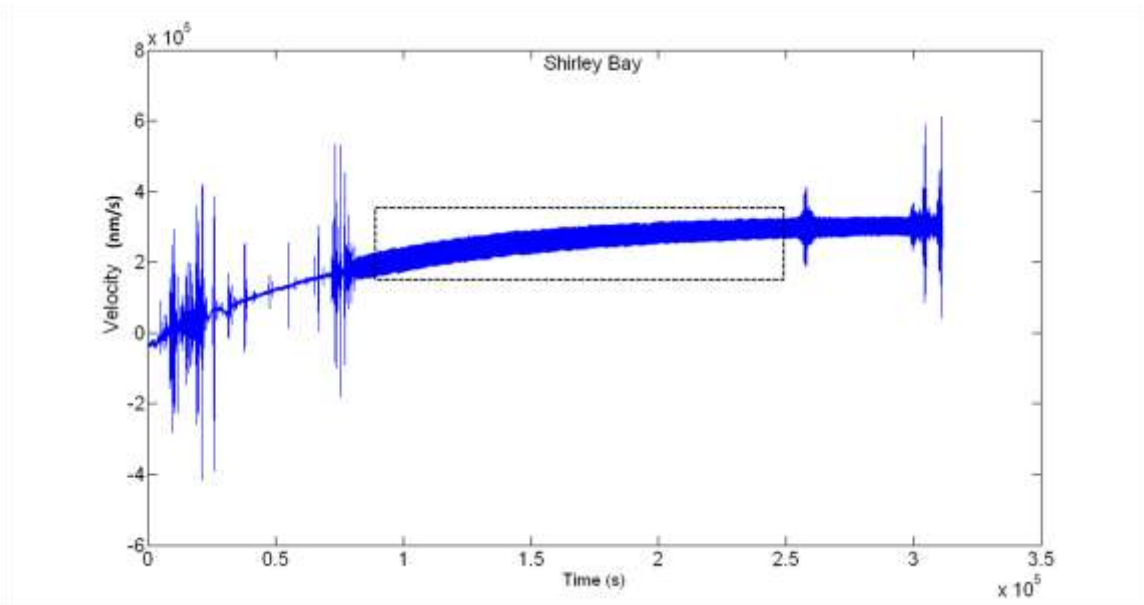


Figure B-3. Raw data and selected time segment used in analysis for site Shirley Bay.

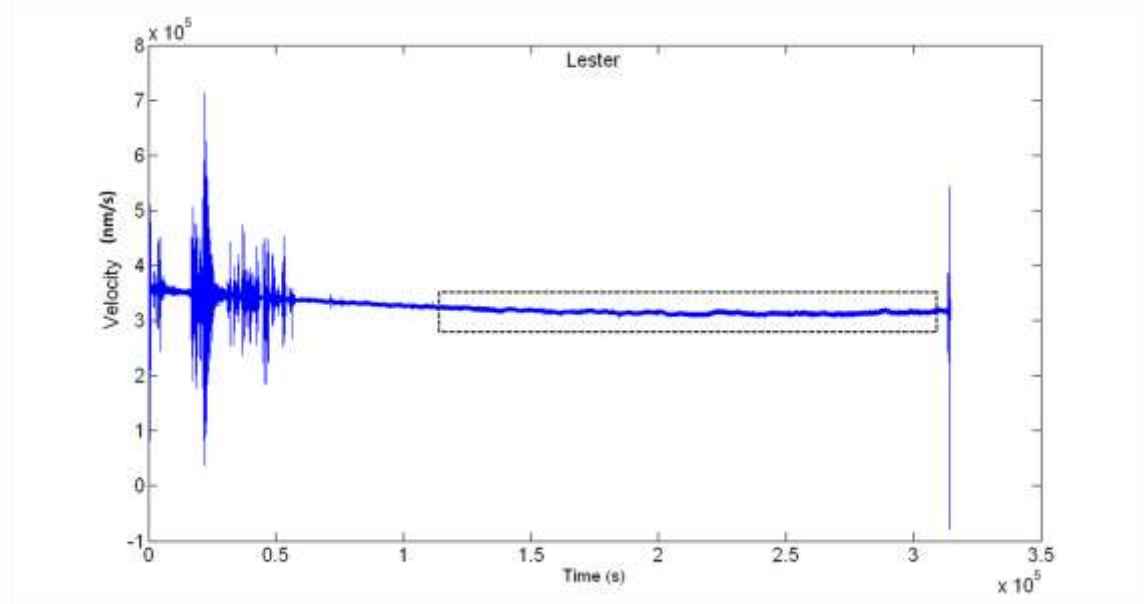


Figure B-4. Raw data and selected time segment used in analysis for site Lester.

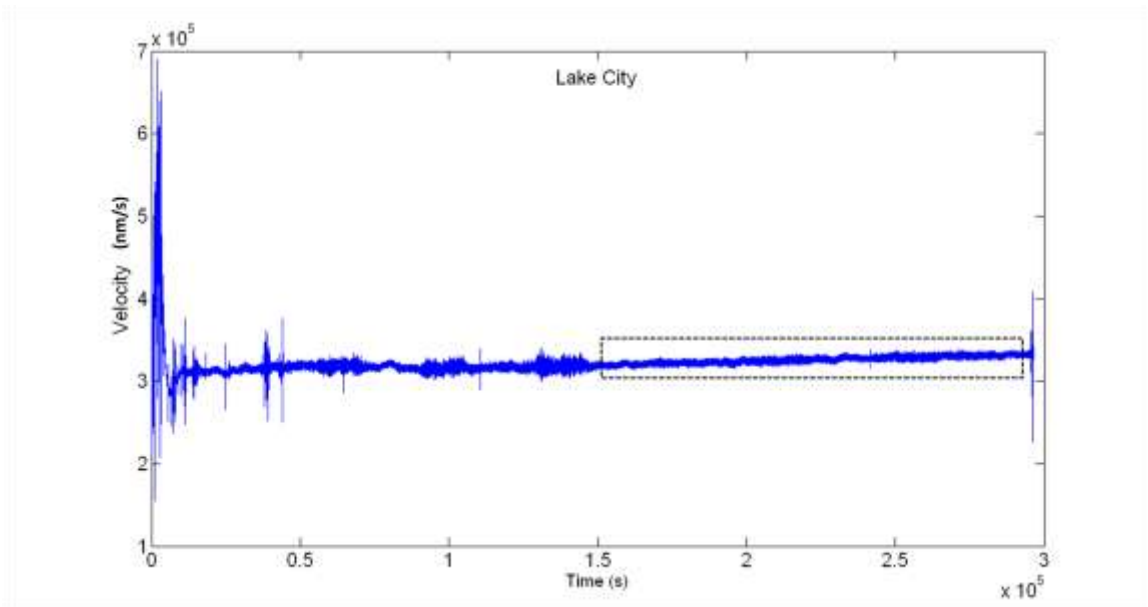


Figure B-5. Raw data and selected time segment used in analysis for site Lake City.

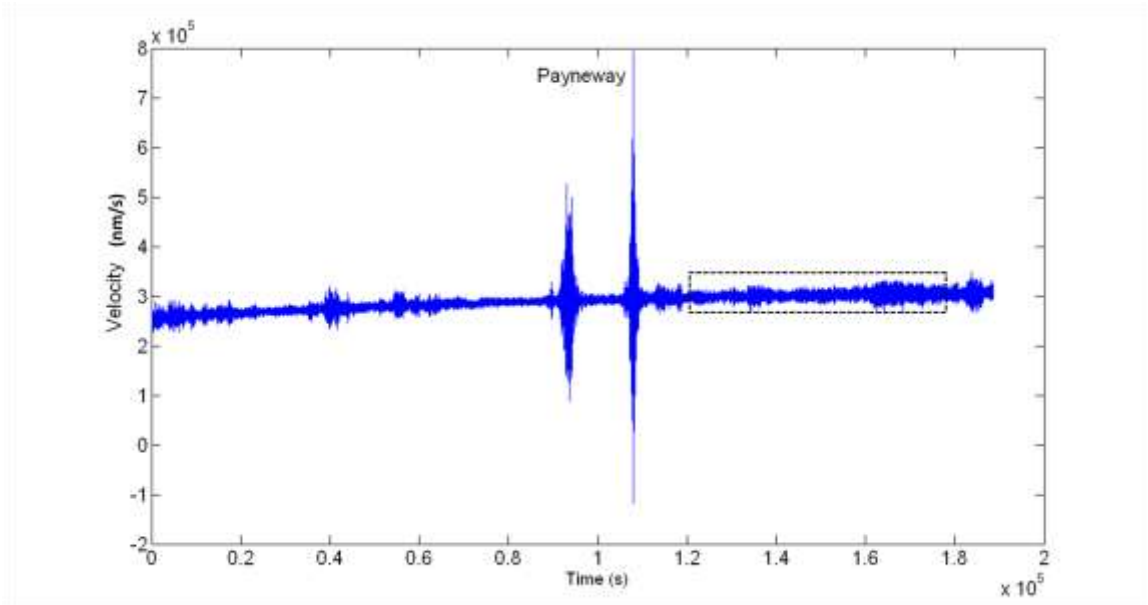


Figure B-6. Raw data and selected time segment used in analysis for site Payneway.

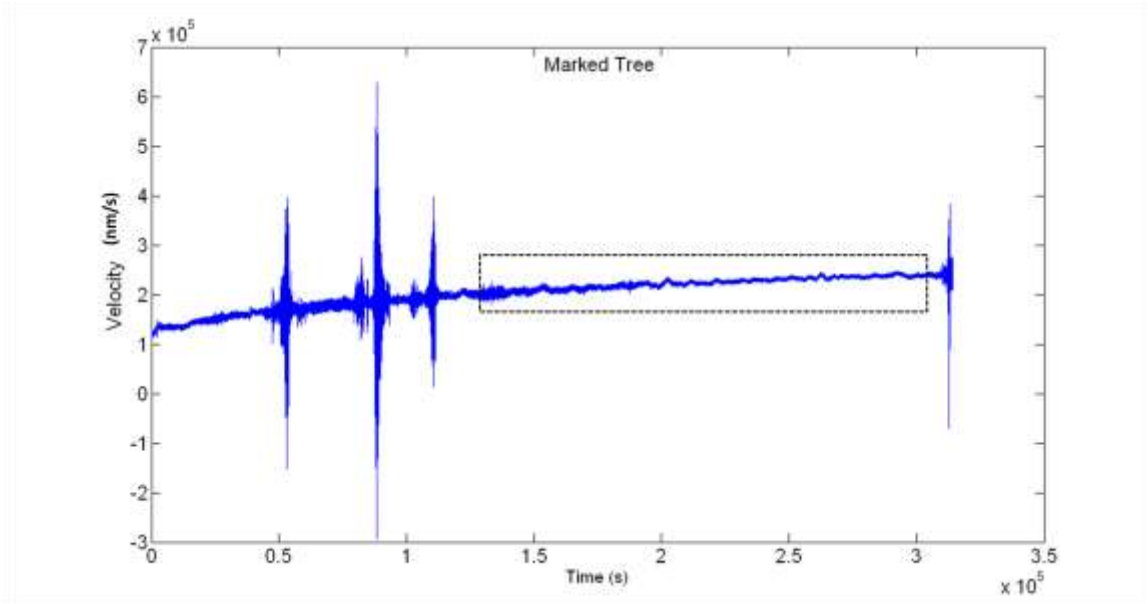


Figure B-7. Raw data and selected time segment used in analysis for site Marked Tree.

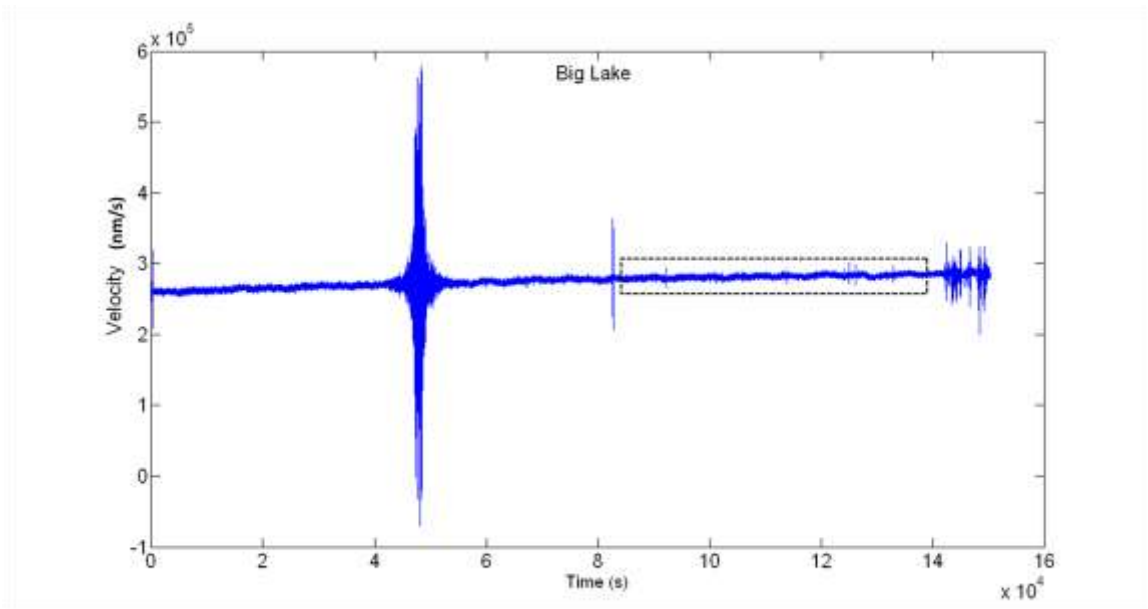


Figure B-8. Raw data and selected time segment used in analysis for site Big Lake.

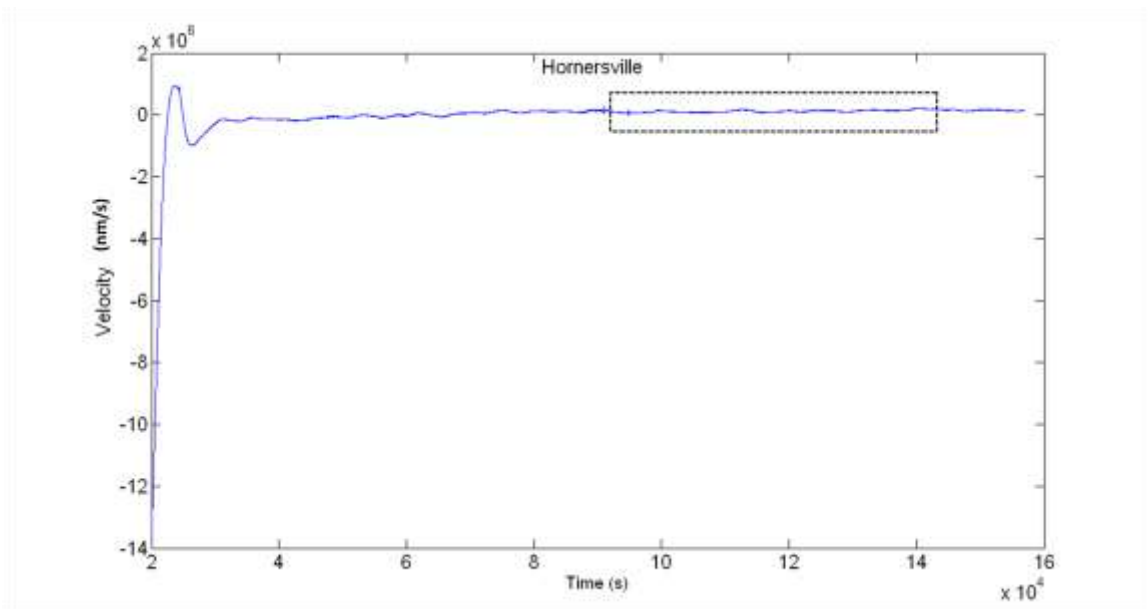


Figure B-9. Raw data and selected time segment used in analysis for site Hornersville.

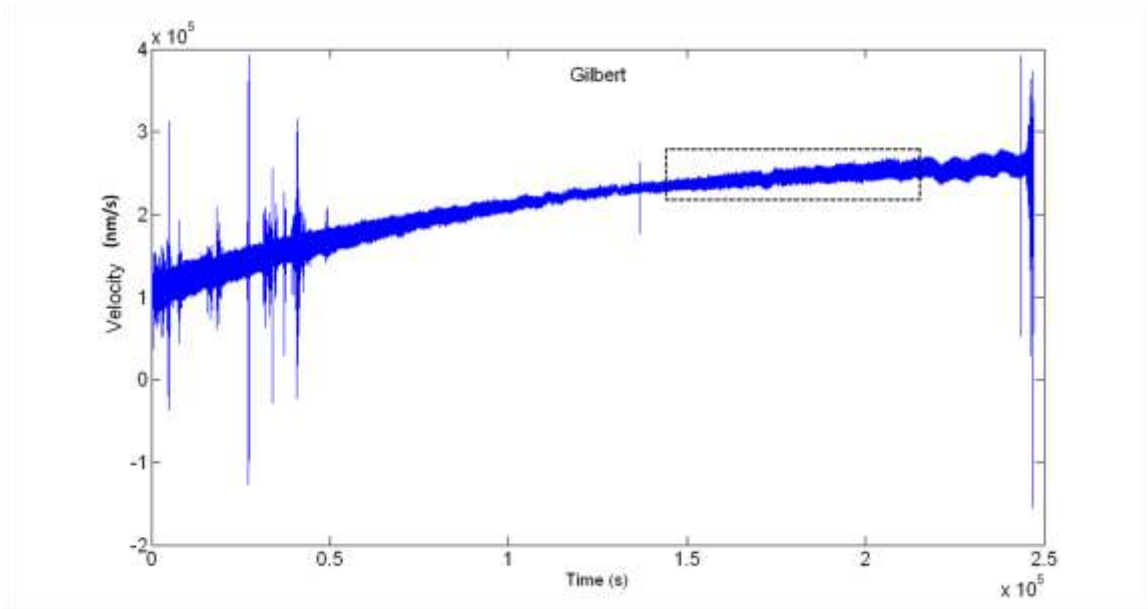


Figure B-10. Raw data and selected time segment used in analysis for site Gilbert.

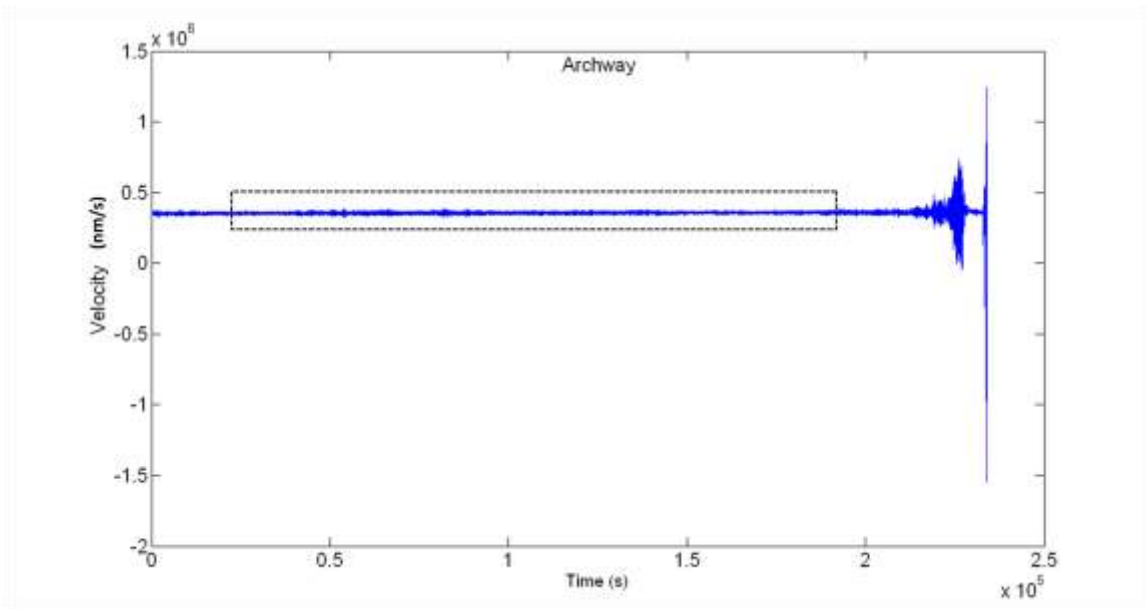


Figure B-11. Raw data and selected time segment used in analysis for site Archway.

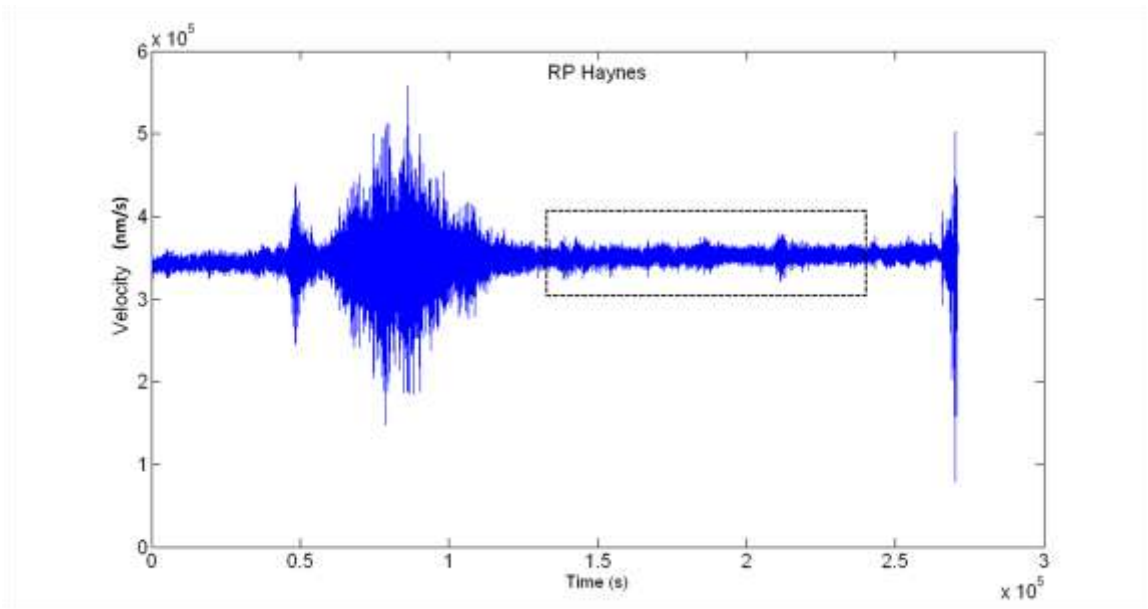


Figure B-12. Raw data and selected time segment used in analysis for site R.P. Haynes.

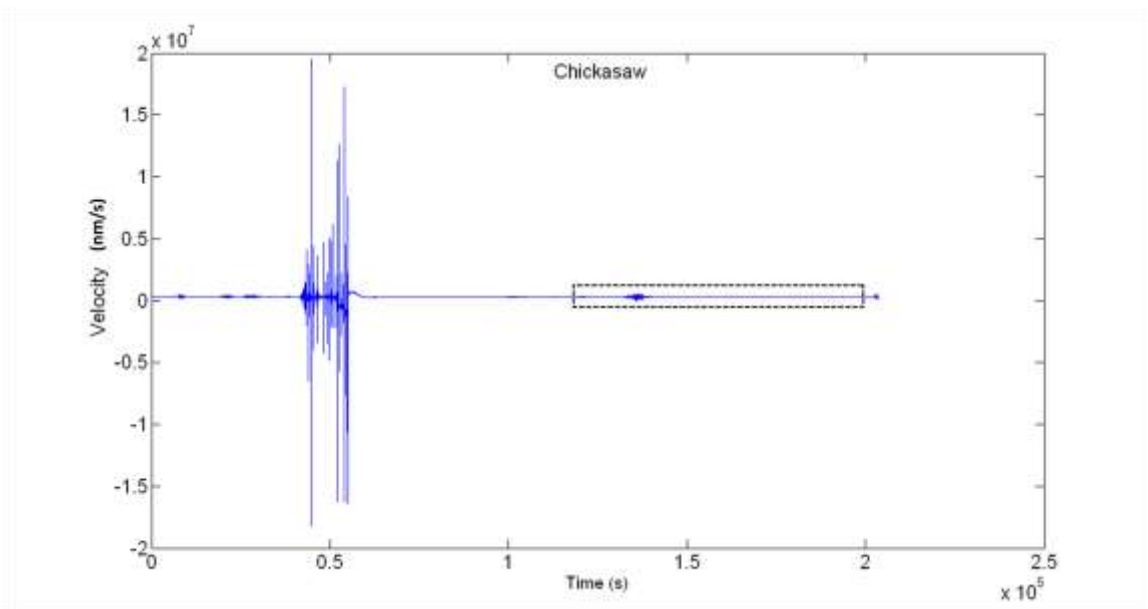


Figure B-13. Raw data and selected time segment used in analysis for site Chickasaw.

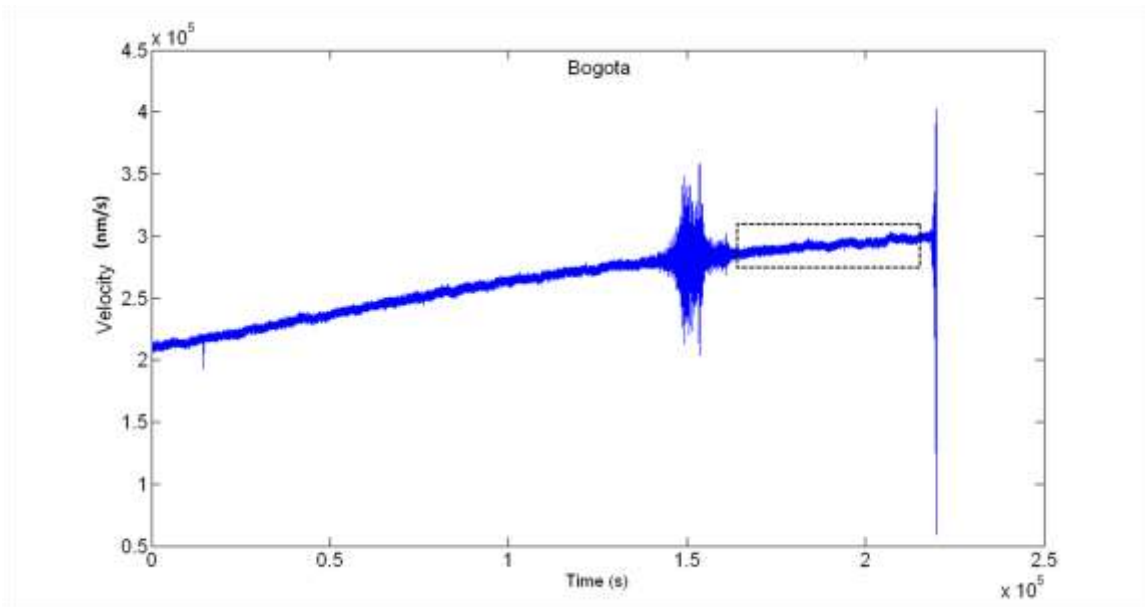


Figure B-14. Raw data and selected time segment used in analysis for site Bogota.

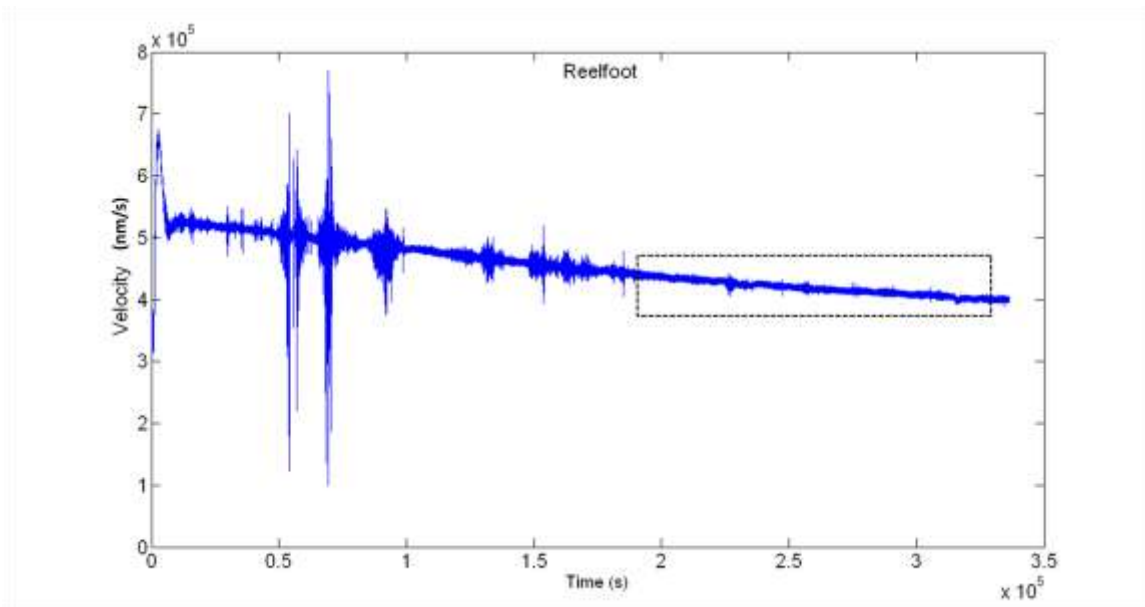


Figure B-15. Raw data and selected time segment used in analysis for site Reelfoot.

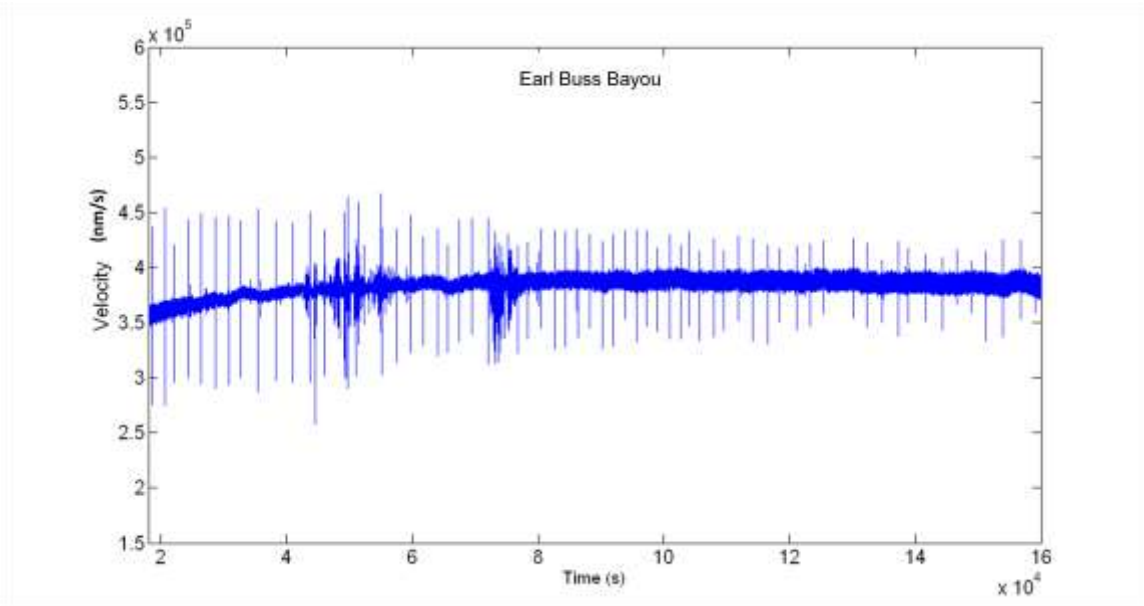


Figure B-16. Raw data not used in analysis for site Earl Buss Bayou.

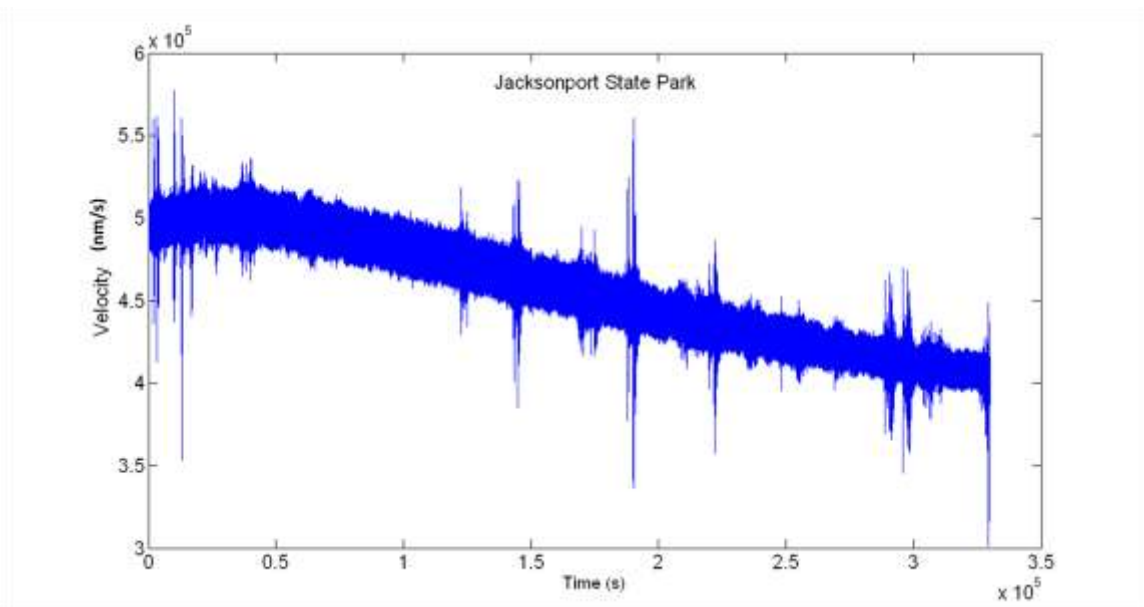


Figure B-17. Raw data not used in analysis for site Jacksonport State Park.

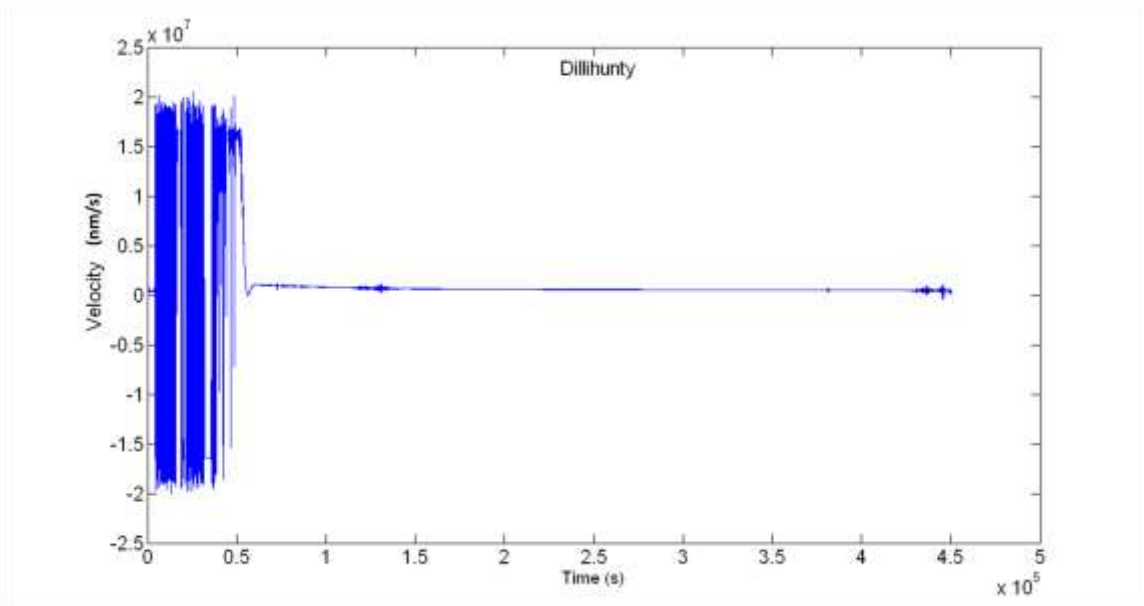


Figure B-18. Raw data not used in analysis for site Dillihunty.

APPENDIX C – Data and MATLAB Programs

The CD insert found in the back sleeve contains data from ground motion recordings made during this study and the MATLAB programs used to calculate the HVPSRs. The CD is labeled “Appendix C” and contains 5 folders, 4 of which contain subfolders. The data are in a UNIX structured database. Appendix A provides file names of the time series used to compute the respective spectral ratios. Most of the spectral ratios are shown in the Result section. The MATLAB programs used to view raw data and to compute the spectral ratios are the ‘load_sac’ and ‘ibs’ M-files, respectively. The data is organized as follows.

FOLDER: Lowlands

SUBFOLDERS: Black River WMA, Earl Buss Bayou, Jacksonport State Park, Lake Ashbaugh, and Shirley Bay WMA.

Time series recorded at each site are in SAC format. The MATLAB programs used for raw data and spectral ratios are M-files. HVPSRs computed for each site are seen in MATLAB figures.

FOLDER: Braided Stream

SUBFOLDERS: Hornersville, Lake City, Lester, and Payneway

Time series recorded at each site are in SAC format. The MATLAB programs used for raw data and spectral ratios are M-files. HVPSRs computed for each site are seen in MATLAB figures.

FOLDER: Transitional

SUBFOLDERS: Big Lake, Gilbert, Marked Tree

Time series recorded at each site are in SAC format. The MATLAB programs used for raw data and spectral ratios are M-files. HVPSRs computed for each site are seen in MATLAB figures.

FOLDER: Meander Flood Plain

SUBFOLDERS: Archway, Bogota, Chickasaw, Chickasaw 2, Dillihunty, Reelfoot, Reelfoot 2, and RP Haynes

Time series recorded at each site are in SAC format. The MATLAB programs used for raw data and spectral ratios are M-files. HVPSRs computed for each site are seen in MATLAB figures.

FOLDER: Cross-Section Sites

Data from various sites in SAC format, along with the MATLAB programs used for raw data and spectral ratios as M-files. HVPSRs computed are seen in MATLAB figures.